

# REDUCIBLE $M$ -CURVES FOR LE-NETWORKS IN THE TOTALLY-NONNEGATIVE GRASSMANNIAN AND KP-II MULTILINE SOLITONS

SIMONETTA ABENDA AND PETR G. GRINEVICH

**ABSTRACT.** We associate real and regular algebraic-geometric data to each multi-line soliton solution of Kadomtsev-Petviashvili II (KP) equation. These solutions are known to be parametrized by points of the totally non-negative part of real Grassmannians  $Gr^{\text{TNN}}(k, n)$ . In [3] we were able to construct real algebraic-geometric data for soliton data in the main cell  $Gr^{\text{TP}}(k, n)$  only. Here we do not just extend that construction to all points in  $Gr^{\text{TNN}}(k, n)$ , but we also considerably simplify it, since both the reducible rational  $M$ -curve  $\Gamma$  and the real regular KP divisor on  $\Gamma$  are directly related to the parametrization of positroid cells in  $Gr^{\text{TNN}}(k, n)$  via the Le-networks introduced in [61]. Finally, we apply our construction to soliton data in  $Gr^{\text{TP}}(2, 4)$  and we compare it with that in [3].

2010 MSC. 37K40; 37K20, 14H50, 14H70.

**KEYWORDS.** Total positivity, totally non-negative Grassmannians, KP hierarchy, real solitons,  $M$ -curves, Le-diagrams, planar bipartite networks in the disk, Baker-Akhiezer function.

## CONTENTS

1. Introduction	2
2. KP-II multi-line solitons	8
2.1. The heat hierarchy and the dressing transformation	8
2.2. Finite-gap KP solutions and their multi-line soliton limits	12
3. Algebraic-geometric approach for KP soliton data in $Gr^{\text{TNN}}(k, n)$ : the main construction	15
3.1. The reducible rational curve $\Gamma$	16
3.2. The planar representation of the desingularized curve.	22
3.3. The KP divisor on $\Gamma$	24

---

This research has been partially supported by GNFM-INDAM and RFO University of Bologna, by the Russian Foundation for Basic Research, grant 17-01-00366, by the program “Fundamental problems of nonlinear dynamics”, Presidium of RAS. Partially this research was fulfilled during the visit of the second author (P.G.) to IHES, Universit Paris-Saclay, France in November 2017.

4. A system of vectors on the Le-network	29
4.1. Representation of the rows of the RREF matrix using the Le-tableau	30
4.2. Recursive construction of the row vectors $E^{(r)}[l]$ using the Le-diagram	32
5. Proof of Theorem 3.1 on $\Gamma$	37
5.1. Vacuum and dressed edge wave functions on the modified Le-network	39
5.2. The vacuum and dressed network divisors	43
5.3. The vacuum wave function on $\Gamma$ and its pole divisor	47
6. Construction of the plane curve and the divisor to soliton data in $Gr^{\text{TP}}(2, 4)$ and comparison with the construction in [3]	52
6.1. A spectral curve for the reduced Le-network for soliton data in $Gr^{\text{TP}}(2, 4)$ and its desingularization	54
6.2. Construction of $\Gamma(\xi)$ as in [3] starting from $\Gamma(\mathcal{G}_{\text{red}})$	56
6.3. The KP divisors on $\Gamma(\mathcal{G}_{\text{red}})$ and on $\Gamma(\xi)$	59
Appendix A. The totally nonnegative Grassmannian	60
References	67

## 1. INTRODUCTION

The deep relation between real boundedness of multi-line KP soliton solutions, asymptotic web networks and total positivity has been unveiled in a series of papers (see [10, 11, 16, 17, 19, 42, 43, 44, 45, 70] and references therein). These results have inspired us in the search of new relations between total positivity in Grassmannians [50, 51, 61, 62, 63] and M-curves [37, 36, 58, 68], by connecting two relevant approaches used in KP theory to classify solutions, the Sato Grassmannian [64] and KP finite-gap theory [46, 47, 24]. Before continuing, we stress that, in our text, the notation KP **always means KP II**, with the heat conductivity operator in the Lax pair. In [3] we have established a new connection between classical total positivity [40, 60] and rational degenerations of M-curves in the case of KP soliton data belonging to the main cell,  $Gr^{\text{TP}}(k, n)$ . Here we continue our project and establish a canonical relation between points in  $g$  dimensional positroid cells of totally non-negative Grassmannians  $Gr^{\text{TN}}(k, n)$  [61] and real and regular degree  $g$  divisors on reducible rational M-curves which are rational degenerations of smooth genus  $g$  M-curves. We stress that, by construction, the genus  $g$  is minimal for generic soliton data.

Real regular multi-line KP solitons are obtained in well-defined finite-dimensional reductions of the Sato Grassmannian. In this setting, if one starts from the following soliton data: a set of ordered phases  $\mathcal{K} = \{\kappa_1 < \dots < \kappa_n\}$  and a point in the totally non-negative real Grassmannian  $[A] \in Gr^{\text{TNN}}(k, n)$ , then the corresponding KP multiline soliton solution is real regular for real times [52]. More recently, in [44], it has been proven that total non-negativity remains necessary for the real regularity of multi-line solutions of the KP equation itself, when only the first three real KP times  $x, y, t$  are considered.

In principle, soliton solutions can also be obtained by degenerating finite-gap solutions as was first observed in [59] in the case of the Korteweg-de Vries equation. Finite-gap KP solutions were constructed in [46, 47]. They are parametrized by degree  $g$  non-special divisors on a genus  $g$  Riemann surface with a marked point and fixed local parameter near this point, while soliton solutions are obtained in the limit when some gaps degenerate to double points. Let us remark that, using other degenerations analogous to those in [22], one can construct other interesting classes of KP solutions, including the rational ones. For additional information about singular spectral curves in soliton theory see [66]. Real regular finite-gap KP solutions correspond to algebraic data on genus  $g$  M-curves satisfying natural constraints [24]: by definition, the curve has  $g + 1$  real ovals, and one of them contains the marked point, while each other oval contains exactly one divisor point.

As it was pointed out by S.P. Novikov, in problems of **real regular** degenerate solutions it is natural to check whether they may be obtained by degenerating **real regular** quasi-periodic solutions. In [3] we have proven that this is indeed the case when the KP soliton data belong to the main cell  $Gr^{\text{TP}}(k, n)$  by using classical total positivity [40, 60]. Here, we extend our construction to all KP soliton data in  $Gr^{\text{TNN}}(k, n)$  by associating an universal reducible rational M-curve equipped with a real and regular divisor to any point of any given positroid stratum. We recall that the positroid stratification of  $Gr^{\text{TNN}}(k, n)$  [61] is naturally related to the Gelfand-Serganova stratification of the complex Grassmannian  $Gr(k, n)$  [32, 33]. We remark that the real positivity condition essentially simplifies the problem since the geometrical structure of the strata for complex Grassmannians can be as complicated as essentially any algebraic variety [53]. Let us point out that Gelfand-Serganova stratification corresponds to the action of all complex KP flows on the Grassmannians. The factor-space of the Grassmannians by the action of compact tori corresponding to pure imaginary times has interesting topology studied in [14, 15].

For the multiline KP soliton solutions considered in this paper, the Darboux dressing transformation provides a real  $k$  point divisor on a rational curve  $\Gamma_0$ , with has  $n$  marked points corresponding to the phases  $\mathcal{K}$  and a marked point corresponding to the essential singularity of the KP wave function [52]. However, these spectral data are, in general, insufficient to reconstruct soliton data varying in a  $|D|$  dimensional irreducible positroid cell of  $Gr^{\text{TNN}}(k, n)$  since  $\max\{k, n - k\} \leq |D| \leq k(n - k)$ . Therefore, following the approach of [48] for degenerate finite-gap solutions, we make the ansatz that these soliton solutions are rational degenerations of real regular finite-gap KP solutions and we look for a **reducible** curve realized from the rational degeneration of a M-curve of genus  $g \geq |D|$ . In the present paper we extend the construction in [3] to all positroid cells of  $Gr^{\text{TNN}}(k, n)$  using their parametrization by Le-networks in the disk introduced in [61]:

- (1) We associate a canonical reducible M-curve  $\Gamma$  to the Le-graph  $\mathcal{G}$  describing the corresponding cell, therefore proving that for any soliton data  $g$  may be chosen equal to the dimension  $|D|$  of the positroid cell. This curve  $\Gamma$  contains  $\Gamma_0$  as one of its irreducible components;
- (2) We provide a parametrization of each  $|D|$ -dimensional positroid cell by real regular degree  $|D|$  divisors  $\mathcal{D}_{\text{KP}, \Gamma}$ . The Sato divisor coincides with  $\mathcal{D}_{\text{KP}, \Gamma} \cap \Gamma_0$ .

In [4] we further generalize such construction by associating a canonical curve and a real regular KP divisor to any network in Postnikov equivalence class representing a given soliton data and we prove the invariance of the KP divisor with respect to changes of orientation of the network and of the position of the Darboux points. We treat the Le-network case separately here both because in this case the reducible curve is the rational degeneration of a smooth M-curve of **minimal genus** equal to the dimension of the positroid cell and also to evidence the relations with the construction in [3].

Before outlining our construction, we would like to point out that there are other well-known relations of different nature between networks, algebraic curves and integrable systems in literature. In dimer models with periodic boundary conditions (models on tori) the Riemann surfaces arise as the spectral curves for operators on networks on tori [41], and such spectral curves, which are generically regular, may be associated to classical or quantum integrable systems [34]. Another big area of activity is currently associated with the use of planar networks in the disk for the computation of scattering amplitudes in  $N = 4$  super Yang-Mills on-shell diagrams, see [7, 8, 9] and references therein. We have noticed an analogy between the momentum-helicity

conservation relations in the trivalent planar networks in the approach of [7, 8] and the relations satisfied by the vacuum and dressed edge wave functions in our approach. It is unclear to us whether our approach for KP may be interpreted as a scalar analog of a field theoretic model.

Total positivity itself, since its appearance in [65], naturally arises in many applications in connection with some reality properties of the system. Important connections between positivity and oscillatory properties of mechanical systems were found in [29, 30]. The extensions of positivity property to integral kernels were investigated in [40]. Extension of total positivity to split reductive connected algebraic groups and flag manifolds was developed in [50, 51]. Total positivity in classical and generalized sense is also one of the basic concepts in the theory of cluster manifolds and cluster algebras [26, 27], see also the book [31]. Applications of the theory of total positivity in Lie groups to the study of homomorphisms of the fundamental group of a closed surface into a Lie group is considered in [25]. Non-negativity of systems of modified Bessel functions of the first kind arising in the solutions to a model of overdamped Josephson junction was studied in [12, 13]. Of course, this list of literature is far from being complete.

Finally a direction which we plan to investigate is the asymptotic behavior of KP zero divisors on  $\Gamma$  in relation to that of the multiline soliton solutions in the  $(x, y)$ -plane for large time  $t$ . Indeed, the latter is known to give rise to webs interpreted in terms of real tropical geometry and cluster algebras [45]. For an introduction to real tropical geometry and its applications see [56] and references therein.

**Outline of the main construction.** The main results in this paper are: we associate a canonical rational degeneration of a M-curve of minimal genus to any positroid cell in  $Gr^{\text{TNN}}(k, n)$ , and we parametrize these cells via real regular divisors of KP multiline solitons on these curves. In our construction an essential tool is the parametrization of all positroid cells in  $Gr^{\text{TNN}}(k, n)$  by the Le-networks introduced in [61], which, in particular, guarantees the minimality of the genus.

Given  $n$  real phases  $\mathcal{K}$  and the planar trivalent bipartite Le-graph in the disk  $\mathcal{G}$  representing the chosen  $g$ -dimensional positroid cell  $\mathcal{S}_{\mathcal{M}}^{\text{TNN}} \subset Gr^{\text{TNN}}(k, n)$ , we associate a unique reducible rational curve  $\Gamma = \Gamma(\mathcal{G})$  to such data using the following natural correspondence:

- (1) The boundary of the disk corresponds to the rational component  $\Gamma_0$  containing the essential singularity of the KP wave function and the Sato divisor, while the  $n$  boundary vertexes correspond to the  $n$  marked phases on  $\Gamma_0$ ;
- (2) Each bivalent or trivalent internal vertex corresponds to a rational component of  $\Gamma$ . The black and white colors are related to the different analytic properties of the KP wave

function on the corresponding rational components. The divisor points are associated to white trivalent vertexes through linear relations;

- (3) Each edge corresponds to a double point of  $\Gamma$  where different components are glued. Thanks to the trivalency assumption, each  $\mathbb{CP}^1$  component carries three marked points and we avoid the introduction of parameters marking double points;
- (4) Faces of the graph correspond to ovals of  $\Gamma$ ;
- (5) The canonical acyclic orientation of the Le-graph in [61] is associated to a well-defined choice of coordinates on the rational components of  $\Gamma$ .

We remark that the above correspondence is a minor modification of a special case in the representation of reducible curves by dual graphs (see, for example, [6], Section X). Non rational components are allowed in degenerate finite-gap theory on reducible curves as well; however, the rational ansatz for  $\Gamma \setminus \Gamma_0$  considerably simplifies the overall construction.

By our construction,  $\Gamma$  is a real curve with  $g+1$  ovals and is the rational degeneration of an M-curve of genus  $g$ . If the soliton data belong to the top cell  $Gr^{\text{TP}}(k, n)$ , then  $g = k(n-k)$  and the curve  $\Gamma(\xi)$  constructed in [3] corresponds to a particular desingularization of  $\Gamma(\mathcal{G})$  which reduces the number of rational components to  $k+1$ . We thoroughly discuss such desingularization in the simplest non-trivial case of soliton data in  $Gr^{\text{TP}}(2, 4)$ .

Then, we fix a point  $[A] \in \mathcal{S}_{\mathcal{M}}^{\text{TN}}^{\text{NN}}$  and construct its KP wave function on  $\Gamma$  using the Le-network  $\mathcal{N}$  representing  $[A]$ . On  $\mathcal{N}$  we first define a system of **edge** vectors satisfying linear relations at the vertexes. Each component of a given edge vector is computed by summing the weights of all paths starting at the given edge and ending at the same boundary sink vertex. We remark that, for soliton data in  $Gr^{\text{TP}}(k, n)$ , the recursive construction of such system of vectors generalizes the algebraic construction in [3]. We then use this system of vectors to construct both a vacuum edge wave function  $\Phi(\vec{t})$  and its dressing  $\Psi(\vec{t})$  on the Le-network. At this step, we modify the original network adding an univalent internal vertex next to each boundary source vertex using Postnikov move (M2) in order that the vacuum edge wave function satisfies Sato boundary conditions on  $\Gamma_0$  and an edge vector corresponds to each Darboux point in  $\Gamma$ . Then, using the linear relations at the vertexes, we associate a vacuum network divisor number to each trivalent white vertex of the modified network  $\mathcal{N}'$ . We also associate a dressed network divisor number to any trivalent white vertex of  $\mathcal{N}'$  not containing a Darboux edge.

Both  $\mathcal{N}$  and  $\mathcal{N}'$  have  $g+1$  faces, the number of trivalent white vertexes is  $g-k$  in the Le-network  $\mathcal{N}$ , and  $g$  in the modified network  $\mathcal{N}'$ . Therefore the vacuum network divisor has

degree  $g$  while the dressed network divisor has degree  $g - k$ . We then construct a unique vacuum divisor  $\mathcal{D}_{\text{vac},\Gamma}$  and a unique dressed divisor  $\mathcal{D}_{\text{KP},\Gamma}$  on  $\Gamma \setminus \{P_0\}$  for any soliton data  $(\mathcal{K}, [A])$  with the desired properties:

- (1) The vacuum (resp. dressed) network divisor number associated to a trivalent white vertex provides the coordinate of the vacuum (resp. dressed) divisor point on the corresponding component of  $\Gamma \setminus \Gamma_0$ ;
- (2) The vacuum divisor  $\mathcal{D}_{\text{vac},\Gamma}$  on  $\Gamma$  is the collection of these points;
- (3) The dressed divisor  $\mathcal{D}_{\text{KP},\Gamma}$  is the set of points in  $\Gamma$  which correspond to the union of the degree  $k$  Sato divisor on  $\Gamma_0$  and of the degree  $n - k$  dressed divisor on  $\Gamma \setminus \Gamma_0$ ;
- (4) Both divisors are effective, of degree  $g$  and contained in the union of all ovals;
- (5)  $\mathcal{D}_{\text{KP},\Gamma}$  satisfies the required reality and regularity property: each finite oval possesses exactly one dressed divisor point and no dressed divisor point belongs to the infinite oval.

The above properties are proven using the correspondence between edges in the graph and marked points on rational components of  $\Gamma$ : we build a unique vacuum normalized wave function  $\hat{\phi}(P, \vec{t})$  and a unique dressed normalized wave function  $\hat{\psi}(P, \vec{t})$  on  $\Gamma \setminus \{P_0\}$  for the given soliton data, by imposing that at all marked points they respectively coincide with the normalized vacuum and dressed edge wave functions. Property (5) then follows from the reality and regularity characterization of  $\mathcal{D}_{\text{vac},\Gamma}$  in Theorem 5.1 and the fact that Darboux dressing acts on divisors as a shift. Finally  $\hat{\psi}(P, \vec{t})$  is the desired KP wave function and has the following properties:

- (1) It coincides with the normalized Sato dressed wave function on  $\Gamma_0$  for all  $\vec{t}$ ;
- (2) Its values coincide at each double point of  $\Gamma$  for all times  $\vec{t}$ ;
- (3)  $\hat{\psi}$  is independent of the spectral parameter for all  $\vec{t}$  on each rational component corresponding to a bivalent vertex or a trivalent black vertex;
- (4)  $\hat{\psi}$  is meromorphic of degree at most one in the spectral parameter for all  $\vec{t}$  on each rational component corresponding to a trivalent white vertex;
- (5)  $\mathcal{D}_{\text{KP},\Gamma}$  is its divisor:  $(\hat{\psi}(P, \vec{t})) + \mathcal{D}_{\text{KP},\Gamma} \geq 0$ , for all  $\vec{t}$ .

In [4] we prove that the KP divisor  $\mathcal{D}_{\text{KP},\Gamma}$  depends only on the soliton data  $(\mathcal{K}, [A])$  and on the network chosen to construct  $\Gamma$ , while, the vacuum divisor  $\mathcal{D}_{\text{vac},\Gamma}$  depends also on the base  $I$  in the matroid of  $[A]$  and on the positions of the Darboux points.

**Plan of the paper:** We did our best to make the paper self-contained. In Section 2 and in Appendix A, we briefly present a review of the necessary results respectively for KP soliton theory and totally non-negative Grassmannians. Section 3 contains the main construction and the statements of the principal theorems. The construction of the system of vectors on the L-network  $\mathcal{N}$  and the proof of the main Theorem on the characterization of the vacuum divisor are carried out respectively in Sections 4 and 5. In section 6 we apply our construction to soliton data in  $Gr^{\text{TP}}(2, 4)$  and compare it with [3].

**Notations:** We use the following notations throughout the paper:

- (1)  $k$  and  $n$  are positive integers such that  $k < n$ ;
- (2) for  $s \in \mathbb{N}$  let  $[s] = \{1, 2, \dots, s\}$ ; if  $s, j \in \mathbb{N}$ ,  $s < j$ , then  $[s, j] = \{s, s+1, s+2, \dots, j-1, j\}$ ;
- (3)  $\vec{t} = (t_1, t_2, t_3, \dots)$ , where  $t_1 = x$ ,  $t_2 = y$ ,  $t_3 = t$ ;
- (4)  $\theta(\zeta, \vec{t}) = \sum_{s=1}^{\infty} \zeta^s t_s$ ,
- (5) we denote the real phases  $\kappa_1 < \kappa_2 < \dots < \kappa_n$  and  $\theta_j \equiv \theta(\kappa_j, \vec{t})$ .

## 2. KP-II MULTI-LINE SOLITONS

In this section, we review the characterization of real bounded regular multiline KP soliton solutions via Darboux transformations, Sato's dressing transformations and finite gap-theory. The KP-II equation [39]

$$(2.1) \quad (-4u_t + 6uu_x + u_{xxx})_x + 3u_{yy} = 0,$$

is the first non-trivial flow of an integrable hierarchy [18, 23, 38, 57, 64]. In the following we denote  $\vec{t} = (t_1 = x, t_2 = y, t_3 = t, t_4, \dots)$ . The family of solutions we consider belong to the class of real regular exact KP solutions used, in particular, to model the shallow water waves in the approximation where the surface tension is negligible.

**2.1. The heat hierarchy and the dressing transformation.** Multiline KP solitons may be realized starting from the soliton data  $(\mathcal{K}, [A])$ , where  $\mathcal{K}$  is a set of real ordered phases  $\kappa_1 < \dots < \kappa_n$ ,  $A = (A_j^i)$  is a  $k \times n$  real matrix of rank  $k$  and  $[A]$  denotes the point in the finite dimensional real Grassmannian  $Gr(k, n)$  corresponding to  $A$ . Following [55], see also [28], multiline KP soliton solutions to the KP equation are defined as

$$(2.2) \quad u(\vec{t}) = 2\partial_x^2 \log(\tau(\vec{t})),$$



where

$$(2.3) \quad \tau(\vec{t}) = Wr(f^{(1)}, \dots, f^{(k)}) \equiv \det \begin{vmatrix} f^{(1)} & \dots & f^{(k)} \\ \partial_x f^{(1)} & \dots & \partial_x f^{(k)} \\ \vdots & \ddots & \vdots \\ \partial_x^{n-1} f^{(1)} & \dots & \partial_x^{n-1} f^{(k)} \end{vmatrix} = \sum_I \Delta_I(A) \prod_{\substack{i_1 < i_2 \\ i_1, i_2 \in I}} (\kappa_{i_2} - \kappa_{i_1}) e^{i \sum \theta_i}$$

is the Wronskian of  $k$  linear independent solutions to the heat hierarchy  $\partial_{t_l} f = \partial_x^l f$ ,  $l = 2, 3, \dots$ , of the form  $f^{(i)}(\vec{t}) = \sum_{j=1}^n A_j^i e^{\theta_j}$ ,  $i \in [k]$ . In (2.3), the sum is over all  $k$ -element ordered subsets  $I$  in  $[n]$ , *i.e.*  $I = \{1 \leq i_1 < i_2 < \dots < i_k \leq n\}$  and  $\Delta_I(A)$  are the maximal minors of the matrix  $A$ . Since we obtain the same KP solution by linearly recombining the heat hierarchy solutions,  $u(\vec{t})$  is associated to the equivalence class  $[A]$  of  $A$ , which is a point in the Grassmannian  $Gr(k, n)$ .

$u(x, y, t, \vec{0})$  is regular and bounded for all real  $x, y, t$  if and only if  $\Delta_I(A) \geq 0$ , for all  $I$  [45]. In such case, let  $Mat_{k,n}^{\text{TNN}}$  and  $GL_k^+$ , respectively denote the set of real  $k \times n$  matrices of maximal rank  $k$  with non-negative maximal minors  $\Delta_I(A)$ , and the group of  $k \times k$  matrices with positive determinants. Since left multiplication by elements in  $GL_k^+$  preserves  $u(\vec{t})$  in (2.2), we conclude that the soliton data  $[A]$  is a point in the totally non-negative Grassmannian [61]  $Gr^{\text{TNN}}(k, n) = GL_k^+ \backslash Mat_{k,n}^{\text{TNN}}$ .

Any given soliton solution is associated to an infinite set of soliton data  $(\mathcal{K}, [A])$ , but there exists a unique minimal pair  $(k, n)$ , such that the soliton solution can be realized with  $n$  phases  $\kappa_1 < \dots < \kappa_n$  and  $[A] \in Gr^{\text{TNN}}(k, n)$ , but not with  $n-1$  phases and  $[A'] \in Gr^{\text{TNN}}(k', n')$ , where  $(k', n')$  is either  $(k, n-1)$  or  $(k-1, n-1)$ .

**Definition 2.1. Regular and irreducible soliton data** [16]. *We call  $(\mathcal{K}, [A])$  regular soliton data if  $\mathcal{K} = \{\kappa_1 < \dots < \kappa_n\}$  and  $[A] \in Gr^{\text{TNN}}(k, n)$ . We call the regular soliton data  $(\mathcal{K}, [A])$  irreducible if  $[A]$  is a point in the irreducible part of the real Grassmannian, *i.e.* if the reduced row echelon matrix  $A$  has the following properties:*

- (1) *Each column of  $A$  contains at least a non-zero element;*
- (2) *Each row of  $A$  contains at least one nonzero element in addition to the pivot.*

*If either (1) or (2) doesn't occur, we call the soliton data  $(\mathcal{K}, [A])$  reducible.*

**Remark 2.1. Reducible soliton data** [16]. *If (1) in Definition 2.1 is violated for column  $l$ , then the phase  $\kappa_l$  does not appear in the solution (2.2). Then, one may remove such phase from  $\mathcal{K}$ , remove the zero column from  $A$  (see also Remark A.2) and realize the soliton in  $Gr^{\text{TNN}}(k, n-1)$ .*

If (2) in Definition 2.1 is violated for the row  $l$  corresponding to the pivot index  $i_l$ , then the heat hierarchy solution  $f^{(l)}(\vec{t})$  contains only the phase  $\kappa_{i_l}$ , and such phase is missing in all other heat hierarchy solutions associated to RREF matrix.  $f^{(l)}(\vec{t})$  is factored out in (2.3), and again,  $\kappa_{i_l}$  is missing in (2.2). So one may eliminate such phase from  $\mathcal{K}$ , remove the corresponding row and pivot column from  $A$ , change all signs in the new matrix to the right of the removed column and above the removed row and realize the soliton in  $Gr^{TNN}(k-1, n-1)$  (see also Remark A.2).

For generic choices of the phases  $\mathcal{K}$ , the combinatorial classification of the irreducible part  $Gr^{TNN}(k, n)$  rules the classification of the asymptotic properties of multi-soliton solutions both in the  $(x, y)$  plane at fixed time  $t$  and in the tropical limit ( $t \rightarrow \pm\infty$ ) (see [10, 11, 16, 17, 19, 42, 43, 44, 45, 70] and references therein).

The following spectral data are associated to each soliton data  $(\mathcal{K}, [A])$ ,  $[A] \in Gr^{TNN}(k, n)$ : an irreducible rational curve, which we denote  $\Gamma_0$ , a marked point  $P_0 \in \Gamma_0$ , a degree  $k$  real divisor, which we call Sato divisor, and a KP wavefunction meromorphic on  $\Gamma_0 \setminus \{P_0\}$ , which we call the Sato KP wave function. The unnormalized Sato wave function can be obtained from the dressing (inverse gauge) transformation [64] of the vacuum (zero-potential) eigenfunction  $\phi^{(0)}(\zeta, \vec{t}) = \exp(\theta(\zeta, \vec{t}))$ , which solves

$$(2.4) \quad \partial_x \phi^{(0)}(\zeta, \vec{t}) = \zeta \phi^{(0)}(\zeta, \vec{t}), \quad \partial_{t_l} \phi^{(0)}(\zeta, \vec{t}) = \zeta^l \phi^{(0)}(\zeta, \vec{t}), \quad l \geq 2.$$

The operator  $W = 1 - \mathfrak{w}_1(\vec{t})\partial_x^{-1} - \dots - \mathfrak{w}_k(\vec{t})\partial_x^{-k}$ , where  $\mathfrak{w}_1(\vec{t}), \dots, \mathfrak{w}_k(\vec{t})$  are the solutions to the following linear system of equations  $\partial_x^k f^{(i)} = \mathfrak{w}_1 \partial_x^{k-1} f^{(i)} + \dots + \mathfrak{w}_k f^{(i)}, i \in [k]$ , is the dressing (*i.e.* gauge) operator for the soliton data  $(\mathcal{K}, [A])$ . Indeed  $W$  satisfies Sato equations  $\partial_{t_l} W = B_l W - W \partial_x^l$ ,  $l \geq 1$ , with  $B_l = (W \partial_x^l W^{-1})_+$  (the symbol  $(H)_+$  denotes the differential part of the operator  $H$ ). Therefore  $L = W \partial_x W^{-1} = \partial_x + \frac{u(\vec{t})}{2} \partial_x^{-1} + \dots$ ,  $u(\vec{t}) = 2\partial_x \mathfrak{w}_1(\vec{t})$  and  $\psi^{(0)}(\zeta; \vec{t}) = W \phi^{(0)}(\zeta; \vec{t})$  are, respectively, the KP-Lax operator, the KP-potential (KP solution) and the KP-eigenfunction, *i.e.*  $L\psi^{(0)}(\zeta; \vec{t}) = \zeta \psi^{(0)}(\zeta; \vec{t})$ ,  $\partial_{t_l} \psi^{(0)}(\zeta; \vec{t}) = B_l \psi^{(0)}(\zeta; \vec{t})$ , for all  $l \geq 2$ .

The Darboux dressing operator  $\mathfrak{D}$  is defined as

$$(2.5) \quad \mathfrak{D} \equiv W \partial_x^k = \partial_x^k - \mathfrak{w}_1(\vec{t}) \partial_x^{k-1} - \dots - \mathfrak{w}_k(\vec{t})$$

and the KP-eigenfunction may be also represented by

$$(2.6) \quad \mathfrak{D} \phi^{(0)}(\zeta; \vec{t}) = W \partial_x^k \phi^{(0)}(\zeta; \vec{t}) = \left( \zeta^k - \mathfrak{w}_1(\vec{t}) \zeta^{k-1} - \dots - \mathfrak{w}_k(\vec{t}) \right) \phi^{(0)}(\zeta; \vec{t}) = \zeta^k \psi^{(0)}(\zeta; \vec{t}).$$

**Definition 2.2. Sato divisor** *Let the regular soliton data be  $(\mathcal{K}, [A])$ ,  $\mathcal{K} = \{\kappa_1 < \dots < \kappa_n\}$ ,  $[A] \in Gr^{TNN}(k, n)$ . We call Sato divisor at time  $\vec{t}_0$ ,  $\mathcal{D}_{S, \Gamma_0}(\vec{t}_0)$ , the set of the roots of the characteristic equation associated to the Dressing transformation*

$$(2.7) \quad \mathcal{D}_{S, \Gamma_0}(\vec{t}_0) = \{\gamma_j^{(S)}(\vec{t}_0), j \in [k] : (\gamma_j^{(S)}(\vec{t}_0))^k - \mathfrak{w}_1(\vec{t})(\gamma_j^{(S)}(\vec{t}_0))^{k-1} - \dots - \mathfrak{w}_k(\vec{t}_0) = 0\}.$$

In [52] it is proven the following proposition

**Proposition 2.1. The Sato divisor** [52]. *Let the regular soliton data be  $(\mathcal{K}, [A])$ ,  $\mathcal{K} = \{\kappa_1 < \dots < \kappa_n\}$ ,  $[A] \in Gr^{TNN}(k, n)$ . Then for all real  $\vec{t}_0$  the Sato divisor  $\mathcal{D}_{S, \Gamma_0}(\vec{t}_0)$  is real and satisfies  $\gamma_j^{(S)}(\vec{t}) \in [\kappa_1, \kappa_n]$ ,  $j \in [k]$ . Moreover for almost all  $\vec{t}_0$  the Sato divisor points are distinct.*

**Remark 2.2. Sato divisor for reducible regular soliton data** *In the case of reducible regular soliton data  $(\mathcal{K}, [A])$ ,  $\mathcal{K} = \{\kappa_1 < \dots < \kappa_n\}$ ,  $[A] \in Gr^{TNN}(k, n)$  (see Remark 2.1), we use the reduced Sato divisor  $\mathcal{D}'_{S, \Gamma_0}(\vec{t}_0)$  of the corresponding maximally reduced positroid cell  $Gr^{TNN}(k', n')$ .*

*More precisely, if the representative RREF matrix  $A$  in  $Gr^{TNN}(k, n)$ , contains a zero column in position  $l$ , then  $k' = k$  and  $\mathcal{D}_{S, \Gamma_0}(\vec{t}_0) = \mathcal{D}'_{S, \Gamma_0}(\vec{t}_0)$  for any  $\vec{t}_0$ , since the reducible and the reduced Darboux transformations coincide  $\mathfrak{D}^{(k)} = \mathfrak{D}^{(k')}$ .*

*Instead, if for some  $r \in [k]$  and  $i_r \in [r, n]$ , the  $r$ -th row of the RREF matrix  $A$  contains only the pivot element:  $A_j^r = \delta_{j, i_r}$ , then, for all  $\vec{t}_0$ ,  $\kappa_{i_r} \in \mathcal{D}_{S, \Gamma_0}(\vec{t}_0)$ ,  $k' = k - 1$  and  $\mathcal{D}'_{S, \Gamma_0}(\vec{t}_0) = \mathcal{D}_{S, \Gamma_0}(\vec{t}_0) \setminus \{\kappa_{i_r}\}$ . Indeed, the characteristic polynomial associated to the Darboux differential operator  $\mathfrak{D}$  satisfies  $\zeta^k - \zeta^{k-1}\mathfrak{w}_1(\vec{t}) - \dots - \mathfrak{w}_k(\vec{t}) = (\zeta - \kappa_{i_r})(\zeta^{k-1} - \mathfrak{w}'_1(\vec{t})\zeta^{k-2} - \dots - \mathfrak{w}'_{k-1}(\vec{t}))$ . Then  $\mathfrak{D}' = W' \partial_x^{k-1} = \partial_x^{k-1} - \mathfrak{w}'_1(\vec{t})\partial_x^{k-2} - \dots - \mathfrak{w}'_{k-1}(\vec{t})$  is the Darboux transformation associated to the reduced soliton data  $(\mathcal{K}', [A'])$ , with  $\mathcal{K}' = \mathcal{K} \setminus \{\kappa_{i_r}\}$ ,  $[A'] \in Gr^{TNN}(k-1, n-1)$  and  $A'$  related to  $A$  as in Remark 2.1.*

**Definition 2.3. Sato algebraic-geometric data** *Let  $(\mathcal{K}, [A])$  be given regular soliton data with  $[A]$  belonging to a  $|D|$  dimensional positroid cell in  $Gr^{TNN}(k, n)$ . Let  $\vec{t}_0$  such that the Sato divisor consists of  $k$  simple poles. Let  $\Gamma_0$  be a copy of  $\mathbb{CP}^1$  with marked points  $P_0$ , local coordinate  $\zeta$  such that  $\zeta^{-1}(P_0) = 0$  and  $\zeta(\kappa_1) < \zeta(\kappa_2) < \dots < \zeta(\kappa_n)$ .*

*Then to the data  $(\mathcal{K}, [A], \Gamma_0 \setminus \{P_0\}, \vec{t}_0)$  we associate the Sato divisor  $\mathcal{D}_{S, \Gamma_0} = \mathcal{D}_{S, \Gamma_0}(\vec{t}_0)$  as in Definition (2.2) and the normalized Sato wave function*

$$(2.8) \quad \hat{\psi}(P, \vec{t}) = \frac{\mathfrak{D}\phi^{(0)}(P; \vec{t})}{\mathfrak{D}\phi^{(0)}(P; \vec{t}_0)} = \frac{\psi^{(0)}(P; \vec{t})}{\psi^{(0)}(P; \vec{t}_0)}, \quad \forall P \in \Gamma_0 \setminus \{P_0\},$$

with  $\mathfrak{D}\phi^{(0)}(\zeta; \vec{t})$  as in (2.6).

By definition  $(\hat{\psi}_0(P, \vec{t})) + \mathcal{D}_{S, \Gamma_0}(\vec{t}_0) \geq 0$ , for all  $\vec{t}$ .

**Remark 2.3. Ill posedness of the inverse spectral problem for the Sato divisor** Let  $1 \leq k < n$  and let  $\vec{t}_0$  be fixed. Given the phases  $\kappa_1 < \dots < \kappa_n$  and the spectral data  $(\Gamma_0 \setminus \{P_0\}, \mathcal{D}_{S, \Gamma_0})$ , where  $\mathcal{D}_{S, \Gamma_0} = \mathcal{D}_{S, \Gamma_0}(\vec{t}_0)$  is a  $k$  point divisor satisfying Proposition 2.1, it is, in general, impossible to identify uniquely the point  $[A] \in Gr^{TNN}(k, n)$  corresponding to such spectral data. Indeed, if none of the Sato divisor points coincides with a phase, then the soliton data belong to an irreducible positroid cell of dimension  $|D|$  such that  $\max\{k, n-k\} \leq |D| \leq k(n-k)$ . Otherwise, one preliminarily eliminates all coinciding phases and divisor points and gets an analogous inequality for the reduced Sato divisor.

**2.2. Finite-gap KP solutions and their multi-line soliton limits.** Soliton KP solutions can be obtained from the finite-gap ones by proper degenerations of the spectral curve [47, 23].

The spectral data for periodic and quasiperiodic solutions of the KP equation (2.1) in the finite-gap approach [46, 47] are: a finite genus  $g$  compact Riemann surface  $\Gamma$  with a marked point  $P_0$ , a local parameter  $1/\zeta$  near  $P_0$  and a non-special divisor  $\mathcal{D} = \gamma_1 + \dots + \gamma_g$  of degree  $g$  in  $\Gamma$ . The Baker-Akhiezer function  $\hat{\psi}(P, \vec{t})$ ,  $P \in \Gamma$ , is defined by the following analytic properties:

- (1) For any fixed  $\vec{t}$  the function  $\hat{\psi}(P, \vec{t})$  is meromorphic in  $P$  on  $\Gamma \setminus P_0$ .
- (2) On  $\Gamma \setminus P_0$  the function  $\hat{\psi}(P, \vec{t})$  is regular outside the divisor points  $\gamma_j$  and has at most first order poles at the divisor points. Equivalently, if we consider the line bundle  $\mathcal{L}(\mathcal{D})$  associated to  $\mathcal{D}$ , then for each fixed  $\vec{t}$  the function  $\hat{\psi}(P, \vec{t})$  is a holomorphic section of  $\mathcal{L}(\mathcal{D})$  outside  $P_0$ .
- (3)  $\hat{\psi}(P, \vec{t})$  has an essential singularity at the point  $P_0$  with the following asymptotic:

$$\hat{\psi}(\zeta, \vec{t}) = e^{\zeta x + \zeta^2 y + \zeta^3 t + \dots} \left( 1 - \chi_1(\vec{t})\zeta^{-1} - \dots - \chi_k(\vec{t})\zeta^{-k} - \dots \right).$$

For generic data these properties define an unique function, which is a common eigenfunction to all KP hierarchy auxiliary linear operators  $-\partial_{t_j} + B_j$ , where  $B_j = (L^j)_+$ , and the Lax operator is  $L = \partial_x + \frac{u(\vec{t})}{2}\partial_x^{-1} + u_2(\vec{t})\partial_x^{-2} + \dots$ . All these operators commute and the potential  $u(\vec{t})$  satisfies the KP hierarchy. In particular, the KP equation arises in the Dryuma-Zakharov-Shabat commutation representation [20], [69] as the compatibility for the second and the third operator:  $[-\partial_y + B_2, -\partial_t + B_3] = 0$ , with  $B_2 \equiv (L^2)_+ = \partial_x^2 + u$ ,  $B_3 = (L^3)_+ = \partial_x^3 + \frac{3}{4}(u\partial_x + \partial_x u) + \tilde{u}$  and  $\partial_x \tilde{u} = \frac{3}{4}\partial_y u$ .

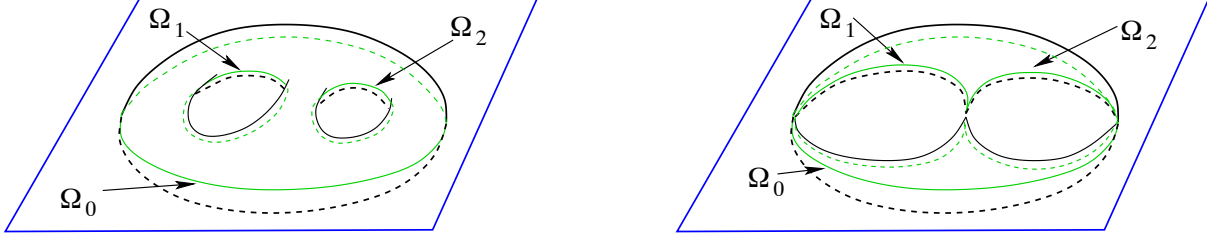


FIGURE 1. *Left: a genus 2 regular M-curve with 3 real ovals invariant w.r.t. the involution  $\sigma$  (orthogonal reflection with respect to the horizontal plane). Right: its degeneration is a reducible M-curve still possessing 3 real ovals.*

The Its-Matveev formula represents the KP hierarchy solution  $u(\vec{t})$  in terms of the Riemann theta-functions associated with  $\Gamma$  (see, for example, [21]). After fixing a canonical basis of cycles  $a_1, \dots, a_g, b_1, \dots, b_g$  and a basis of normalized holomorphic differentials  $\omega_1, \dots, \omega_g$  on  $\Gamma$  such that  $\oint_{a_j} \omega_l = 2\pi i \delta_{jl}$ ,  $\oint_{b_j} \omega_l = B_{lj}$ ,  $j, l \in [g]$ , the KP solution takes the form  $u(\vec{t}) = 2\partial_x^2 \log \theta(\sum_j t_j U^{(j)} + z_0) + c_1$ , where  $\theta$  is the Riemann theta function and  $U^{(j)}$  are the vectors of the  $b$ -periods of the following normalized meromorphic differentials, holomorphic on  $\Gamma \setminus \{P_0\}$  and with principal parts  $\hat{\omega}^{(j)} = d(\zeta^j) + O(1)$ , at  $P_0$  (see [46, 24]).

The real regular solutions are the most relevant in physical applications. In [24] the necessary and sufficient conditions on spectral data to generate real regular KP hierarchy solutions for all real  $\vec{t}$  were established, under the assumption that  $\Gamma$  is smooth and has genus  $g$ :

- (1)  $\Gamma$  possesses an antiholomorphic involution  $\sigma : \Gamma \rightarrow \Gamma$ ,  $\sigma^2 = \text{id}$ , which has the maximal possible number of fixed components (real ovals). This number is equal to  $g + 1$ , therefore  $(\Gamma, \sigma)$  is an M-curve.
- (2)  $P_0$  lies in one of the ovals, and each other oval contains exactly one divisor points. The oval containing  $P_0$  is called “infinite” and all other ovals are called “finite”.

The set of real ovals divides  $\Gamma$  into two connected components. Each of these components is homeomorphic to a sphere with  $g + 1$  holes. In Figure 1(left) we show an example for  $g = 2$ .

The sufficient condition of the Theorem in [24] still holds true if the spectral curve  $\Gamma$  degenerates in such a way that the divisor remains in the finite ovals at a finite distance from the essential singularity [24]. Of course, this condition is not necessary for degenerate curves, but

the properties of the Sato divisor established in [52] are compatible with such an ansatz. Moreover, in [48], it has been proven that the algebraic–geometric approach goes through also for degenerate finite-gap solutions on **reducible** curves. The inverse spectral problem is ill-posed also in this case, since there is not a unique reducible curve associated to the given soliton data. Finally there is also no a priori reason why, given one such reducible curve, the divisor on it should satisfy any reality condition.

In [3], we have proven that the multiline soliton solutions corresponding to points in  $Gr^{TP}(k, n)$  may indeed be obtained as limits of real regular finite-gap solutions on smooth M-curves: to any soliton datum in  $Gr^{TP}(k, n)$  and any  $\xi \gg 1$ , we have associated a curve  $\Gamma_\xi$ , which is the rational degeneration of a smooth M-curve of minimal genus  $k(n - k)$  and a degree  $k(n - k)$  divisor satisfying the reality conditions of Dubrovin and Natanzon’s theorem. In Figure 1(right) we show the rational degeneration of the genus  $g = 2$  curve associated to soliton data in  $Gr^{TP}(1, 3)$  and  $Gr^{TP}(2, 3)$  in [1, 3].

The main objective of this paper is therefore twofold: **provide a canonical construction of a reducible rational M-curve of minimal genus  $g = |D|$  for any fixed positroid cell in  $Gr^{TNN}(k, n)$  and show that real and regular divisors on such curve provide a parametrization of the cell.** We therefore give the following definition:

**Definition 2.4.** *Real regular algebraic-geometrical data associated with a given soliton solution.* Assume that we have fixed soliton data  $(\mathcal{K}, [A])$ , where  $\mathcal{K}$  is a collection of real phases  $\kappa_1 < \kappa_2 < \dots < \kappa_n$ ,  $[A] \in Gr^{TNN}(k, n)$ . Let  $|D|$  be the dimension of the positroid cell to which  $[A]$  belongs.

Assume that we have a reducible connected curve  $\Gamma$  with a marked point  $P_0$ , a local parameter  $1/\zeta$  near  $P_0$ . In addition, assume that the curve  $\Gamma$  may be obtained from a rational degeneration of a smooth M-curve of genus  $g$ , with  $g \geq |D|$ , and that the antiholomorphic involution preserves the maximum number of the ovals in the limit, so that  $\Gamma$  possesses  $g + 1$  real ovals.

Assume that  $\mathcal{D}$  is a degree  $g$  non-special divisor on  $\Gamma \setminus P_0$ , and that  $\hat{\psi}$  is the normalized Baker-Akhiezer function associated to such data, i.e. for any  $\vec{t}$  its pole divisor is contained in  $\mathcal{D}$ :  $(\hat{\psi}(P, \vec{t})) + \mathcal{D} \geq 0$  on  $\Gamma \setminus P_0$ , where  $(f)$  denotes the divisor of  $f$ .

We say that **the algebraic-geometrical data  $\Gamma, \mathcal{D}$  are associated to the soliton data  $(\mathcal{K}, [A])$** , if the irreducible component  $\Gamma_0$  of  $\Gamma$  containing  $P_0$  is  $\mathbb{CP}^1$ , and the restriction of  $\hat{\psi}$  to  $\Gamma_0$  coincides with Sato normalized dressed wave function for the soliton data  $(\mathcal{K}, [A])$ . In particular, for such data the restriction of  $\mathcal{D}$  to  $\Gamma_0$  coincides with the Sato divisor.

We say that the **divisor**  $\mathcal{D}$  *satisfies the reality and regularity conditions* if  $P_0$  belongs to one of the fixed ovals and the boundary of each other finite oval contains exactly one divisor point.

We remark that the simplicity and reality of the Sato divisor points proven in [52] is compatible with the reality and regularity of the algebraic-geometrical data associated with a given soliton solution in the Definition above, provided that the reducible curve  $\Gamma$  possesses  $k$  distinct ovals containing the Sato divisor points.

### 3. ALGEBRAIC-GEOMETRIC APPROACH FOR KP SOLITON DATA IN $Gr^{\text{TNN}}(k, n)$ : THE MAIN CONSTRUCTION

Since  $Gr^{\text{TNN}}(k, n)$  is topologically the closure of  $Gr^{\text{TP}}(k, n)$ , one can try to extend **indirectly** the construction of [3] to soliton data in  $Gr^{\text{TNN}}(k, n)$  considering the latter as the limit of a sequence of soliton data in  $Gr^{\text{TP}}(k, n)$ . But this limiting procedure is very non-trivial, and it provides only an upper bound for the genus:  $g \leq k(n - k)$ .

In the following we present a **direct** construction of algebraic geometric data associated to points in  $Gr^{\text{TNN}}(k, n)$  which is naturally related to the characterization of positroid cells in [61] and provides optimal genus spectral curves. Moreover, the present construction unveils the relation of the algebraic construction in [3] with Le-networks in  $Gr^{\text{TP}}(k, n)$ . The starting point are the algebraic geometric data associated to  $(\mathcal{K}, [A])$  via Sato dressing (see Definition 2.3):

- (1) A rational curve  $\Gamma_0$  equipped with a finite number of marked points: the ordered real phases  $\kappa_1 < \dots < \kappa_n$ , and the essential singularity  $P_0$  of the wave function;
- (2) The Sato divisor  $\mathcal{D}_{\text{S}, \Gamma_0}(\vec{t}_0)$  for the soliton data defined in Definition 2.2;
- (3) The normalized wave function  $\hat{\psi}(P, \vec{t})$  on  $\Gamma_0 \setminus \{P_0\}$  defined in (2.8).

As pointed out in Section 2.1, in general, the Sato divisor does not parametrize the whole positroid cell to which  $[A]$  belongs to. Therefore, in general, we cannot reconstruct the soliton data  $[A]$  just from the Sato divisor at  $\vec{t}_0$ .

Below, to any regular soliton data  $(\mathcal{K}, [A])$ , we associate a well-defined curve  $\Gamma$  containing  $\Gamma_0$  as a connected component, and a unique KP divisor on it using the Le-network  $\mathcal{N}$  representing  $[A]$ .  $\Gamma$  is reducible and a rational degeneration of a M-curve having the minimal possible genus under genericity assumption on the soliton data. Finally, the set of poles of  $\hat{\psi}$  exactly coincides with  $\mathcal{D}_{\text{KP}, \Gamma}$  for generic  $\vec{t}$ .

**Main construction** Assume we are given a real regular bounded multiline KP soliton solution generated by the following soliton data:

- (1) A set of  $n$  real ordered phases  $\mathcal{K} = \{\kappa_1 < \kappa_2 < \dots < \kappa_n\}$ ;
- (2) A point  $[A] \in \mathcal{S}_{\mathcal{M}}^{\text{TNN}} \subset \text{Gr}^{\text{TNN}}(k, n)$ , where  $\mathcal{S}_{\mathcal{M}}^{\text{TNN}}$  is a positroid stratum of dimension  $|D|$ .

We represent  $[A]$  with its canonically oriented bipartite trivalent Le-network  $\mathcal{N}$ . We recall that  $\mathcal{N}$  provides a representation of the points of the cell depending exactly by  $|D|$  parameters. Let us also denote  $\mathcal{G}$  the Le-graph representing  $\mathcal{S}_{\mathcal{M}}^{\text{TNN}}$ . Then, we associate the following algebraic-geometric objects to the soliton data  $(\mathcal{K}, [A])$ :

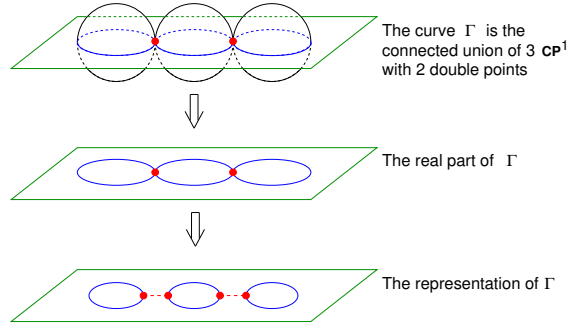
- (1) A reducible M-curve  $\Gamma = \Gamma(\mathcal{G})$  with  $g + 1$  ovals which is the rational degeneration of a smooth M-curve of genus  $g = |D|$ . In our approach,  $\Gamma_0$  is one of the irreducible components of  $\Gamma$ . The marked point  $P_0$  belongs to the intersection of  $\Gamma_0$  with an oval (infinite oval);
- (2) An unique real and regular degree  $g$  non-special KP divisor  $\mathcal{D}_{\text{KP}, \Gamma} = \mathcal{D}_{\text{KP}, \Gamma}(\mathcal{K}, [A]) \subset \Gamma \setminus \{P_0\}$  such that any finite oval contains exactly one divisor point and  $\mathcal{D}_{\text{KP}, \Gamma} \cap \Gamma_0$  coincides with Sato divisor  $\mathcal{D}_{\text{S}, \Gamma_0}(\vec{t}_0)$  for some initial time  $\vec{t}_0$ ;
- (3) An unique KP wave-function  $\hat{\psi}$  as in Definition 2.4 such that
  - (a) Its restriction to  $\Gamma_0 \setminus \{P_0\}$  coincides with the normalized Sato wave function (2.6);
  - (b) Its pole divisor has degree  $\mathfrak{d} \leq g$  and is contained in  $\mathcal{D}_{\text{KP}, \Gamma}$ .

**Remark 3.1.** Here and in the following, when we refer to the Sato divisor for reducible real and regular soliton data, we mean the reduced Sato divisor defined in Remark 2.2. In particular, the KP divisor  $\mathcal{D}_{\text{KP}, \Gamma}$  restricted to  $\Gamma_0$  is the reduced Sato divisor.

**Remark 3.2.** In [4] we extend the main construction using any oriented bipartite trivalent network in the disk representing  $[A]$  in Postnikov equivalence class [61].

**3.1. The reducible rational curve  $\Gamma$ .** Given the oriented graph  $\mathcal{G}$  representing a given positroid cell  $\mathcal{S}_{\mathcal{M}}^{\text{TNN}} \subset \text{Gr}^{\text{TNN}}(k, n)$ , the curve  $\Gamma = \Gamma(\mathcal{G})$  is obtained gluing a finite number of copies of  $\mathbb{CP}^1$ , corresponding to the internal vertexes in  $\mathcal{G}$ , and one copy of  $\mathbb{CP}^1 = \Gamma_0$ , corresponding to the boundary of the disk. We glue these components at pairs of points corresponding to its edges. We also fix a local affine coordinate  $\zeta$  on each component (see Definition 3.1), therefore we have complex conjugation  $\zeta \rightarrow \bar{\zeta}$  at each component. The points with real  $\zeta$  form the real part of the given component. By construction (see Definition 3.1), the coordinates at each pair of glued points  $P, Q$ , are real. We then topologically represent the real part of  $\Gamma$  as a union of circles (ovals), where the latter correspond to the faces of  $\mathcal{G}$ .



FIGURE 2. The model of a reducible rational curve  $\Gamma$  with three components and one oval.

We use the same representation for real rational curves as in [3] (see Fig. 2). We draw only the real part of each component and we represent it with a circle. Then we schematically represent the real part of  $\Gamma$  by drawing these circles separately and connecting the glued points by dashed lines. The planarity of the Le-graph implies that  $\Gamma$  is a reducible rational M-curve.

**Construction 3.1.** *The curve  $\Gamma = \Gamma(\mathcal{G})$ . Let  $\mathcal{K} = \{\kappa_1 < \dots < \kappa_n\}$  and let  $\mathcal{S}_{\mathcal{M}}^{TNN} \subset Gr^{TNN}(k, n)$  be the positroid cell corresponding to the realizable matroid  $\mathcal{M}$ . Let  $\mathcal{G}$  be the planar connected acyclically oriented trivalent bipartite Le-graph in the disk of Definition A.4 representing  $\mathcal{S}_{\mathcal{M}}^{TNN}$ . Let  $I = \{1 \leq i_1 < \dots < i_k \leq n\}$  be the set of the pivot indexes (i.e the lexicographically minimal base of  $\mathcal{M}$ ) and, for any  $r \in [k]$ , let  $N_r$  be the number of filled boxes in the  $r$ -th row of corresponding Le-diagram (see (A.3) in Appendix A). Finally, let  $1 \leq j_1 < j_2 < \dots < j_{N_r} \leq n$  be the non-pivot indexes of the boxes  $B_{i_r, j_s}$  with index  $\chi_{j_s}^{i_r} = 1$ ,  $s \in [N_r]$ , as in (A.3) and (A.4) in Appendix A.*

TABLE 1. The Le-graph  $\mathcal{G}$  vs the reducible rational curve  $\Gamma$ 

$\mathcal{G}$	$\Gamma$
Boundary of disk	Copy of $\mathbb{CP}^1$ denoted $\Gamma_0$
Boundary vertex $b_l$	Marked point $\kappa_l$ on $\Gamma_0$
Black vertex $V'_{ij}$	Copy of $\mathbb{CP}^1$ denoted $\Sigma_{ij}$
White vertex $V_{ij}$	Copy of $\mathbb{CP}^1$ denoted $\Gamma_{ij}$
Internal Edge	Double point
Face	Oval

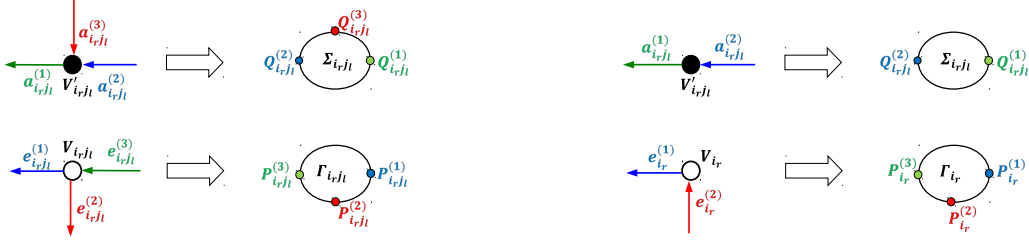


FIGURE 3. The correspondence between marked points on copies  $\Gamma_{i_r j_l}$  and  $\Sigma_{i_r j_l}$  and edges of white and black vertexes. The rule at the marked points corresponding to the edges of a bivalent white vertex at a boundary source  $b_{i_r}$  is justified by the necessity of adding a third marked point (Darboux point) on  $\Gamma_{i_r}$ .

The curve  $\Gamma = \Gamma(\mathcal{G})$  is associated to  $\mathcal{G}$  according to Table 1, after reflecting the graph w.r.t. a line orthogonal to the one containing the boundary vertexes (we reflect the graph to have the natural increasing order of the phases on  $\Gamma_0 \subset \Gamma$ ). More precisely,  $\Gamma$  is the connected union of  $2n + k + 1$  copies of  $\mathbb{CP}^1$  denoted as  $\Gamma_0, \Sigma_{i_r j_s}, \Gamma_{i_r j_s}, \Gamma_{i_r}$ , for  $r \in [k], s \in [N_r]$

$$\Gamma = \Gamma_0 \bigsqcup_{r=1}^k \left( \Gamma_{i_r} \sqcup \left( \bigsqcup_{s=1}^{N_r} \Gamma_{i_r j_s} \sqcup \Sigma_{i_r j_s} \right) \right)$$

according to the following rules (see also Figures 3 and 4):

- (1)  $\Gamma_0$  is the copy of  $\mathbb{CP}^1$  corresponding to the boundary of the disk. It has  $n + 1$  marked points:  $P_0$  such that  $\zeta^{-1}(P_0) = 0$  and the points  $\kappa_1 < \dots < \kappa_n$  corresponding to the boundary vertexes  $b_1, \dots, b_n$  on  $\mathcal{G}$ ;
- (2) A copy of  $\mathbb{CP}^1$  corresponds to any internal vertex of  $\mathcal{G}$ . For any fixed  $r \in [k]$  and  $s \in [N_r]$  we denote  $\Gamma_{i_r j_s}$  (resp.  $\Sigma_{i_r j_s}$ ) the copy of  $\mathbb{CP}^1$  corresponding to the white vertex  $V_{i_r j_s}$  (resp. black vertex  $V'_{i_r j_s}$ );
- (3) We denote  $\Gamma_{i_r}$  the copy of  $\mathbb{CP}^1$  corresponding to the internal white vertex  $V_{i_r}$  joined by an edge to the source  $b_{i_r}$ ,  $r \in [k]$ ;
- (4) On each copy of  $\mathbb{CP}^1$  corresponding to an internal vertex  $V$ , we mark as many points as edges at  $V$ . We number the edges at  $V$  anticlockwise in increasing order, so that, on the corresponding copy of  $\mathbb{CP}^1$ , the marked points are numbered clockwise because of the mirror rule (see Figure 3). We use the following numbering rule:
  - (a) The unique horizontal edge pointing inward at the white vertex  $V_{i_r j_s}$  is numbered 3, for any  $r \in [k], s \in [N_r]$ . Therefore  $\Gamma_{i_r j_s}$ ,  $r \in [k], s \in [N_r - 1]$ , has 3 real

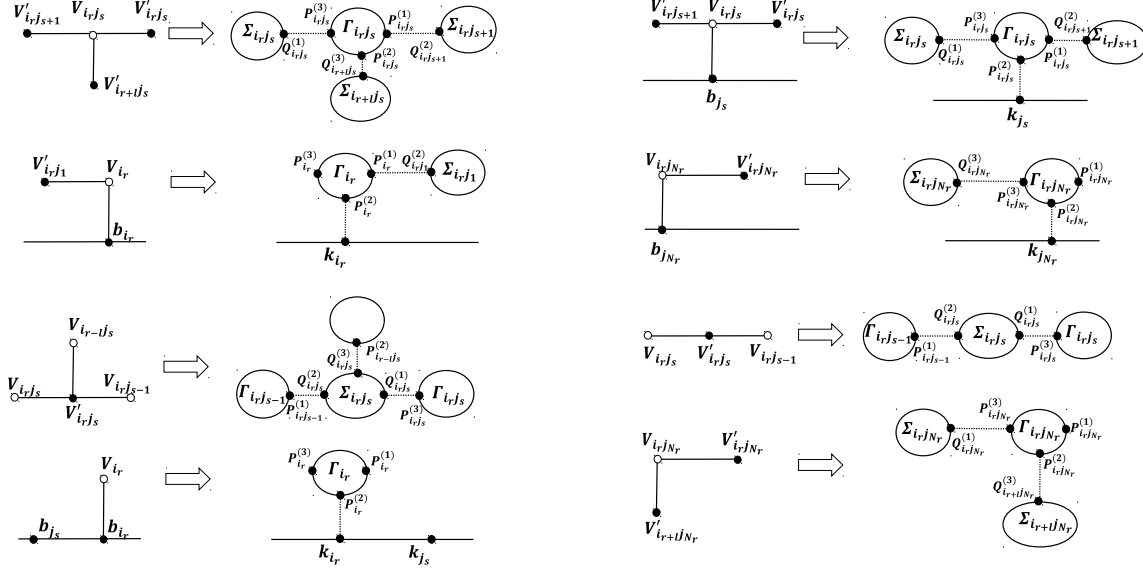


FIGURE 4. The gluing rules on  $\Gamma$  are modeled on the bipartite Le-graph  $\mathcal{G}$  reflected w.r.t. the vertical axis. The dotted lines mark the points where we glue different copies of  $\mathbb{CP}^1$ .

ordered marked points which we denote  $P_{i_rj_s}^{(1)}, P_{i_rj_s}^{(2)}, P_{i_rj_s}^{(3)}$  (see Figure 3[bottom, left]) and  $\Gamma_{i_rj_{N_r}}$  has two marked points  $P_{i_rj_s}^{(2)}, P_{i_rj_s}^{(3)}$ ;

(b) At each white vertex  $V_{i_r}$  we have a horizontal edge marked  $e_{i_r}^{(1)}$  and a vertical edge marked  $e_{i_r}^{(2)}$  which correspond to the marked points  $P_{i_r}^{(1)}, P_{i_r}^{(2)} \in \Gamma_{i_r}$ . On each  $\Gamma_{i_r}$ ,  $r \in [k]$ , we add an extra point, the Darboux point  $P_{i_r}^{(3)}$ , which we use to rule the position of the vacuum divisor;

(c) The unique edge pointing outward at a black vertex  $V'_{i_rj_s}$ ,  $r \in [k]$ ,  $s \in [N_r - 1]$ , is always numbered 1. We denote  $Q_{i_rj_s}^{(m)}$ ,  $m \in [3]$  (resp.  $m \in [2]$ ) the marked points on  $\Sigma_{i_rj_s}$  corresponding to the trivalent (resp. bivalent) black vertex  $V'_{i_rj_s}$ .

(5) We glue copies of  $\mathbb{CP}^1$  in pairs at the marked points corresponding to the end points of the corresponding edge on  $\mathcal{G}$  (see Figure 4). More precisely:

(6) **Horizontal gluing rules for fixed  $r \in [k]$ :**

- (a) If, for some  $r \in [k]$ ,  $N_r = 0$ , then  $P_{i_r}^{(1)} \in \Gamma_{i_r}$  is not glued to any other marked point;
- (b) If, for some  $r \in [k]$ ,  $N_r > 0$ , then  $P_{i_r}^{(1)} \in \Gamma_{i_r}$  is glued to  $Q_{i_rj_1}^{(2)} \in \Sigma_{i_rj_1}$ ;
- (c) For any  $s \in [N_r - 1]$ ,  $P_{i_rj_s}^{(1)} \in \Gamma_{i_rj_s}$  is glued to  $Q_{i_rj_{s+1}}^{(2)} \in \Sigma_{i_rj_{s+1}}$ ;
- (d) For any  $s \in [N_r]$ ,  $P_{i_rj_s}^{(3)} \in \Gamma_{i_rj_s}$  is glued to  $Q_{i_rj_s}^{(1)} \in \Sigma_{i_rj_s}$ ;
- (e)  $P_{i_rj}^{(3)} \in \Gamma_{i_r}$  is not glued to any other marked point.

(7) **Vertical gluing rules:**

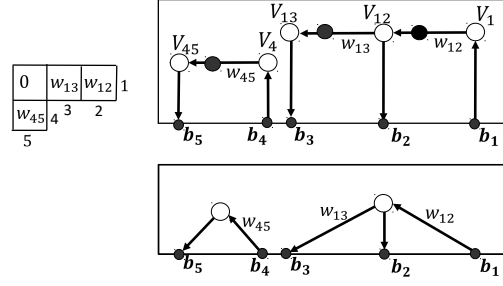


FIGURE 5. The Le-networks corresponding to the Le-graph  $\mathcal{G}$  [top] and its reduction  $\mathcal{G}_{\text{red}}$  [bottom] for the same Le-tableau of a positroid cell of dimension  $|D| = 3$  in  $Gr^{TNN}(2, 5)$  [left].

The weight is one for any edge not marked in the Figure.

- (a) For any  $r \in [k]$ ,  $\kappa_{i_r} \in \Gamma_0$  is glued to  $P_{i_r}^{(2)} \in \Gamma_{i_r}$ ;
- (b) For any  $j \in \bar{I}$  such that  $\bar{r} = \max\{r \in [k] : \chi_j^{i_r} = 1\} > 0$ ,  $\kappa_j \in \Gamma_0$  is glued to  $P_{i_{\bar{r}j}}^{(2)} \in \Gamma_{i_{\bar{r}j}}$ ;
- (c) If, for some  $j \in \bar{I}$ ,  $\chi_j^{i_r} = 0$  for all  $r \in [k]$ , then  $\kappa_j \in \Gamma_0$  is not glued to any other marked point;
- (d) For any fixed  $r \in [2, k]$  and any fixed  $s \in [N_r]$ , let  $\bar{r} = \max\{l \in [1, r-1] : \chi_{j_s}^{i_l} = 1\}$ . Then  $Q_{i_r j_s}^{(3)} \in \Sigma_{i_r j_s}$  is glued to  $P_{i_{\bar{r}j_s}}^{(2)} \in \Gamma_{i_{\bar{r}j_s}}$ .
- (8) The faces of  $\mathcal{G}$  correspond to the ovals of  $\Gamma$ . We label the ovals  $\Omega_0, \Omega_{i_r j_s}, s \in [N_r], r \in [k]$ , as the corresponding faces of  $\mathcal{N}$ .

**Remark 3.3. Universality of the reducible rational curve  $\Gamma$  and local parametrization of positroid cells.** Let us point out that, for any fixed positroid cell  $\mathcal{S} = \mathcal{S}_{\mathcal{M}}^{TNN}$ , the construction of  $\Gamma$  does **not** require the introduction of any parameter. Therefore it provides an **universal** curve  $\Gamma$  for the whole positroid cell. From our construction below it follows that the points of  $\mathcal{S}$  are locally parametrized by the divisor positions at the finite ovals for given  $\vec{t}_0$ . To obtain global parametrization, one has to consider also special divisor, which in our construction occur when some of the divisor points coincide with double points, and this case requires a separate analysis.

**Remark 3.4. The role of bivalent vertexes, the reduced graph  $\mathcal{G}_{\text{red}}$  and the reduced M-curve  $\Gamma(\mathcal{G}_{\text{red}})$**  The number of copies of  $\mathbb{CP}^1$  used to construct  $\Gamma$  above is **excessive** in the sense that both the number of ovals and the **KP divisor** are invariant if we eliminate from  $\mathcal{G}$  all copies of  $\mathbb{CP}^1$  corresponding to bivalent vertexes and change edge weights following [61]. In this procedure we maintain a bivalent vertex in  $\mathcal{G}_{\text{red}}$  for each component which disconnects from the

graph upon removing the boundary of the disk and consists of a single boundary source connected to a single boundary sink. We show a simple example in Figure 5. In the following, we denote the reduced trivalent graph and the reducible rational curve associated to it  $\mathcal{G}_{\text{red}}$  and  $\Gamma(\mathcal{G}_{\text{red}})$ , respectively.

For the construction of the **reducible rational** M-curve we can use both  $\mathcal{G}$  and  $\mathcal{G}_{\text{red}}$  graphs. In Sections 4 and 5 we use the Le-graph  $\mathcal{G}$  to evidence the recursive construction in the proof. However, it is also possible to directly construct the KP wave function and its divisor on  $\Gamma(\mathcal{G}_{\text{red}})$ , since, by our construction, the KP wave function is constant with respect to the spectral parameter on each  $\mathbb{CP}^1$  corresponding to a bivalent vertex.

For constructing a regular perturbed M-curve of genus equal to  $|D|$  it is convenient to start from  $\Gamma(\mathcal{G}_{\text{red}})$  since it corresponds to a nodal plane curve of degree lesser than that for  $\Gamma(\mathcal{G})$ . In Section 6, we use  $\Gamma(\mathcal{G}_{\text{red}})$  in the construction of the plane curve and of the KP divisor for soliton data in  $Gr^{TP}(2, 4)$ .

**Remark 3.5. Comparison with the construction in [3].** In [3], to any given soliton data  $(\mathcal{K}, [A])$ ,  $[A] \in Gr^{TP}(k, n)$ , we associate a curve obtained gluing  $k + 1$  copies of  $\mathbb{CP}^1$  at double points whose position is ruled by a parameter  $\xi \gg 1$ . We then control the asymptotic leading behavior in  $\xi$  of the vacuum wave function via an algebraic construction using the positivity properties of a specific representative matrix of  $[A]$ . In this approach the number of  $\mathbb{CP}^1$  components is much smaller, but we have to introduce extra parameters marking the positions of the glued points. In practice one can obtain such curve from the universal one by a proper desingularization of some double point (see also Section 6, where we desingularize explicitly  $\Gamma(\mathcal{G}_{\text{red}})$  to  $\Gamma(\xi)$  when  $[A] \in Gr^{TP}(2, 4)$ ).

**Proposition 3.1. The oval structure of  $\Gamma$ .** Let  $\mathcal{K} = \{\kappa_1 < \dots < \kappa_n\}$  and  $\mathcal{S}_{\mathcal{M}}^{TNN} \subset Gr^{TNN}(k, n)$  be a positroid cell of dimension  $|D|$ . Let  $\Gamma$  be as in Construction 3.1. Then  $\Gamma$  possesses  $|D| + 1$  ovals which we label  $\Omega_0, \Omega_{i_r j_s}$ ,  $s \in [N_r]$ ,  $r \in [k]$ ,  $N_r \geq 1$ . Moreover the ovals are uniquely identified by the following properties:

- (1)  $\Omega_0$  is the unique oval whose boundary contains both  $\kappa_1$  and  $\kappa_n$ ;
- (2) For any  $r \in [k]$ ,  $s \in [2, N_r]$ ,  $\Omega_{i_r j_s}$  is the unique oval whose boundary contains both  $P_{i_r j_s}^{(2)} \in \Gamma_{i_r j_s}$  and  $P_{i_r j_{s-1}}^{(2)} \in \Gamma_{i_r j_{s-1}}$ ;
- (3) For any  $r \in [k]$ ,  $\Omega_{i_r j_1}$  is the unique oval whose boundary contains both  $P_{i_r j_1}^{(2)} \in \Gamma_{i_r j_1}$  and  $P_{i_r}^{(2)} \in \Gamma_{i_r}$ .

The proof is straightforward and we omit it. We remark that  $\Gamma(\mathcal{G}_{\text{red}})$  has the same number of ovals as  $\Gamma(\mathcal{G})$ .

Let  $|D|$  be the dimension of the **irreducible** positroid cell  $\mathcal{S}_{\mathcal{M}}^{\text{TNN}} \subset \text{Gr}^{\text{TNN}}(k, n)$ . Let  $\mathcal{G}_{\text{red}}$  be its reduced graph as in Remark 3.4 and suppose that it has  $n_b$  bivalent vertexes after the reduction. Then  $\Gamma(\mathcal{G}_{\text{red}})$  is a partial normalization [6] of a connected reducible nodal plane curve with  $|D| + 1$  ovals obtained by gluing  $2|D| - n + n_b + 1$  copies of  $\mathbb{CP}^1$ . The curve  $\Gamma(\mathcal{G}_{\text{red}})$  is a rational degeneration of a genus  $|D|$  smooth M-curve. The total number of edges of  $\mathcal{G}_{\text{red}}$  is  $3|D| - n + n_b$ , and each of them corresponds to an handle of the desingularized M-curve. In the next Proposition we verify that the genus of the latter coincides with the dimension of  $\mathcal{S}_{\mathcal{M}}^{\text{TNN}}$ .

**Proposition 3.2.**  *$\Gamma(\mathcal{G}_{\text{red}})$  is the rational degeneration of a smooth M-curve of genus  $|D|$ . Let  $\mathcal{K} = \{\kappa_1 < \dots < \kappa_n\}$  and  $\mathcal{S}_{\mathcal{M}}^{\text{TNN}} \subset \text{Gr}^{\text{TNN}}(k, n)$  be an irreducible positroid cell of dimension  $|D|$ . Let  $\Gamma$  be as in Construction 3.1 and  $\Gamma(\mathcal{G}_{\text{red}})$  be the its reduction obtained by eliminating the components corresponding to bivalent vertexes eliminated in  $\mathcal{G}_{\text{red}}$ . Then  $\Gamma(\mathcal{G}_{\text{red}})$  is a rational degeneration of a regular M-curve of genus  $|D|$  equal to the dimension of the positroid cell, possessing  $|D| + 1$  ovals.*

*Proof.* The only untrivial statement is the one concerning the genus of the perturbed curve. Let  $n_b$  be the number of bivalent vertexes survived the reduction of the graph  $\mathcal{G}$  according to Remark 3.4. By definition,  $\Gamma(\mathcal{G}_{\text{red}})$  is represented by  $2|D| - n + n_b + 1$  copies of  $\mathbb{CP}^1$  connected at  $3|D| - n + n_b$  pairs of double points. The regular curve is obtained opening a gap at each pair of these double points. We perform this desingularization respecting the real structure and keeping the number of real ovals fixed.

By construction, the desingularized curve has genus  $g = \# \text{handles} - \# \mathbb{CP}^1 + 1 = 3|D| - n + n_b - (2|D| - n + n_b + 1) + 1 = |D|$ , and it possesses  $|D| + 1$  real ovals, therefore it is an M-curve.  $\square$

**3.2. The planar representation of the desingularized curve.** Generic Riemann surfaces cannot be holomorphically mapped into  $\mathbb{CP}^2$  without self-intersections [35], therefore partial normalization is necessary if the number of  $\mathbb{CP}^1$  copies is sufficiently high. In our construction we have  $2|D| - n + n_b + 1$  copies of  $\mathbb{CP}^1$ , which may be lines, quadrics or rational cubics. Denote the numbers of lines, quadrics and cubics by  $n_1, n_2, n_3$  respectively. Clearly  $n_1 + n_2 + n_3 = 2|D| - n + n_b + 1$ , the total degree of the rational reducible curve  $\Gamma(\mathcal{G}_{\text{red}})$  is  $d = n_1 + 2n_2 + 3n_3$ . The total number of singularities before normalization is

$$n_s = \frac{n_1(n_1 - 1)}{2} + 2n_1n_2 + 3n_1n_3 + 2n_2(n_2 - 1) + 6n_2n_3 + \frac{9n_3(n_3 - 1)}{2} + n_3$$

The last term in the above sum takes into account that all cubics are rational and each has one cusp. When we desingularize  $\Gamma(\mathcal{G}_{\text{red}})$  to the genus  $|D|$  curve,  $n_s - 3|D| + n - n_b$  intersections have to remain intersections for its plane curve model, and they are resolved after normalization.

Let us provide evidence that we have enough parameters. Let us assume that  $\Gamma_0$  is defined by  $\mu = 0$ , and we have 3 systems of linear functions  $l_j = a_j\lambda + b_j\mu$ ,  $j \in [n_1]$ ,  $l'_j = a'_j\lambda + b'_j\mu$ ,  $j \in [n_2]$ ,  $l''_j = a''_j\lambda + b''_j\mu$ ,  $j \in [n_3]$  such that

- (1) All slopes are pairwise distinct and all  $a_j$ ,  $a'_j$ ,  $a''_j$  are non-zero;
- (2) The system of lines  $\Gamma_0$ ,  $\mathcal{L}_j : \{l_j - \alpha_j = 0\}$  intersect only in pairs.

The quadrics and cubics are represented by  $\mathcal{Q}_j = 0$ ,  $j \in [n_2]$  and  $\mathcal{C}_i = 0$ ,  $i \in [n_3]$  respectively, where  $\mathcal{Q}_j = y - \alpha'_{j,2}(l'_j)^2 - \alpha'_{j,1}l'_j - \alpha'_{j,0}$  and  $\mathcal{C}_i = y - \alpha''_{i,3}(l''_i)^3 - \alpha''_{i,2}(l''_i)^2 - \alpha''_{i,1}l''_i - \alpha''_{i,0}$ .

The coefficients  $\alpha$ ,  $\alpha'$ ,  $\alpha''$  have to be chosen so that all lines, quadrics and cubics intersect  $\Gamma_0$  at correct points. We also assume that all  $\alpha'_{j,2}$ ,  $\alpha''_{i,3}$  are sufficiently large, so that all quadrics and cubics are small perturbations of pairs or triples of parallel lines respectively, and all intersections of components are real.

The unperturbed curve has the following form

$$\Pi_0(\lambda, \mu) = 0, \quad \text{where} \quad \Pi_0(\lambda, \mu) = \mu \prod_{i_1 \in [n_1]} \mathcal{L}_{i_1} \prod_{i_2 \in [n_2]} \mathcal{Q}_{i_2} \prod_{i_3 \in [n_3]} \mathcal{C}_{i_3}.$$

We use the following collection of perturbative terms:  $\{\Pi_{i_1}^{[0,1]}; \Pi_{i_2}^{[0,2],k}, k \in [2]; \Pi_{i_3}^{[0,3],k}, k \in [3]; \Pi_{i_1,j_1}^{[1,1]}; \Pi_{i_1,i_2}^{[1,2],k}, k \in [2]; \Pi_{i_1,i_3}^{[1,3],k}, k \in [3]; \Pi_{i_2,j_2}^{[2,2],k_1,k_2}, k_1, k_2 \in [2]; \Pi_{i_2,i_3}^{[2,3],k_1,k_2}, k_1 \in [2], k_2 \in [3]; \Pi_{i_3,j_3}^{[3,3],k_1,k_2}, k_1, k_2 \in [3]\}$ .

Here  $i_l, j_l \in [n_l]$ ,  $l \in [3]$ ,  $i_1 < j_1$ ,  $i_2 < j_2$ ,  $i_3 < j_3$ .

$$\begin{aligned} \Pi_{i_1}^{[0,1]} &= \frac{\Pi_0}{\mu \mathcal{L}_{i_1}}, \quad \Pi_{i_2}^{[0,2],k} = \frac{\Pi_0(l'_{i_2})^{k-1}}{\mu \mathcal{Q}_{i_2}}, \quad \Pi_{i_3}^{[0,3],k} = \frac{\Pi_0(l''_{i_3})^{k-1}}{\mu \mathcal{C}_{i_3}}, \\ \Pi_{i_1,j_1}^{[1,1]} &= \frac{\Pi_0}{\mathcal{L}_{i_1} \mathcal{L}_{j_1}}, \quad \Pi_{i_1,i_2}^{[1,2],k} = \frac{\Pi_0(l'_{i_2})^{k-1}}{\mathcal{L}_{i_1} \mathcal{Q}_{i_2}}, \quad \Pi_{i_1,i_3}^{[1,3],k} = \frac{\Pi_0(l''_{i_3})^{k-1}}{\mathcal{L}_{i_1} \mathcal{C}_{i_3}}, \\ \Pi_{i_2,j_2}^{[2,2],k_1,k_2} &= \frac{\Pi_0(l'_{i_2})^{k_1-1}(l'_{j_2})^{k_2-1}}{\mathcal{Q}_{i_2} \mathcal{Q}_{j_2}}, \quad \Pi_{i_2,i_3}^{[2,3],k_1,k_2} = \frac{\Pi_0(l'_{i_2})^{k_1-1}(l''_{i_3})^{k_2-1}}{\mathcal{Q}_{i_2} \mathcal{C}_{i_3}}, \quad \Pi_{i_3,j_3}^{[3,3],k_1,k_2} = \frac{\Pi_0(l''_{i_3})^{k_1-1}(l''_{j_3})^{k_2-1}}{\mathcal{C}_{i_3} \mathcal{C}_{j_3}}. \end{aligned}$$

Consider the following perturbation of our rational curve  $\Pi_0(\lambda, \mu) = 0$ :

$$(3.1) \quad \Pi(\lambda, \mu) = 0, \quad \text{where} \quad \Pi(\lambda, \mu) = \Pi_0 + \sum \epsilon_s^r \Pi_s^r,$$

where the sum runs over all perturbation terms described above. Then the perturbed curve has the same structure at the infinite line as the original rational curve. The number of perturbation

parameters  $\epsilon_s^r$  in (3.1) coincides with the number of intersections in  $\Pi_0(\lambda, \mu) = 0$ . For sufficiently small  $\epsilon_s^r$  we have the following map

$$(3.2) \quad \{\epsilon_s^r\} \rightarrow \Pi(\mathcal{R}_s^r),$$

where  $\mathcal{R}_s^r$  are the solutions of the system

$$(3.3) \quad \partial_\lambda \Pi(\lambda, \mu) = 0, \quad \partial_\mu \Pi(\lambda, \mu) = 0.$$

For the unperturbed curve, the set  $\{\mathcal{R}_s^r\}$  coincides with the intersection points, therefore for small  $\epsilon_s^r$  we have a natural enumeration. The map (3.2) is analytic for  $|\epsilon_s^r| \ll 1$  and its Jacobian is non-zero, therefore it is locally invertible, and at each double point we can open a gap in the desired direction, or keep the point double.

Let us remark that these arguments are analogous to arguments used in [49].

**3.3. The KP divisor on  $\Gamma$ .** Throughout this section we fix the set of phases  $\mathcal{K} = \{\kappa_1 < \dots < \kappa_n\}$  and the  $g = |D|$  dimensional positroid cell  $\mathcal{S}_{\mathcal{M}}^{\text{TNN}} \subset Gr^{\text{TNN}}(k, n)$ .  $\Gamma$  is the curve of Construction 3.1 associated to such data with marked point  $P_0 \in \Gamma_0$ .

**In this section we state the main results of our paper: for any soliton data  $(\mathcal{K}, [A])$ ,  $[A] \in \mathcal{S}_{\mathcal{M}}^{\text{TNN}}$ , we construct a unique real and regular degree  $g$  KP divisor  $\mathcal{D}_{\text{KP}, \Gamma}$  on  $\Gamma$  as follows:**

- (1) We first construct a unique degree  $g$  effective real and regular **vacuum** divisor  $\mathcal{D}_{\text{vac}, \Gamma}$  and a unique real and regular **vacuum** wave function  $\hat{\phi}(P, \vec{t})$  on  $\Gamma$  satisfying appropriate boundary conditions (Theorem 3.1);
- (2) We then apply the Darboux dressing to such vacuum wave function and define the normalized **dressed divisor**  $\mathcal{D}_{\text{KP}, \Gamma}$ , which, by construction is effective and of degree  $g$ ;
- (3)  $\mathcal{D}_{\text{KP}, \Gamma}$  is the **KP divisor** for the given soliton data on the spectral curve  $\Gamma$ , since its restriction to  $\Gamma_0$  coincides with the Sato divisor defined in Section 2.1, and, by construction, it satisfies the reality and regularity conditions of Definition 2.4 (see Theorem 3.2).

In particular,  $\mathcal{D}_{\text{KP}, \Gamma}$  has minimal degree  $g$ . As a byproduct, we obtain a local bijection between KP divisors on  $\Gamma$  and points in the positroid cell  $\mathcal{S}_{\mathcal{M}}^{\text{TNN}}(k, n)$ .

We start introducing local affine coordinates on each copy of  $\mathbb{CP}^1$  and we use the same symbol  $\zeta$  for any such affine coordinate to simplify notations (see also Figure 6).

**Definition 3.1. Local affine coordinate on  $\Gamma$**  *On each copy of  $\mathbb{CP}^1$  the local coordinate  $\zeta$  is uniquely identified by the following properties:*



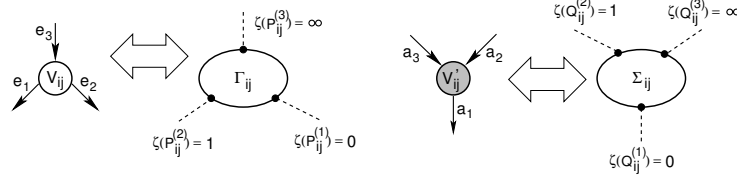


FIGURE 6. Local coordinates on the components  $\Gamma_{ij}$  and  $\Sigma_{ij}$ : the marked point  $P_{ij}^{(s)} \in \Gamma_{ij}$  corresponds to the edge  $e_s$  at the white vertex  $V_{ij}$  and the marked point  $Q_s \in \Gamma_{ij}$  corresponds to the edge  $a_s$  at the black vertex  $V'_{ij}$ .

- (1) On  $\Gamma_0$ ,  $\zeta^{-1}(P_0) = 0$  and  $\zeta(\kappa_1) < \dots < \zeta(\kappa_n)$ . To abridge notations, we identify the  $\zeta$ -coordinate with the marked points  $\kappa_j = \zeta(\kappa_j)$ ,  $j \in [n]$ ;
- (2) On the component  $\Gamma_{ij}$  corresponding to the internal white vertex  $V_{ij}$ :

$$\zeta(P_{ij}^{(1)}) = 0, \quad \zeta(P_{ij}^{(2)}) = 1, \quad \zeta(P_{ij}^{(3)}) = \infty,$$

while on the component  $\Sigma_{ij}$  corresponding to the internal black vertex  $V'_{ij}$ :

$$\zeta(Q_{ij}^{(1)}) = 0, \quad \zeta(Q_{ij}^{(2)}) = 1, \quad \zeta(Q_{ij}^{(3)}) = \infty.$$

In the following Definitions we state the desired properties for both the vacuum divisor and the vacuum wave function on  $\Gamma$ .

**Definition 3.2.** *Real and regular vacuum divisor compatible with  $\mathcal{S}_M^{TNN}$ .* Let  $\Omega_0$  be the infinite oval containing the marked point  $P_0 \in \Gamma_0$  and let  $\Omega_j$ ,  $j \in [g]$  be the finite ovals of  $\Gamma$ . Let  $P_3^{(ir)}$ ,  $r \in [k]$  be the Darboux points in  $\Gamma$ .

We call a degree  $g$  divisor  $\mathcal{D}_{\text{vac}, \Gamma} \in \Gamma \setminus \Gamma_0$  a real and regular vacuum divisor compatible with  $\mathcal{S}_M^{TNN}$  if:

- (1)  $\mathcal{D}_{\text{vac}, \Gamma}$  is contained in the union of all the ovals of  $\Gamma$ ;
- (2) There is exactly one divisor point on each component of  $\Gamma$  corresponding to a trivalent white vertex or a bivalent white vertex containing a Darboux point;
- (3) In any  $\Omega_j$ ,  $j \in [g]$ , the total number of vacuum divisor poles plus the number of Darboux points is 1 mod 2;
- (4) In  $\Omega_0$ , the total number of vacuum divisor poles plus the number of Darboux points plus  $k$  is 0 mod 2.

**Definition 3.3.** *A real and regular vacuum wave function on  $\Gamma$  corresponding to  $\mathcal{D}_{\text{vac}, \Gamma}$ :* Let  $\mathcal{D}_{\text{vac}, \Gamma}$  be a degree  $g$  real regular divisor on  $\Gamma$  as in Definition 3.2 A function  $\hat{\phi}(P, \vec{t})$ ,

where  $P \in \Gamma \setminus \{P_0\}$  and  $\vec{t}$  are the KP times, is called a real and regular vacuum wave function on  $\Gamma$  corresponding to  $\mathcal{D}_{\text{vac}, \Gamma}$  if:

- (1) There exists  $\vec{t}_0$  such that  $\hat{\phi}(P, \vec{t}_0) = 1$  at all points  $P \in \Gamma \setminus \{P_0\}$ ;
- (2) The restriction of  $\hat{\phi}$  to  $\Gamma_0 \setminus \{P_0\}$  coincides with the following normalization of Sato's wave function,  $\hat{\phi}(\zeta(P), \vec{t}) = e^{\theta(\zeta, \vec{t} - \vec{t}_0)}$ , where  $\theta(\zeta, \vec{t}) = \sum_{l \geq 1} t_l \zeta^l$ ;
- (3) For all  $P \in \Gamma \setminus \Gamma_0$  the function  $\hat{\phi}(P, \vec{t})$  satisfies all equations (2.4) of the vacuum hierarchy;
- (4) If both  $\vec{t}$  and  $\zeta(P)$  are real, then  $\hat{\phi}(\zeta(P), \vec{t})$  is real. Here  $\zeta(P)$  is the local affine coordinate on the corresponding component of  $\Gamma$  as in Definition 3.1;
- (5)  $\hat{\phi}$  takes equal values at pairs of glued points  $P, Q \in \Gamma$ , for all  $\vec{t}$ :  $\hat{\phi}(P, \vec{t}) = \hat{\phi}(Q, \vec{t})$ ;
- (6) For each fixed  $\vec{t}$  the function  $\hat{\phi}(P, \vec{t})$  is meromorphic of degree  $\leq g$  in  $P$  on  $\Gamma \setminus \{P_0\}$ : for any fixed  $\vec{t}$  we have  $(\hat{\phi}(P, \vec{t})) + \mathcal{D}_{\text{vac}, \Gamma} \geq 0$  on  $\Gamma \setminus P_0$ , where  $(f)$  denotes the divisor of  $f$ . Equivalently, for any fixed  $\vec{t}$  on  $\Gamma \setminus \{P_0\}$  the function  $\hat{\phi}(\zeta, \vec{t})$  is regular outside the points of  $\mathcal{D}_{\text{vac}, \Gamma}$  and at each of these points either it has a first order pole or is regular;
- (7) For each  $P \in \Gamma \setminus \{P_0\}$  outside  $\mathcal{D}_{\text{vac}, \Gamma}$  the function  $\hat{\phi}(P, \vec{t})$  is regular in  $\vec{t}$  for all times.

**Definition 3.4. A real and regular vacuum wave function on  $\Gamma$  for the soliton data  $(\mathcal{K}, [A])$ :** Let  $\mathcal{K}$ ,  $\Gamma$  and  $\hat{\phi}(P, \vec{t})$  be as in Construction 3.1 and in Definition 3.3. Let  $[A] \in \mathcal{S}_{\mathcal{M}}^{TNN}$ . The function  $\hat{\phi}(P, \vec{t})$  is a real and regular vacuum wave function for the soliton data  $(\mathcal{K}, [A])$  if, at each Darboux point  $P_{i_r}^{(3)}$ ,  $r \in [k]$  and for all  $\vec{t}$ ,

$$(3.4) \quad \hat{\phi}(P_{i_r}^{(3)}, \vec{t}) \equiv f^{(r)}(\vec{t}),$$

where  $f^{(r)}(\vec{t})$ ,  $r \in [k]$ , generate the Darboux transformation for the soliton data.

**Theorem 3.1. Existence and uniqueness of a real and regular divisor and vacuum wave function on  $\Gamma$  satisfying appropriate boundary conditions.** Let  $(\mathcal{K}, [A])$  be given soliton data with  $[A] \in \mathcal{S}_{\mathcal{M}}^{TNN}$  of dimension  $g$ , and let  $\Gamma$  be as in Construction 3.1 with Darboux points  $\{P_{i_r}^{(3)}, r \in [k]\}$ . Then, we can fix an initial time  $\vec{t}_0$  such that to the following data  $(\mathcal{K}, [A]; \Gamma, P_0, P_{i_1}^{(3)}, \dots, P_{i_k}^{(3)}; \vec{t}_0)$  we associate

- (1) A **unique** real and regular degree  $g$  vacuum divisor  $\mathcal{D}_{\text{vac}, \Gamma}$  as in Definition 3.2,
- (2) A **unique** real and regular vacuum wave function  $\hat{\phi}(P, \vec{t})$  corresponding to this divisor satisfying Definitions 3.3 and 3.4.

Moreover, at the Darboux points,  $\hat{\phi}(P, \vec{t})$  satisfies

$$(3.5) \quad \hat{\phi}(P_{i_r}^{(3)}, \vec{t}) \equiv \frac{\sum_{l=1}^n A_l^r \exp(\theta_l(\vec{t}))}{\sum_{l=1}^n A_l^r \exp(\theta_l(\vec{t}_0))}, \quad r \in [k], \quad \forall \vec{t},$$

where  $f^{(r)}(\vec{t})$  are the generators of the Darboux transformation associated to the RRE representative matrix  $A$ .

We prove Theorem 3.1 in Section 5. More precisely, we construct a unique vacuum wave function on  $\Gamma$  using the algebraic recursion settled in Section 4.2. We first modify the Le-network moving the boundary sources to convenient inner vertexes, added in correspondence of the Darboux points in  $\Gamma$ . Then we assign a vector constructed in Section 4.1 to each vertical edge of this modified network and use the linear relations at the inner vertexes to extend this system of vectors to all its edges. We use this system of vectors to define a unique vacuum edge wave function (v.e.w.) satisfying the necessary boundary conditions. By construction, the linear relations at trivalent white vertexes define a degree  $g$  divisor with the required reality and regularity conditions (see Lemma 5.3). Finally, we construct the degree  $g$  real and regular vacuum wave function on  $\Gamma$  imposing that it takes the value of the normalized v.e.w. at the marked points (double points and Darboux points) which correspond to the edges (see Theorem 5.1).

**Definition 3.5.** *The dressing of the vacuum wave function on  $\Gamma$ . Let  $\Gamma$  and  $\hat{\phi}$  be as in Theorem 3.1 for given soliton data  $(\mathcal{K}, [A])$ . Then the corresponding **Darboux transformed wave function** is defined by:*

$$(3.6) \quad \psi(P, \vec{t}) = \mathfrak{D}\hat{\phi}(P, \vec{t}), \quad P \in \Gamma \setminus \{P_0\}, \quad \forall \vec{t},$$

where  $\mathfrak{D}$  is the  $k$ -th order ordinary differential operator associated to such soliton data as in (2.5). Let the initial condition  $\vec{t}_0$  be such that  $\mathfrak{D}\hat{\phi}(P, \vec{t}_0) \neq 0$  at all double points  $P \in \Gamma$ . We define the **normalized dressed wave function**  $\hat{\psi}(P, \vec{t})$  as

$$(3.7) \quad \hat{\psi}(P, \vec{t}) = \frac{\psi(P, \vec{t})}{\psi(P, \vec{t}_0)}.$$

We define the **normalized dressed divisor** as

$$(3.8) \quad \mathcal{D}_{\text{KP}, \Gamma} = \mathcal{D}_{\text{dr}, \Gamma} + (\psi(P, \vec{t}_0)).$$

where the non-effective divisor  $\mathcal{D}_{\text{dr}, \Gamma}$  is defined by

$$(3.9) \quad \mathcal{D}_{\text{dr}, \Gamma} = \mathcal{D}_{\text{vac}, \Gamma} + kP_0 - \sum_{r=1}^k P_{i_r}.$$

**Remark 3.6.** *For reducible soliton data  $[A]$  in  $Gr^{TNN}(k, n)$  with  $s$  isolated boundary sources we have two Darboux dressings: the reducible  $k$ -th order dressing operator and the reduced  $(k - s)$ -order dressing operator (see Remarks 2.1 and 2.2). The normalized dressed wave function is the same for both dressings, while the  $\mathcal{D}_{KP, \Gamma}$  divisor associated to the reducible dressing operator contains  $s$  extra points in the intersection of the finite ovals with  $\Gamma_0$ , so that we have more than one divisor point in some of the finite ovals. Therefore, in such case, in the Definition above we use the  $(k - s)$ -th order reduced dressing operator. The extra  $s$  divisor points may be interpreted as being originated from real and regular divisor data on regular  $\mathbb{M}$ -curves of genus  $g + s$  under the assumption that  $s$  ovals degenerate to points in the solitonic limit.*

**Lemma 3.1.** (1) *For any  $\vec{t}$  we have the following inequality on  $\Gamma \setminus P_0$ :*

$$(3.10) \quad (\psi(P, \vec{t})) + \mathcal{D}_{dr, \Gamma} \geq 0.$$

(2) *The number of poles minus the number of zeroes for  $\mathcal{D}_{dr, \Gamma}$  (counted with multiplicities, if necessary) at each finite oval is odd and at the infinite oval it is even.*

The first property follows directly from the definition of  $\psi(P, \vec{t})$ . The second statement simply follows from properties of the vacuum wave function constructed in Theorem 3.1, namely equation (3.4) in Definition 3.4, properties (3)-(4) in Definition 3.2 and formula (3.9).

**Lemma 3.2.** (1) *For any  $\vec{t}$  we have the following inequality on  $\Gamma \setminus P_0$ :*

$$(3.11) \quad (\hat{\psi}(P, \vec{t})) + \mathcal{D}_{KP, \Gamma} \geq 0.$$

(2) *The divisor  $\mathcal{D}_{KP, \Gamma}$  is effective and has degree  $g$ .*

(3) *All poles of  $\mathcal{D}_{KP, \Gamma}$  lie at the finite ovals, and each finite oval contains exactly one pole of  $\mathcal{D}_{KP, \Gamma}$ .*

The first statement follows immediately from the definition of  $\hat{\psi}(P, \vec{t})$  and  $\mathcal{D}_{KP, \Gamma}$ . The second statement follows immediately from (3.8). The third statement follows from the fact that  $\psi(P, \vec{t}_0)$  is real at all real ovals and from Lemma 3.1.

**Theorem 3.2.** *The effective divisor on  $\Gamma$ . Assume that  $\hat{\phi}$  is the real and regular vacuum wave function on  $\Gamma$  of Theorem 3.1 for the given soliton data  $(\mathcal{K}, [A])$ . Let  $\hat{\psi}$  be the normalized dressed wave function from Definition 3.5.*

*Then the divisor  $\mathcal{D}_{KP, \Gamma}$  is the KP divisor, and it satisfies the reality and regularity conditions of Definition 2.4 and  $\hat{\psi}$  is the KP wave function on  $\Gamma$  for the soliton data  $(\mathcal{K}, [A])$ . Moreover,*

the degree  $\mathfrak{d}$  of the effective pole divisor of  $\hat{\psi}$  coincides with the dimension of the positroid cell of  $[A]$ ,  $\mathfrak{d} = g$ .

The proof of the Theorem easily follows from Lemmas 3.1, 3.2 and Theorem 3.1. We remark that the Darboux transformation automatically creates the Sato divisor on  $\Gamma_0$ .

**Remark 3.7.**  $\mathcal{D}_{\text{KP},\Gamma}$  is the KP divisor on  $\Gamma(\mathcal{G}_{\text{red}})$ . In our construction each KP divisor point either belongs to  $\Gamma_0$  or to a copy of  $\mathbb{CP}^1$  represented by a trivalent white vertex. Below we prove that the value of the normalized KP wavefunction is constant with respect to the spectral parameter on each component corresponding to a bivalent vertex; therefore the elimination of bivalent vertexes doesn't affect the value of the normalized KP wavefunction on the  $\mathbb{CP}^1$  components corresponding to trivalent white vertexes and the position of the KP divisor points is unaffected by this reduction.

**Remark 3.8. Invariance of the divisor** In [4] we prove that  $\hat{\psi}$  and  $\mathcal{D}_{\text{KP},\Gamma}$  do not depend neither on the orientation of the network nor on the choice of the position of the Darboux points.

#### 4. A SYSTEM OF VECTORS ON THE LE-NETWORK

In the previous Section we constructed the spectral curve  $\Gamma$  associated with the given positroid cell. The next step of the main construction is the computation of the divisor corresponding to a given point  $[A]$  of this cell. At this aim, we first compute the values of the vacuum and dressed wave functions at all marked points of the curve using an algebraic procedure based on the construction of a system of vectors at the edges of the Le-network.

In [3], we introduced an analogous algebraic construction on the main cell: we related a specific representation of the rows of the banded matrix in  $[A] \in Gr^{\text{TP}}(k, n)$  to the leading order behavior in the parameter  $\xi$  of the vacuum wave function at double points and Darboux points. Here we use an excessive number of copies of  $\mathbb{CP}^1$  to relate the system of vectors to the **exact behavior** of both the vacuum and dressed wave functions at the marked points. Moreover, both the vectors and the wave functions satisfy linear relations at the vertexes of the Le-network which are used to construct both the vacuum and the dressed divisors.

In this section we first use the Le-network  $\mathcal{N}$  to express each row of the RREF representative matrix as a linear combination with positive coefficients of a minimal number of some basic row vectors. This construction is a generalization of the Principal Algebraic Lemma in [3] and easily follows from [61]. Then, in Section 4.2 we present a recursive construction of these basic

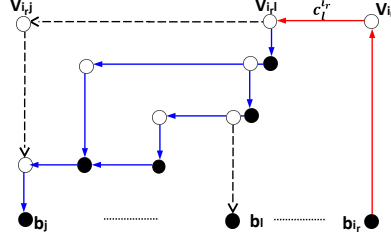


FIGURE 7. The coefficient  $c_{l^r}^{i_r}$  is the weight of the directed path from the source  $b_{i_r}$  to the white internal vertex  $V_{i_r, l}$ , while  $E_j^{(r)}[l]$ , the  $j$ -th component of  $E^{(r)}[l]$ , has absolute value equal to the sum of the weights of all the directed paths which start downwards at the internal vertex  $V_{i_r, l}$  and zig-zag to the boundary sink  $b_j$ . The sign of  $E_j^{(r)}[l]$  is equal to the number of boundary sources  $b_{i_s}$  with  $i_s \in ]i_r, j[$ .

vectors, generalizing the corresponding theorem in [3]. In [4], we generalize this construction to any planar trivalent bipartite network  $\mathcal{N}$  in the disk representing a given point of  $Gr^{\text{TNN}}(k, n)$ .

**4.1. Representation of the rows of the RREF matrix using the Le-tableau.** The notations used in this section are the same as in the Appendix:  $\mathcal{N} = (\mathcal{G}, T)$  is the planar bipartite trivalent acyclically oriented network associated to the Le-tableau  $T$  for the given point  $[A] \in Gr^{\text{TNN}}(k, n)$  and  $A$  is the representative matrix in RREF of  $[A]$ .  $I$  is the lexicographically minimal base in the associated matroid and  $\bar{I} = [n] \setminus I$ . Each row  $r$  of  $A$  may be expressed as a linear combination with **positive coefficients**  $c_{l_s}^r$  of  $N_r + 1$  vectors  $E^{(r)}[l_s]$ ,  $s \in [0, N_r]$ , computed using  $\mathcal{N}$ . Each coefficient  $c_{l_s}^r$  is the weight of the directed path from the boundary source  $b_{i_r}$  to the internal white vertex  $V_{i_r, l_s}$ . The absolute value of the  $j$ -th component of the vector  $E^{(r)}[l_s]$  is the sum of the weights of all possible paths starting downwards at  $V_{i_r, l_s}$  and zig-zagging to the destination  $b_j$ , while its sign depends on the number of boundary sources passed before reaching the destination (see Lemma 4.1).

Let us fix  $r \in [k]$  and let  $i_r \in I$  be the corresponding pivot index. Let  $l \in \bar{I}$  such that the box  $B_{i_r, l}$  has index  $\chi_l^{i_r} = 1$  and let  $V_{i_r, l}$  be the corresponding white vertex in  $\mathcal{N}_l$ . Let us consider all directed paths  $P$  starting at  $b_{i_r}$ , moving horizontally from  $V_{i_r}$  to  $V_{i_r, l}$ , moving downwards at  $V_{i_r, l}$  and then zigzagging towards any possible destination  $j \in \bar{I}$ . Necessarily  $j \geq l$ ; moreover, for  $l = j$ , there is exactly one such path from  $b_{i_r}$  to  $b_l$ . For  $j \in \bar{I}$  and  $j \geq l$ , let us define

$$(4.1) \quad \begin{aligned} \mathcal{P}_{l_j}^{(r)} &= \{ P_{l_j}^{(r)} : b_{i_r} \mapsto b_j : P_{l_j}^{(r)} \text{ moves downwards at the white vertex } V_{i_r, l} \}, \\ \bar{\mathcal{P}}_{l_j}^{(r)} &= \{ \bar{P}_{l_j}^{(r)} : V_{i_r, l} \mapsto b_j : \bar{P}_{l_j}^{(r)} \text{ moves downwards at the white vertex } V_{i_r, l} \}, \end{aligned}$$

and denote by  $P_{i_r l}$  the path from the source  $b_{i_r}$  to the white vertex  $V_{i_r l}$ . Then for any  $P_{lj}^{(r)} \in \mathcal{P}_{lj}^{(r)}$  there exists a unique path  $\bar{P}_{lj}^{(r)} \in \bar{\mathcal{P}}_{lj}^{(r)}$  such that  $P_{lj}^{(r)} = P_{i_r l} \sqcup \bar{P}_{lj}^{(r)}$ . Define

$$(4.2) \quad c_l^i \equiv \prod_{e \in P_{i_r l}} w_e.$$

Then the weight of the path  $P_{lj}^{(r)}$  is  $w(P_{lj}^{(r)}) = \prod_{e \in P_{lj}^{(r)}} w_e = c_l^i \left( \prod_{e \in \bar{P}_{lj}^{(r)}} w_e \right) = c_l^i w(\bar{P}_{lj}^{(r)})$  and, for any  $j \in \bar{I}$ ,  $j > i_r$ , the matrix entry in reduced row echelon form as in (A.2), may be re-expressed as

$$A_j^{r_i} = (-1)^{\sigma_{i_r j}} \sum_{s=1}^{N_r} c_{l_s}^i \sum_{\substack{\bar{P}_{l_s j}^{(r)} \in \bar{\mathcal{P}}_{l_s j}^{(r)}}} w(\bar{P}_{l_s j}^{(r)}) = (-1)^{\sigma_{i_r j}} \sum_{l \leq j} c_l^i \sum_{\substack{\bar{P}_{lj}^{(r)} \in \bar{\mathcal{P}}_{lj}^{(r)}}} w(\bar{P}_{lj}^{(r)}),$$

where  $\sigma_{i_r j}$  is the number of boundary sources in  $]i_r, j[$ . In [61] the matrix elements  $A_j^{r_i}$  are computed using columns instead of rows.

Finally, for any  $r \in [k]$ ,  $i_r \in I$ ,  $l \in \bar{I}$ ,  $l > i_r$ , and such that  $\chi_{l_s}^{i_r} = 1$ , let us define the row vector  $E^{(r)}[l] = (E_1^{(i)}[l], \dots, E_n^{(i)}[l])$ , with

$$(4.3) \quad E_j^{(r)}[l] = \begin{cases} 0 & \text{if } j < l \text{ or } j \in I, \\ (-1)^{\sigma_{i_r j}} \sum_{\substack{\bar{P}_{lj}^{(r)} \in \bar{\mathcal{P}}_{lj}^{(r)}}} w(\bar{P}_{lj}^{(r)}) & \text{if } l, j \in \bar{I} \text{ and } j \geq l. \end{cases}$$

In the expression above the entry  $E_j^{(r)}[l] = 0$  if there is no path moving downwards at the vertex  $V_{i_r l}$  and reaching destination  $b_j$ . Finally we associate to the boundary source a vector

$$(4.4) \quad E^{(r)}[i_r] = (0, \dots, 0, 1, 0, \dots, 0),$$

with non zero entry in the  $i_r$ -th column. Then the following Lemma holds true.

**Lemma 4.1.** *Let  $A$  be the reduced row echelon form matrix representing a given point in the matroid stratum  $\mathcal{S}_{\mathcal{M}}^{TNN} \subset Gr^{TNN}(k, n)$  and let  $D$  be the corresponding Le-diagram. Let  $E^{(r)}[i]$ ,  $E^{(r)}[l]$ ,  $c_l^i$  as in (4.2), (4.3) and (4.4), with  $r \in [k]$ ,  $i_r \in I$ ,  $l \in \bar{I}$ , such that the box  $B_{i_r l}$  is filled by 1. Then, the  $r$ -th row of  $A$  is*

$$(4.5) \quad A[r] = E^{(r)}[i_r] + \sum_{s=1}^{N_r} c_{l_s}^r E^{(r)}[l_s],$$

where the sum runs over the indexes  $l_s \in \bar{I}$  such that the index in (A.4) is  $\chi_{l_s}^{i_r} = 1$ .

The proof is trivial and is omitted. Let us remark that the vectors  $E^{(r)}[i_r]$ ,  $E^{(r)}[l_s]$ ,  $s \in N_r$ , form a minimal system of vectors to represent the  $r$ -th row of the reduced row echelon matrix.

**4.2. Recursive construction of the row vectors  $E^{(r)}[l]$  using the Le-diagram.** In Theorem 4.1 we provide a recursive representation for the above system of vectors using the Le-tableau starting from the last row ( $r = k$ ) and moving upwards till the first row ( $r = 1$ ).

For any fixed  $r \in [k]$ , we first complete the system of vectors introduced in the previous section to a convenient basis in  $\mathbb{R}^n$ , given by the rows of  $n \times n$  matrix  $\hat{E}^{(r)}$ . For  $r = k$ , we use the canonical basis in  $\mathbb{R}^n$ . We pass from the basis associated to the  $r$ -th row to the one associated to the  $(r - 1)$ -th row applying a transition matrix  $C^{[r-1,r]}$ :  $\hat{E}^{(r-1)} = C^{[r-1,r]} \hat{E}^{(r)}$ . Each transition matrix  $C^{[r-1,r]}$  keeps track of empty and non-empty boxes of the  $r$ -th row of the Le-tableau, and is upper triangular by definition. The choice of signs in  $C^{[r-1,r]}$  in (4.6) keeps track of the sign changes when passing a pivot column. We also complete each set of coefficients  $c_l^r$  in (4.2) to a row vector  $\hat{c}^{(r)}$ , with  $l$  indexing the column position.

This construction is a corollary to the Lindström lemma in the case of acyclic graphs and, for points  $[A] \in Gr^{\text{TP}}(k, n)$ , is also the combinatorial version of the recursive algebraic construction in [3] for a different choice of the basic vectors and therefore of the representative matrix  $A$ . In [4] we give general rules to construct well defined systems of vectors on any network and for any orientation.

Theorem 4.1 is used in section 5.1 to define a vacuum edge wave function and its dressing on the bipartite Le-network  $\mathcal{N}$ . Such vacuum edge wave function (respectively its dressing)

- (1) rules the behavior of the vacuum wave function (respectively the dressed wave function) on  $\Gamma$  at all marked points;
- (2) satisfies linear relations at the inner vertexes of  $\mathcal{N}$  which are used to detect the position of the vacuum (resp. dressed) divisor points.

**Theorem 4.1. (The recursive algebraic construction)** *Let  $[A] \in \mathcal{S}_{\mathcal{M}}^{TNN} \subset Gr^{TNN}(k, n)$  with pivot set  $I = \{1 \leq i_1 < i_2 < \dots < i_k \leq n\}$ . Let  $D$  and  $\mathcal{N}$  respectively be the Le-diagram and its acyclically oriented bipartite Le-network. For any  $r \in [k]$ ,  $j \in \bar{I}$ , let the index  $\chi_j^{i_r}$  be as in (A.4). Let us define the following collections of  $n \times n$  invertible matrices  $\hat{E}^{(r)}$ ,  $n \times n$  transition matrices  $C^{[r-1,r]}$  and row vectors  $\hat{c}^{(r)}$ ,  $r \in [k]$ , associated to the graph of the network:*

- (1)  $\hat{E}^{(k)}$  is the  $n \times n$  identity matrix and we denote its row vectors as  $\hat{E}^{(k)}[l]$ ,  $l \in [n]$ ;



(2) For  $r \in [k]$ , define the  $n \times n$  transition matrix  $C^{[r-1, r]}$  as follows:

$$(4.6) \quad C_j^{[r-1, r], l} = \begin{cases} \delta_j^l, & \text{if } l \in [1, i_r[, \quad j \in [n], \\ -1 & \text{if } l = j = i_r, \\ -\hat{w}_{i_r j}^{(r)}, & \text{if } l = i_r, \quad j \in ]i_r, n] \text{ and } \chi_j^{i_r} = 1, \\ -\hat{w}_{lj}^{(r)}, & \text{if } l, j \in \bar{I} \cap ]i_r, n], \quad j \geq l, \quad \chi_j^{i_r} \chi_l^{i_r} = 1, \\ -\delta_j^l, & \text{if } l \in \bar{I} \cap ]i_r, n], \quad \chi_l^{i_r} = 0, \quad j \in [n], \\ -\delta_j^l, & \text{if } l \in I \cap ]i_r, n], \quad j \in [n], \\ 0 & \text{otherwise,} \end{cases}$$

where

- (a) for  $l, j \in \bar{I} \cap ]i_r, n], j \geq l$ ,  $\hat{w}_{lj}^{(r)}$  is the weight of the directed horizontal path from the black vertex  $V'_{i_r l}$  to the white vertex  $V_{i_r j}$ . In particular  $\hat{w}_{ll}^{(r)} = 1$ ;
- (b) for  $l = i_r$  and  $j \in \bar{I}$ ,  $\hat{w}_{i_r j}^{(r)}$  is the weight of the directed horizontal path from the vertex  $V_{i_r}$  to the white vertex  $V_{i_r j}$ .

(3) The matrices  $\hat{E}^{(r-1)}$  are recursively computed as  $r$  decreases from  $k$  to 2, by

$$(4.7) \quad \hat{E}^{(r-1)} = C^{[r-1, r]} \hat{E}^{(r)}.$$

(4) For any  $r \in [k]$ , the  $l$ -element of the row vector  $\hat{c}^{(r)}$ ,  $l \in [n]$ , is

$$(4.8) \quad \hat{c}_l^{(r)} = \begin{cases} 1 & \text{if } l = i_r, \\ c_l^r & \text{if } \chi_l^{i_r} = 1, \\ 0 & \text{otherwise,} \end{cases}$$

with  $c_l^r$  as in (4.2).

Then

(1) For  $r \in [k-1]$   $\hat{E}^{(r)}$  is the  $n \times n$  matrix such that

$$(4.9) \quad \hat{E}^{(r)}[l] = \begin{cases} \hat{E}^{(k)}[l] & \text{if } l \leq i_r, \\ (-1)^{\sigma_{sr}} A[s] & \text{if } l = i_s, \text{ and } s \in ]r, k], \\ E^{(r)}[l] & \text{if } l \in \bar{I} \cap ]i_r, n], \text{ and } \chi_l^r = 1, \end{cases}$$

with  $E^{(r)}[l]$  as in (4.3) and  $\sigma_{sr} = \#\{i_t \in I, r \leq t < s\}$ ;

(2) For any  $r \in [k]$ ,

$$(4.10) \quad A[r] = \sum_{l=1}^n \hat{c}_l^r \hat{E}^{(r)}[l] \equiv E^{(r)}[i_r] + \sum_{s=1}^{N_r} c_{l_s}^r E^{(r)}[l_s],$$

where the second sum is over the indexes such that  $\chi_{l_s}^{i_r} = 1$ .

**Remark 4.1. Changing the orientation of the graph** *Any change of orientation in  $\mathcal{N}$  corresponds to the composition of elementary changes of orientation [61]. The latter either correspond to a change of the base in the matroid  $\mathcal{M}$  of  $[A]$  or to a change of orientation in a cycle of the graph. We postpone to [4] a thorough explanation of how the system of vectors on any given network representing  $[A]$  is effected by such elementary changes and the proof that both the normalized dressed wave function and the effective KP divisor are not affected by them.*

*Proof.* (4.10) follows immediately from Lemma 4.1, (4.8) and (4.9).

The first statement in (4.9),  $\hat{E}^{(r)}[l] = \hat{E}^{(k)}[l]$  for  $l \leq i_r$ ,  $r \in [k]$  is trivial by definition of the transition matrix (4.6). The remaining statements in (4.9) follow by induction in the index  $r$  as it decreases from  $k$  to 1. Indeed, for  $r = k$ , the transition matrix  $C^{[k-1,k]}$

- (1) Leaves invariant all canonical basis vectors  $\hat{E}^{(k)}[l]$  for all  $l < i_k$ ;
- (2) Transforms the canonical basis vector  $\hat{E}^{(k)}[i_k]$  to  $-A[k]$ , if  $l = i_k$ ;
- (3) Changes the sign of the canonical basis vector,  $\hat{E}^{(k-1)}[l] = -\hat{E}^{(k)}[l]$ , if  $l \in \bar{I} \cap ]i_k, n]$  and  $\chi_l^{i_k} = 0$ ;
- (4) Acts untrivially only if  $l \in \bar{I} \cap ]i_k, n]$  and  $\chi_l^{i_k} = 1$ . In such case, the components of  $\hat{E}^{(k-1)}[l]$  are transformed to

$$\hat{E}_j^{(k-1),l} = \begin{cases} 0 & \text{if } j < l, \\ -1 & \text{if } j = l, \\ 0 & \text{if } j > l \text{ and } \chi_j^{i_k} = 0, \\ -\hat{w}_{lj}^{(k)} & \text{if } j > l \text{ and } \chi_j^{i_k} = 1. \end{cases}$$

It is straightforward to verify that  $\hat{E}^{(k-1)}[l] = E^{(k-1)}[l]$ , if  $l = i_{k-1}$  or  $\chi_l^{i_{k-1}} = 1$ , for  $l \geq i_{k-1}$ . Indeed if both  $\chi_l^{i_{k-1}} = 1$  and  $\chi_l^{i_k} = 1$ , the white vertex  $V_{i_{k-1}l}$  is joined to the black vertex  $V'_{i_k l}$  by an edge of weight 1 so that by definition  $\hat{E}^{(k-1)}[l] = E^{(k-1)}[l]$ . If  $\chi_l^{i_{k-1}} = 1$  and  $\chi_l^{i_k} = 0$ , the white vertex  $V_{i_{k-1}l}$  is joined to the boundary vertex  $b_l$  by an edge of unit weight and  $\hat{E}^{(k-1)}[l] = E^{(k-1)}[l]$ .

Let us now suppose to have verified (4.9), for any  $s \in [r, k]$  and let's verify it for  $s = r - 1$ . By definition

$$(4.11) \quad \hat{E}^{(r-1)} = C^{[r-1,r]} \hat{E}^{(r)} = C^{[r-1,r]} C^{[r,r+1]} \hat{E}^{(r+1)} = \dots = \left( \prod_{s=r}^k C^{[s-1,s]} \right) \hat{E}^{(k)}.$$

Let  $l \in \bar{I} \cap ]i_{r-1}, n]$  be fixed. If  $\chi_l^{i_{r-1}} = 0$ , then there is no contribution to  $A[r-1]$  from the vector  $\hat{E}^{(r-1)}[l]$  since the coefficient  $\hat{c}_l^{r-1} = 0$ . Suppose now that  $\chi_l^{i_{r-1}} = 1$  and consider the

set  $S = \{s \in [r, k] : \chi_l^{i_s} = 1\}$ . If  $S = \emptyset$ , then the white vertex  $V_{i_{r-1}l}$  is joined directly to the boundary sink  $b_l$  by an edge of unit weight and

$$\hat{E}^{(r-1)}[l] = (-1)^{k-r+1} \hat{E}^{(k)}[l] = (-1)^{k-r+1} E^{(k)}[l] = E^{(r-1)}[l].$$

Otherwise, let  $\bar{s} = \min S$ . In this case moving downwards from the white vertex  $V_{i_{r-1}l}$  the first black vertex that we meet is  $V'_{i_{\bar{s}}l}$  and such edge has unit weight. Then, using (4.11), we have

$$\hat{E}^{(r-1)}[l] = (-1)^{\bar{s}-r+1} \hat{E}^{(\bar{s})}[l] = (-1)^{\bar{s}-r+1} E^{(\bar{s})}[l] = E^{(r-1)}[l].$$

Finally let  $l = i_r$ . In such case

$$\hat{E}^{(r-1)}[i_r] = C^{[r-1,r]}[i_r] \hat{E}^{(r)} = - \sum_{j=1}^n \tilde{c}_j^r \hat{E}^{(r)}[j] = -A[r].$$

since, by definition  $C_j^{[r-1,r],i_r} = -\tilde{c}_j^r$  and  $\tilde{c}_j^r$  is non zero if and only if  $j = i_r$  or  $j \in \bar{I} \cap ]i_r, n]$  is such that  $\chi_j^{i_r} = 1$ .  $\square$

**Remark 4.2.** *Comparison with the algebraic construction in [3] Lemma 4.1 and Theorem 4.1 generalize the algebraic construction in [3] for points in  $Gr^{TP}(k, n)$  to any point in  $Gr^{TNN}(k, n)$ . The main difference is in the choice of the representative matrix: here  $A$  is the RREF matrix while in [3] we use a matrix in banded form.*

**Example 4.1.** *Let us apply Theorem 4.1 to the Le-network in Figure 21 representing Example A.2.  $\hat{E}^{(4)} = Id_{9 \times 9}$ , the only non-zero coefficients associated to the forth row of  $A$  are  $\hat{c}_7^4 = 1$ ,  $\hat{c}_8^4 = w_{78}$  and clearly  $A[4] = \hat{c}^4 \hat{E}^{(4)}$ . Then*

$$\hat{E}^{(3)} \equiv C^{[3,4]} = \begin{pmatrix} I_{6 \times 6} & 0_{6 \times 3} \\ & -1 & -w_{78} & 0 \\ 0_{3 \times 6} & 0 & -1 & 0 \\ & 0 & 0 & -1 \end{pmatrix},$$

where  $0_{i \times j}$  is the  $(i \times j)$  null matrix, while  $I_{l \times l}$  is the  $(l \times l)$  identity matrix. The third row coefficient vector is  $\hat{c}^3 = (0, 0, 0, 1, w_{45}, w_{45}w_{46}, 0, w_{45}w_{46}w_{48}, w_{45}w_{46}w_{48}w_{49})$ , and  $A[3] = \hat{c}^3 \hat{E}^{(3)}$ . The transition matrix from the third to the second row  $C^{[2,3]}$ , the new basis vectors  $\hat{E}^{(2)}$

and the coefficient vector  $\hat{c}^2$  of the second row respectively are

$$C^{[2,3]} = \begin{pmatrix} I_{3 \times 3} & 0_{3 \times 6} \\ 0_{6 \times 3} & \begin{pmatrix} -1 & -w_{45} & -w_{45}w_{46} & 0 & -w_{45}w_{46}w_{48} & -w_{45}w_{46}w_{48}w_{49} \\ 0 & -1 & -w_{46} & 0 & -w_{46}w_{48} & -w_{46}w_{48}w_{49} \\ 0 & 0 & -1 & 0 & -w_{48} & -w_{48}w_{49} \\ 0 & 0 & 0 & -1 & 0 & 0 \\ 0 & 0 & 0 & 0 & -1 & -w_{49} \\ 0 & 0 & 0 & 0 & 0 & -1 \end{pmatrix} \end{pmatrix},$$

$$\hat{E}^{(2)} = C^{[2,3]} \hat{E}^{(3)} = \begin{pmatrix} Id_{3 \times 3} & 0_{3 \times 6} \\ 0_{6 \times 3} & \begin{pmatrix} -1 & -w_{45} & -w_{45}w_{46} & 0 & w_{45}w_{46}w_{48} & w_{45}w_{46}w_{48}w_{49} \\ 0 & -1 & -w_{46} & 0 & w_{46}w_{48} & w_{46}w_{48}w_{49} \\ 0 & 0 & -1 & 0 & w_{48} & w_{48}w_{49} \\ 0 & 0 & 0 & 1 & w_{78} & 0 \\ 0 & 0 & 0 & 0 & 1 & w_{49} \\ 0 & 0 & 0 & 0 & 0 & 1 \end{pmatrix} \end{pmatrix},$$

$\hat{c}^2 = (0, 1, w_{23}, 0, w_{23}w_{25}, 0, 0, 0, 0)$ , and  $A[2] = \hat{c}^2 \hat{E}^{(2)}$ . Finally, the transition matrix from the second to the first row  $C^{[1,2]}$ , the new basis vectors  $\hat{E}^{(1)}$  and the coefficient vector  $\hat{c}^1$  of the first row, respectively, are

$$C^{[1,2]} = \begin{pmatrix} \begin{pmatrix} 1 & 0 & 0 & 0 & 0 \\ 0 & -1 & -w_{23} & 0 & -w_{23}w_{25} \\ 0 & 0 & -1 & 0 & -w_{25} \\ 0 & 0 & 0 & -1 & 0 \\ 0 & 0 & 0 & 0 & -1 \end{pmatrix} & 0_{5 \times 4} \\ 0_{5 \times 1} & -Id_{4 \times 4} \end{pmatrix},$$

$$\hat{E}^{(1)} = C^{[1,2]} \hat{E}^{(2)} = \begin{pmatrix} 1 & 0 & 0 & 0 & 0 & 0 & 0 & 0 & 0 \\ 0 & -1 & -w_{23} & 0 & w_{23}w_{25} & w_{23}w_{25}w_{46} & 0 & -w_{23}w_{25}w_{46}w_{48} & -w_{23}w_{25}w_{46}w_{48}w_{49} \\ 0 & 0 & -1 & 0 & w_{25} & w_{25}w_{46} & 0 & -w_{25}w_{46}w_{48} & -w_{25}w_{46}w_{48}w_{49} \\ 0 & 0 & 0 & 1 & w_{45} & w_{45}w_{46} & 0 & -w_{45}w_{46}w_{48} & -w_{45}w_{46}w_{48}w_{49} \\ 0 & 0 & 0 & 0 & 1 & w_{46} & 0 & -w_{46}w_{48} & -w_{46}w_{48}w_{49} \\ 0 & 0 & 0 & 0 & 0 & 1 & 0 & -w_{48} & -w_{48}w_{49} \\ 0 & 0 & 0 & 0 & 0 & 0 & -1 & -w_{78} & 0 \\ 0 & 0 & 0 & 0 & 0 & 0 & 0 & -1 & -w_{49} \\ 0 & 0 & 0 & 0 & 0 & 0 & 0 & 0 & -1 \end{pmatrix},$$

$\hat{c}^1 = (1, 0, 0, 0, w_{15}, w_{15}w_{16}, 0, 0, w_{15}w_{16}w_{19})$ , and  $A[1] = \hat{c}^1 \hat{E}^{(1)}$ .

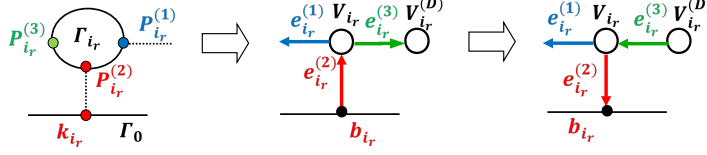


FIGURE 8. The modified graph  $\mathcal{N}'$  is obtained adding an edge  $e_{i_r}^{(3)}$  at each pivot vertex  $V_{i_r}$  and a white vertex  $V_{i_r}^{(D)}$ . The orientation in  $\mathcal{N}'$  is the same as in the initial network  $\mathcal{N}$  except at the edge  $e_{i_r}^{(2)}$ .

## 5. PROOF OF THEOREM 3.1 ON $\Gamma$

Throughout this Section we fix the KP regular soliton data, i.e.  $n$  ordered real phases  $\mathcal{K} = \{\kappa_1 < \dots < \kappa_n\}$  and  $[A] \in \mathcal{S}_{\mathcal{M}}^{\text{TNN}} \subset Gr^{\text{TNN}}(k, n)$ .  $I$  is the lexicographically minimal base of  $\mathcal{M}$ , and  $D$  and  $\mathcal{N}$  respectively are the Le-diagram and the acyclically oriented bipartite Le-network representing  $[A]$ , see [61] and, also, Appendix A. Finally,  $\Gamma$  is the curve associate to the Le-graph as in Construction 3.1.

The proof of Theorem 3.1 goes through several steps. First, we modify the Le-network by adding an edge and an internal vertex in correspondence of each Darboux point in  $\Gamma$  and transforming the boundary sources into boundary sinks (see Figure 8). After this transformation, on each component  $\Gamma_{i_r}$ ,  $r \in [k]$ , the Darboux point  $P_{i_r}^{(3)} \in \Gamma_{i_r}$  corresponds to the edge  $e_{i_r}^{(3)}$  added at  $V_{i_r}$ . The vectors  $E^{(r)}[l]$  introduced in the previous Section are then naturally assigned to the vertical edges of this modified network.

Then, we extend the system of vectors to all horizontal edges of the modified Le-network using the linear relations at internal vertexes. In particular, the vector on  $e_{i_r}^{(3)}$  is the  $r$ -th row of the RREF matrix. We use this system of vectors to define the vacuum and dressed edge wave functions on the modified Le-network and the linear relations to assign a network divisor number (vacuum or dressed) at each trivalent white vertex.

**Remark 5.1.** *The edge vectors, the vacuum edge wave function and its dressing satisfy a consistent system of linear relations at the black and white vertexes (see Definition 5.2 and Figure 9), which are of the same type as those imposed by momentum conservation at trivalent vertexes of on-shell diagrams in [7, 8] (formulas (4.54) and (4.55) in [7]). In [4], we generalize the construction of edge vectors and edge wave functions to any network representing  $[A]$  in Postnikov class.*

We uniquely define the vacuum (resp. dressed) wave function on  $\Gamma$  imposing that:

- (1) At each marked point it coincides with the normalized vacuum (resp. dressed) edge wave function;
- (2) It coincides with the normalized vacuum (resp. dressed) Sato wave function on  $\Gamma_0$ ;
- (3) It is meromorphic of degree 1 on each component corresponding to a trivalent white vertex;
- (4) It is constant with respect to the spectral parameter at each other component.

By construction, the coordinate the divisor point belonging to a given component is equal to the corresponding network divisor number for the corresponding vertex. Finally, we check that we have the correct number of divisor points at each oval.

**Definition 5.1.** *The planar oriented trivalent bipartite network  $\mathcal{N}'$ : Denote  $\mathcal{N}'$  the network obtained from  $\mathcal{N}$  adding a unit edge  $e_{i_r}^{(3)}$  at each pivot vertex  $V_{i_r}$  in the position corresponding to the Darboux point  $P_{i_r}^{(3)} \in \Gamma_{i_r}$  and let  $V_{i_r}^{(D)}$  be the white vertex at the other end of  $e_{i_r}^{(3)}$ . Such move corresponds to Move (M2) - unicolored edge contraction/uncontraction and still represents the same point in the Grassmannian [61]. Then orient all edges in  $\mathcal{N}'$  as in  $\mathcal{N}$  except the edges  $e_{i_r}^{(2)}$ , which point from  $V_{i_r}$  to  $b_{i_r}$ , and  $e_{i_r}^{(3)}$ ,  $r \in [k]$ , which point from  $V_{i_r}^{(D)}$  to  $V_{i_r}$ , for any  $r \in [k]$  (see Figure 8).*

**Remark 5.2. Data and notations.** *From now on we use the modified network  $\mathcal{N}'$  with the orientation as in Definition 5.1 and settle the following notations:*

- (1) *The dimension of the positroid cell is  $g$ ;*
- (2)  *$N_r$ ,  $r \in [k]$ , is the number of filled boxes in the row  $r$  of the Le-tableaux of  $A$ ,  $\chi_j^i \in \{0, 1\}$  is the index of the box  $B_{i,j}$  (see (A.3) and (A.4));*
- (3) *The pivot indexes are denoted  $1 \leq i_1 < \dots < i_k \leq n$  and, for any  $r \in [k]$ ,  $1 \leq j_1 < j_2 < \dots < j_{N_r} \leq n$  are the non-pivot indexes of the boxes  $B_{i_r, j_s}$  of index  $\chi_{j_s}^{i_r} = 1$ ,  $s \in [N_r]$ ;*
- (4) *The index  $j_0 \equiv 0$  is associated to the vertexes,  $V_{i_r, 0} \equiv V_{i_r}$ , and to any quantity referring to them;*
- (5) *The edges  $e_{i_r j_l}^{(m)}$ ,  $m \in [3]$ , are enumerated with the indexes of its incident white vertex  $V_{i_r j_l}$ ,  $r \in [k]$  and  $l \in [0, N_r]$  (see Figures 3 and 8). Finally, the vertexes  $V_{i_r j_{N_r}}$  have two edges which we label  $e_{i_r j_l}^{(2)}$  and  $e_{i_r j_l}^{(3)}$ ;*
- (6) *The families of matrices  $\hat{E}^{(r)}$  and vectors  $\hat{c}^{(r)}$ ,  $r \in [k]$ , are as in Theorem 4.1;*

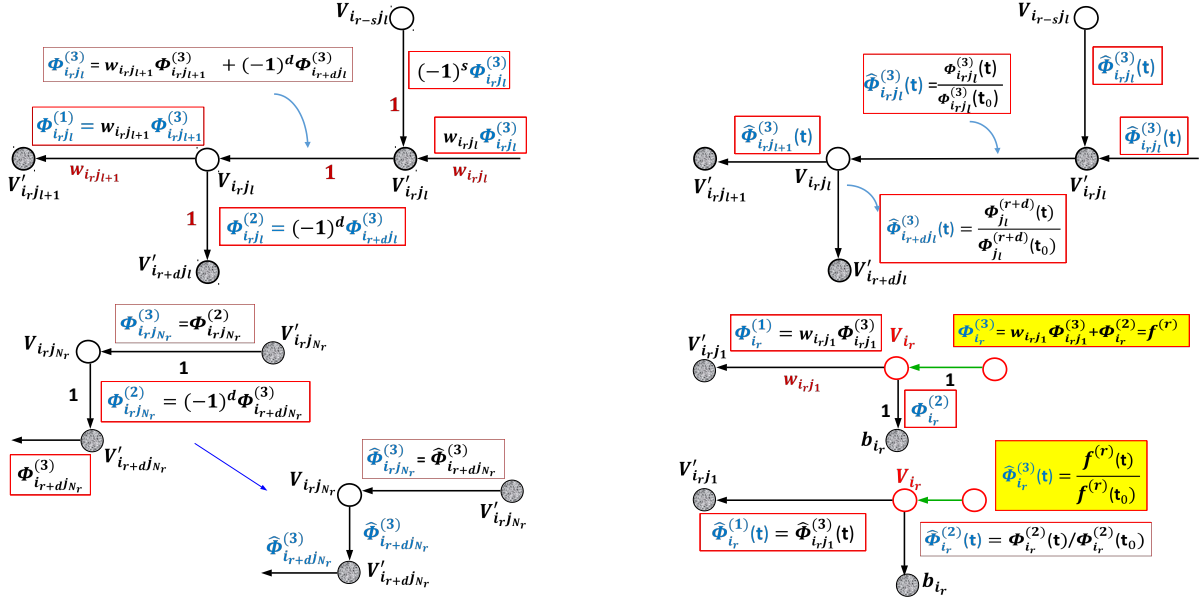


FIGURE 9. The linear relations for the vacuum edge wave function  $\Phi_{i_r j_l}^{(m)}(\vec{t})$  at white and black vertexes [top, left]. The normalized v.e.w.  $\hat{\Phi}_{i_r j_l}^{(m)}(\vec{t})$  takes the same value at all the edges at a given black vertex  $V'_{i_r j_l}$  and different values at the edges at a given trivalent white vertex  $V_{i_r j_l}$  [top right]. The same linear relations also hold for the dressed edge wave function. The same at the bivalent white vertex  $V_{i_r j_{N_r}}$  [bottom, left] and at the vertex  $V_{i_r}$ ,  $i_r \in I$  [bottom, right].

- (7)  $\mathfrak{E}_\theta(\vec{t}) = (e^{\theta_1(\vec{t})}, \dots, e^{\theta_n(\vec{t})})$ , where  $\theta_j(\vec{t}) = \sum_{l \geq 1} \kappa_j^l t_l$  and  $\vec{t} = (t_1 = x, t_2 = y, t_3 = t, t_4, \dots)$  are the KP times, and  $\prec \cdot, \succ$  denotes the usual scalar product;
- (8) On each component of  $\Gamma$ ,  $\zeta$  is the coordinate of Definition 3.1.

In the statements of the Theorems and in the Definitions below we shall not explicitly mention the above data.

**5.1. Vacuum and dressed edge wave functions on the modified Le-network.** We now define a system of vectors  $\mathfrak{E}_{i_r j_l}^{(m)}$  on the edges of  $\mathcal{N}'$  using the vectors introduced in Section 4. First of all, in  $\mathcal{N}'$ , for each fixed  $r \in [k]$  and  $l \in [0, N_r]$  we assign the row vector  $E^{(r)}[j_l]$  to the vertical edge  $e_{i_r j_l}^{(2)}$  at the white vertex  $V_{i_r j_l} \in \mathcal{N}'$ :  $\mathfrak{E}_{i_r j_l}^{(2)} \equiv E^{(r)}[j_l]$ . We then assign a vector also at each horizontal edge using linear relations at inner black and white vertexes (see Definition 5.2). The vacuum edge wave function  $\Phi_{ij}^{(m)}(\vec{t})$  at the edge  $e_{ij}^{(m)} \in \mathcal{N}'$  is just the product of the edge vector  $\mathfrak{E}_{ij}^{(m)}$  with the vector  $\mathfrak{E}_\theta(\vec{t})$ :  $\Phi_{ij}^{(m)}(\vec{t}) = \mathfrak{E}_{ij}^{(m)} \prec \mathfrak{E}_\theta(\vec{t}) \succ$ .

**Definition 5.2.** Edge vectors (e.v.) and vacuum edge wave function (v.e.w.) on  $\mathcal{N}'$ .

Let the soliton data and the notations be fixed as in Remark 5.2. To each edge of  $\mathcal{N}'$ , we associate an edge vector (e.v.) and a vacuum edge wave function (v.e.w.) depending on  $\vec{t}$  as follows:

(1) For any  $r \in [k]$ , to the vertical edge  $e_{i_r}^{(2)}$  joining the white vertex  $V_{i_r}$  to the boundary vertex  $b_{i_r}$ , we assign e.v. and v.e.w.

$$(5.1) \quad \mathfrak{E}_{i_r}^{(2)} = \hat{E}^{(k)}[i_r], \quad \Phi_{i_r}^{(2)}(\vec{t}) \equiv \prec \hat{E}^{(k)}[i_r], \mathfrak{E}_\theta(\vec{t}) \succ = e^{\theta_{i_r}(\vec{t})};$$

(2) For any fixed  $r \in [k]$  and  $l \in [N_r]$ , to the vertical edge  $e_{i_r j_l}^{(2)}$  at  $V_{i_r j_l}$  we assign

$$(5.2) \quad \mathfrak{E}_{i_r j_l}^{(2)} = \hat{E}^{(r)}[j_l], \quad \Phi_{i_r j_l}^{(2)}(\vec{t}) \equiv \prec \mathfrak{E}_{i_r j_l}^{(2)}, \mathfrak{E}_\theta(\vec{t}) \succ;$$

(3) For any  $r \in [k]$ , to the horizontal edge  $e_{i_r j_{N_r}}^{(3)}$  joining  $V'_{i_r j_{N_r}}$  to  $V_{i_r j_{N_r}}$  we assign:

$$(5.3) \quad \mathfrak{E}_{i_r j_{N_r}}^{(3)} = \mathfrak{E}_{i_r j_{N_r}}^{(2)}, \quad \Phi_{i_r j_{N_r}}^{(3)}(\vec{t}) \equiv \prec \mathfrak{E}_{i_r j_{N_r}}^{(3)}, \mathfrak{E}_\theta(\vec{t}) \succ = \Phi_{i_r j_{N_r}}^{(2)}(\vec{t})$$

(4) For any  $r \in [k]$ ,  $l \in [0, N_r - 1]$ , to the horizontal edge  $e_{i_r j_l}^{(1)}$  joining  $V_{i_r j_l}$  to  $V'_{i_r j_{l+1}}$  we assign

$$(5.4) \quad \mathfrak{E}_{i_r j_l}^{(1)} = w_{i_r j_{l+1}} \mathfrak{E}_{i_r j_{l+1}}^{(3)}, \quad \Phi_{i_r j_l}^{(1)}(\vec{t}) \equiv \prec \mathfrak{E}_{i_r j_l}^{(1)}, \mathfrak{E}_\theta(\vec{t}) \succ = w_{i_r j_{l+1}} \Phi_{i_r j_{l+1}}^{(3)}(\vec{t}),$$

where  $w_{i_r j_1}$  is the weight of  $e_{i_r j_1}^{(1)}$ . Here  $j_0 = 0$ ;

(5) For any  $r \in [k]$ ,  $l \in [0, N_r - 1]$ , to the edge  $e_{i_r j_l}^{(3)}$  joining  $V'_{i_r j_l}$  to  $V_{i_r j_l}$  we assign

$$(5.5) \quad \mathfrak{E}_{i_r j_l}^{(3)} = \mathfrak{E}_{i_r j_l}^{(1)} + \mathfrak{E}_{i_r j_l}^{(2)}, \quad \Phi_{i_r j_l}^{(3)}(\vec{t}) \equiv \prec \mathfrak{E}_{i_r j_l}^{(3)}, \mathfrak{E}_\theta(\vec{t}) \succ = \Phi_{i_r j_l}^{(1)}(\vec{t}) + \Phi_{i_r j_l}^{(2)}(\vec{t}),$$

i.e. the sum of the contributions from the edges to the left and below the white vertex  $V_{i_r j_l}$ .

We illustrate Definition 5.2 in Figure 9.

**Definition 5.3. The dressed edge wave function (d.e.w.) on  $\mathcal{N}'$ .** In the setting of Definition 5.2, for any fixed  $r \in [k]$  and  $l \in [0, N_r]$ , we define the dressed edge wave function  $\Psi_{i_r j_l}^{(m)}(\vec{t})$  on the edge  $e_{i_r j_l}^{(m)} \in \mathcal{N}'$  as the dressing of the v.e.w.  $\Phi_{i_r j_l}^{(m)}(\vec{t})$

$$(5.6) \quad \Psi_{i_r j_l}^{(m)}(\vec{t}) = \mathfrak{D} \Phi_{i_r j_l}^{(m)}(\vec{t}),$$

where  $\mathfrak{D}$  is the Darboux transformation associated to the given soliton data  $(\mathcal{K}, [A])$ .

By construction, the system of edge vectors  $\mathfrak{E}_{i_r j_l}^{(m)}$ , the v.e.w.  $\Phi_{i_r j_l}^{(m)}(\vec{t})$  and the d.e.w.  $\Psi_{i_r j_l}^{(m)}(\vec{t})$  on  $\mathcal{N}'$  solve a linear system at the inner vertexes of  $\mathcal{N}'$  under suitable boundary conditions:

**Lemma 5.1. The linear system in  $\mathcal{N}'$**  Let  $G_j(\vec{t})$ ,  $j \in [n]$ , be smooth functions in  $\vec{t}$ . Then there exists a unique function  $G_e(\vec{t})$  defined on the edges  $e$  of  $\mathcal{N}'$  satisfying for all  $\vec{t}$ :



- (1) For any  $r \in [k]$  and  $l \in [0, N_r]$ , on the unit edge  $e_{i_r j_l}^{(3)}$  pointing in at the white vertex  $V_{i_r j_l}$ , define  $G_{e_{i_r j_l}^{(3)}}$  as the sum of the values of  $G_e$  on the edges  $e = e_{i_r j_l}^{(1)}, e_{i_r j_l}^{(2)}$  pointing out at  $V_{i_r j_l}$ :

$$G_{e_{i_r j_l}^{(3)}}(\vec{t}) = G_{e_{i_r j_l}^{(1)}}(\vec{t}) + G_{e_{i_r j_l}^{(2)}}(\vec{t});$$

- (2) For any  $r \in [k]$  and  $l \in [0, N_r - 1]$ , on the horizontal edge  $e_{i_r j_l}^{(1)}$  of weight  $w_{i_r j_l}$  pointing in at the black vertex  $V'_{i_r j_{l+1}}$ , define  $G_{e_{i_r j_l}^{(1)}}$  as

$$G_{e_{i_r j_l}^{(1)}}(\vec{t}) = w_{i_r j_{l+1}} G_{e_{i_r j_{l+1}}^{(3)}}(\vec{t}),$$

where  $e_{i_r j_{l+1}}^{(3)}$  is the unique edge pointing out at  $V'_{i_r j_{l+1}}$ ;

- (3) For any  $r \in [k]$ , the unit vertical edge  $e_{i_r}^{(2)}$  joins  $V_{i_r}$  to the boundary vertex  $b_{i_r}$ . Define

$$G_{e_{i_r}^{(2)}}(\vec{t}) = G_{i_r}(\vec{t});$$

- (4) For any  $r \in [N_r]$ , if the unit vertical edge  $e_{i_r j_l}^{(2)}$  joins  $V_{i_r j_l}$  to the boundary vertex  $b_{j_l}$ , define

$$G_{e_{i_r j_l}^{(2)}}(\vec{t}) = G_{j_l}(\vec{t}).$$

Otherwise, the black vertex  $V'_{i_{\bar{s}} j_l}$ , with  $\bar{s} = \min S$ , with  $S = \{s \in [r+1, k] : \chi_{j_l}^{i_s} = 1\} \neq \emptyset$  as in the proof of Theorem 4.1, is the ending vertex of  $e_{i_r j_l}^{(2)}$ ,  $d = d(i_r j_l) = \bar{s} - r$  is the number of pivot indexes in the interval  $]i_r, j_l[$  and define

$$G_{e_{i_r j_l}^{(2)}}(\vec{t}) = (-1)^d G_{e_{i_r + d j_l}^{(3)}}(\vec{t}).$$

In particular, if we assign the boundary conditions  $G_j(\vec{t}) \equiv \Phi_j^{(2)}(\vec{t})$ , (respectively  $G_j(\vec{t}) \equiv \Psi_j^{(2)}(\vec{t})$ ), for all  $j \in [n]$ , then the edge function coincides with the v.e.w. of Definition 5.2 (respectively with the d.e.w. of Definition 5.3).

*Proof.* First let  $\mathcal{N}'$  correspond to an irreducible positroid cell  $\mathcal{S}_{\mathcal{M}}^{\text{TNN}} \subset Gr^{\text{TNN}}(k, n)$  of dimension  $g$ . Then, the number of variables in the linear system defined in the above Lemma is equal to the number of edges,  $3g + 2k$  ( $g + k$  vertical edges and  $2g + k$  horizontal edges). Any trivalent black vertex carries two equations, while each bivalent black vertex carries one condition. There are  $g$  internal black vertexes and  $g - n + k$  are trivalent. Therefore the total number of equations at black vertexes is  $2g - n + k$ . The total number of equations at white vertexes is  $g + k$ , since the total number of internal white vertexes is  $g + 2k$ , but the univalent Darboux vertexes on  $\mathcal{N}'$  do not carry any extra condition. So we may freely impose a value to  $n$  variables (edges).

The presence of an isolated boundary sink  $b_j$  implies the addition of an internal univalent vertex joined to  $b_j$ : we have a new variable (the univalent edge) and no extra condition. The presence of an isolated boundary source  $b_i$  implies the addition of a bivalent vertex  $V_i$  and of an univalent Darboux vertex  $V_i^{(D)}$ : we have two variables and one equation.

The system is well-defined and the solution is unique because the network is acyclic. Finally the system can be solved recurrently.  $\square$

Comparing Theorem 4.1 and Definition 5.2, it is not difficult to prove that the e.v. at the Darboux edge  $e_{i_r}^{(3)}$  coincides with the  $r$ -th row of the RREF matrix  $A$  (see equation 5.8 below); therefore the v.e.w. at the same edge is  $f^{(r)}(\vec{t})$  as required in Theorem 3.1.

**Lemma 5.2.** *Let the soliton data and the notations be fixed as in Remark 5.2. Let the e.v. and v.e.w. be as in Definition 5.2. Then,*

(1) *for any  $r \in [k]$  and  $l \in [N_r]$ , the edge vector at the edge joining  $V_{i_r j_l}$ ,  $V'_{i_r j_l}$  is*

$$(5.7) \quad \mathfrak{E}_{i_r j_l}^{(3)} = \sum_{s=l}^{N_r} \hat{c}_{j_s}^r \hat{E}^{(r)}[j_s];$$

(2) *for any  $r \in [k]$  the edge vector at the edge  $e_{i_r}^{(3)}$  is the  $r$ -th row of the RREF matrix representing  $[A] \in Gr^{TNN}(k, n)$  and the v.e.w. is the  $r$ -th generator of the dressing transformation associated to the soliton data  $(\mathcal{K}, [A])$*

$$(5.8) \quad \mathfrak{E}_{i_r}^{(3)} = A[r], \quad \Phi_{i_r}^{(3)}(\vec{t}) = f^{(r)}(\vec{t}).$$

*Therefore the d.e.w. satisfies  $\Psi_{i_r}^{(3)}(\vec{t}) \equiv 0$ , for all  $r \in [k]$  and for all  $\vec{t}$ .*

The proof of the Lemma easily follows comparing (5.7) and (5.8) with (4.2), (4.7), (4.8) and (4.10) in Theorem 4.1 and with (5.1)–(5.5) in Definition 5.2.

As remarked in the proof of Lemma 5.1, the edge vectors and vacuum and dressed edge wave functions on  $\mathcal{N}'$  may be recursively computed using Theorem 4.1 starting from the last row of the corresponding Le-diagram ( $r = k$ ) and moving up till decreasing the index  $r$  till  $r = 1$ . For simplicity, we illustrate the algorithm for the edge vectors only (see also Figure 9 for the edge wave functions).

**Algorithm for the edge vectors:** For any  $r \in [k]$ :

- (1) If  $N_r = 0$ , i.e. all the boxes of the  $r$ -th row of the Le-diagram contain zeros, assign to the white vertex  $V_r$  the vector  $\hat{E}^{(r)}[i_r] \equiv \hat{E}^{(k+1)}[i_r]$  and proceed to (3);
- (2) Otherwise:

- (a) Start from the leftmost white vertex of the line,  $V_{irjN_r}$  and assign to the edge joining  $V_{irjN_r}$  and  $V'_{irjN_r}$  the edge vector

$$\mathfrak{E}_{irjN_r}^{(3)} = \hat{E}^{(r)}[jN_r]$$

- (b) For any  $l$  from  $N_r - 1$  to 1, assign to the edge joining  $V'_{irjl}$  and  $V_{irjl}$ , the vector

$$\mathfrak{E}_{irjl}^{(3)} = w_{irjl+1} \mathfrak{E}_{irjl+1}^{(3)} + \hat{E}^{(r)}[jl].$$

- (c) At the white vertex  $V_r$  assign the vector

$$\mathfrak{E}_{ir0}^{(3)} = w_{irj1} \mathfrak{E}_{irj1}^{(3)} + \hat{E}^{(r)}[ir] = A[r],$$

and go to (3).

- (3) If  $r = 1$ , just end. Otherwise set the counter to  $r - 1$  and repeat the whole procedure.

**Example 5.1.** We illustrate such procedure for Example A.2 (see Figure 21). At the horizontal edge joining  $V_{45}$  and  $V'_{45}$  we assign the edge vector

$$\mathfrak{E}_{45}^{(3)} = E^{(3)}[5] + w_{46} \mathfrak{E}_{46}^{(3)} = (0, 0, 0, 0, 1, w_{46}, 0, -w_{46}w_{48}, -w_{46}w_{48}w_{49}),$$

since  $\mathfrak{E}_{46}^{(3)} = E^{(3)}[6] + w_{48} \mathfrak{E}_{48}^{(3)} = E^{(3)}[6] + w_{48}(\hat{E}^{(3)}[8] + w_{49}\hat{E}^{(3)}[9])$ , and the edge wave function

$$\Phi_{45}^{(3)}(\vec{t}) = e^{\theta_5(\vec{t})} + w_{46}e^{\theta_6(\vec{t})} - w_{46}w_{48}e^{\theta_8(\vec{t})} - w_{46}w_{48}w_{49}e^{\theta_9(\vec{t})}.$$

At the horizontal edge joining  $V_{25}$  and  $V'_{25}$  we associate the edge vector  $\mathfrak{E}_{25}^{(3)} = E^{(2)}[5] = -\mathfrak{E}_{45}^{(3)}$  (compare with Example 4.1) and the edge wave function  $\Phi_{25}^{(3)}(\vec{t}) = -\Phi_{45}^{(3)}(\vec{t})$  for all times  $\vec{t}$ .

**5.2. The vacuum and dressed network divisors.** We now assign a vacuum network divisor number  $\gamma_{ij}^{(\text{vac})}$  and a dressed network divisor number  $\gamma_{ij}^{(\text{dr})}$  to each trivalent white vertex of  $\mathcal{N}'$  using the linear system considered in the previous section, after choosing a convenient initial time  $\vec{t}_0$  with respect to which we normalize the wave functions. To simplify the control of the position of the vacuum divisor, we use the fact that both the highest phase and the sign of the corresponding coefficient of the v.e.w.  $\Phi$  are the same at all horizontal edges on the same row. We then can choose  $\vec{t}_0$  so that the sign of  $\Phi(\vec{t}_0)$  is equal to the sign of such highest non zero coefficient.

**Definition 5.4. Choice of the initial time  $\vec{t}_0$ .** Let the Le-network  $\mathcal{N}'$ , the v.e.w.  $\Phi_{ij}^{(m)}(\vec{t})$  and the d.e.w.  $\Psi_{ij}^{(m)}(\vec{t})$  be as in the previous section. Let  $\vec{t}_0 = (x_0, 0 \dots)$  with  $x_0 \in \mathbb{R}$  be such that:

- (1) For any  $l \in [0, N_r]$ ,  $r \in [k]$ , the sign of both  $\Phi_{i_r j_l}^{(1)}(\vec{t}_0)$  and  $\Phi_{i_r j_l}^{(3)}(\vec{t}_0)$  are equal to the sign of their highest non zero coefficient;
- (2) The d.e.w.  $\Psi_{i_r j_{N_r}}^{(m)}(\vec{t}_0) \neq 0$  on any edge  $e_{i_r j_l}^{(m)}$  distinct from the Darboux edges,  $e_{i_r j_l}^{(m)} \notin \{e_{i_r}^{(3)} : r \in [k]\}$ .

We remark that the d.e.w. is identically zero by definition at the Darboux edges  $e_{i_r}^{(3)}$ ,  $r \in [k]$ . We are now ready to assign a vacuum and a dressed divisor number to each trivalent white vertex of  $\mathcal{N}'$ .

**Definition 5.5.** *The vacuum network divisor  $\mathcal{D}_{\text{vac}, \mathcal{N}'}$ . Let  $\Phi_{i_r j_l}^{(m)}(\vec{t})$  be the vacuum edge wave function on the edges  $e_{i_r j_l}^{(m)}$ ,  $m \in [3]$ , at  $V_{i_r j_l}$  of the network  $\mathcal{N}'$ . Let  $\vec{t}_0$  be fixed as in Definition 5.4. We assign a vacuum network divisor number  $\gamma_{i_r j_l}^{(\text{vac})}$  to each trivalent white vertex  $V_{i_r j_l}$  ( $r \in [k]$ ,  $l \in [0, N_r - 1]$ ) :*

$$(5.9) \quad \gamma_{i_r j_l}^{(\text{vac})} = \frac{\Phi_{i_r j_l}^{(1)}(\vec{t}_0)}{\Phi_{i_r j_l}^{(1)}(\vec{t}_0) + \Phi_{i_r j_l}^{(2)}(\vec{t}_0)} = \frac{\Phi_{i_r j_l}^{(1)}(\vec{t}_0)}{\Phi_{i_r j_l}^{(3)}(\vec{t}_0)}.$$

We call the collection of the  $g$  pairs:  $\mathcal{D}_{\text{vac}, \mathcal{N}'} = \{(\gamma_{i_r j_l}^{(\text{vac})}, V_{i_r j_l}), l \in [0, N_r - 1], r \in [k]\}$  the vacuum network divisor on  $\mathcal{N}'$ .

**Remark 5.3.** *We do not assign vacuum network divisor numbers to vertexes connected with isolated boundary vertexes, since these vertexes are not trivalent in our construction.*

**Remark 5.4.** *The vacuum network divisor in Definition 5.5 is associated to a certain orientation of the Le-network for the given regular soliton data  $(\mathcal{K}, [A])$ . In [4], we prove that any change either of base in the matroid  $\mathcal{M}$  or of position of the Darboux edges induces an untrivial change in the values of the v.e.w. and an untrivial transformation of the vacuum network divisor numbers in the above definition.*

In the next Lemma, we normalize the v.e.w. previously defined and characterize the vacuum network divisor.

**Lemma 5.3.** *Let  $(\mathcal{K}, [A])$  and the v.e.w. be as in the Definition 5.2 and let  $\vec{t}_0 = (x_0, 0 \dots)$  be as in Remark 5.4. Then the normalized v.e.w.*

$$(5.10) \quad \hat{\Phi}_{i_r j_l}^{(m)}(\vec{t}) = \frac{\Phi_{i_r j_l}^{(m)}(\vec{t})}{\Phi_{i_r j_l}^{(m)}(\vec{t}_0)}, \quad l \in [0, N_r], \quad r \in [k], \quad m \in [3],$$

*has the following properties:*

- (1)  $\hat{\Phi}_{i_r j_l}^{(m)}(\vec{t})$  is a regular function of  $\vec{t}$  for any  $r \in [k]$ ,  $l \in [0, N_r]$ ,  $m \in [3]$ ;
- (2) For any fixed  $r \in [k]$ ,  $j \in [N_r]$ , the normalized v.e.w. takes the same value on all edges at the (bivalent or trivalent) black vertex  $V'_{i_r j_l}$ ;
- (3) For any fixed  $r \in [k]$ , the normalized v.e.w. takes the same value on both edges at the white vertex  $V_{i_r j_{N_r}}$  for all times  $\vec{t}$ :  $\hat{\Phi}_{i_r j_{N_r}}^{(2)}(\vec{t}) = \hat{\Phi}_{i_r j_{N_r}}^{(3)}(\vec{t})$ ;
- (4) For any fixed  $r \in [k]$ ,  $j \in [N_r - 1]$ , the normalized v.e.w. takes different values on the edges at the white trivalent vertex  $V_{i_r j_l}$  for almost all  $\vec{t}$ , and the vacuum network divisor number  $\gamma_{i_r j_l}^{(\text{vac})}$  defined in (5.9) is the unique **positive** number such that

$$\hat{\Phi}_{i_r j_l}^{(3)}(\vec{t}) \equiv \gamma_{i_r j_l}^{(\text{vac})} \hat{\Phi}_{i_r j_l}^{(1)}(\vec{t}) + (1 - \gamma_{i_r j_l}^{(\text{vac})}) \hat{\Phi}_{i_r j_l}^{(2)}(\vec{t}), \quad \forall \vec{t};$$

- (5) For any  $r \in [k]$ , such that  $b_{i_r}$  is not an isolated boundary vertex, the normalized v.e.w. takes different values on the edges at the white trivalent vertex  $V_{i_r}$  for almost all  $\vec{t}$ , and  $\gamma_{i_r}^{(\text{vac})}$  defined in (5.9) is the unique **positive** number such that

$$\hat{\Phi}_{i_r}^{(3)}(\vec{t}) \equiv \gamma_{i_r}^{(\text{vac})} \hat{\Phi}_{i_r}^{(1)}(\vec{t}) + (1 - \gamma_{i_r}^{(\text{vac})}) \hat{\Phi}_{i_r}^{(2)}(\vec{t}), \quad \forall \vec{t};$$

- (6) If, for some  $r \in [k]$ ,  $b_{i_r}$  is an isolated boundary vertex, the white vertex  $V_{i_r}$  is bivalent and  $\hat{\Phi}_{i_r}^{(3)}(\vec{t}) \equiv \hat{\Phi}_{i_r}^{(2)}(\vec{t}) = \exp(\theta_{i_r}(\vec{t} - \vec{t}_0))$ ,  $\forall \vec{t}$ ;
- (7) The set of normalized v.e.w.  $\hat{\Phi}_{i_r}^{(3)}(\vec{t})$  defined at the vertexes  $V_{i_r}$ ,  $r \in [k]$ ,
  - (a) Form a basis of heat hierarchy solutions which satisfy  $\mathfrak{D} \hat{\Phi}_{i_r}^{(3)}(\vec{t}) \equiv 0$ , for all  $r \in [k]$ ,  $\vec{t}$ , with  $\mathfrak{D} = W \partial_x^k \equiv \partial_x^k - \mathfrak{w}_1(\vec{t}) \partial_x^{k-1} - \mathfrak{w}_2(\vec{t}) \partial_x^{k-2} - \dots - \mathfrak{w}_k(\vec{t})$ , the Darboux transformation and  $W$  the Sato dressing operator for  $(\mathcal{K}, [A])$ ;
  - (b) Generate the KP soliton solution  $u(\vec{t})$  associated to  $(\mathcal{K}, [A])$

$$u(\vec{t}) = 2\partial_{xx} \log(\tau(\vec{t})), \quad \tau(\vec{t}) = \text{Wr}_x(\hat{\Phi}_{i_1}^{(3)}(\vec{t}), \dots, \hat{\Phi}_{i_k}^{(3)}(\vec{t}))$$

where  $\text{Wr}_x$  denotes the Wronskian of  $\hat{\Phi}_{i_r}^{(3)}(\vec{t})$ ,  $r \in [k]$ , with respect to  $x = t_1$ .

The proof is trivial and is omitted. We illustrate the above statement in Figure 9.

**Example 5.2.** Let's compute the normalized vacuum edge wave function for Example 5.1. At the vertex  $V_{45}$  the normalized vacuum edge wave function is

$$\hat{\Phi}_{45}^{(3)}(\vec{t}) = \frac{e^{\theta_5(\vec{t})} + w_{46}e^{\theta_6(\vec{t})} - w_{46}w_{48}e^{\theta_8(\vec{t})} - w_{46}w_{48}w_{49}e^{\theta_9(\vec{t})}}{e^{\theta_5(\vec{t}_0)} + w_{46}e^{\theta_6(\vec{t}_0)} - w_{46}w_{48}e^{\theta_8(\vec{t}_0)} - w_{46}w_{48}w_{49}e^{\theta_9(\vec{t}_0)}}.$$

At the vertex  $V_{25}$  we associate the **opposite** edge wave function  $\Phi_{25}^{(3)}(\vec{t}) = -\Phi_{45}^{(3)}(\vec{t})$  and the **same normalized** edge wave function  $\hat{\Phi}_{25}^{(3)}(\vec{t}) = \hat{\Phi}_{45}^{(3)}(\vec{t})$  for all times  $\vec{t}$ . We leave as an exercise to the reader the computation of the vacuum divisor numbers for this example (see also Figure 10).

**Definition 5.6.** *The dressed network divisor  $\mathcal{D}_{\text{dr}, \mathcal{N}'}$ . Let  $\Psi_{i_r j_l}^{(m)}(\vec{t})$  be the dressed edge wave function on the edges  $e_{i_r j_l}^{(m)}$ ,  $m \in [3]$ , at  $V_{i_r j_l}$  of the network  $\mathcal{N}'$ . Let  $\vec{t}_0$  be fixed as in Definition 5.4. We assign a dressed network divisor number  $\gamma_{i_r j_l}^{(\text{dr})}$  to each trivalent white vertex  $V_{i_r j_l}$  not containing a Darboux edge ( $r \in [k]$ ,  $l \in [N_r - 1]$ ):*

$$(5.11) \quad \gamma_{i_r j_l}^{(\text{dr})} = \frac{\Psi_{i_r j_l}^{(1)}(\vec{t}_0)}{\Psi_{i_r j_l}^{(1)}(\vec{t}_0) + \Psi_{i_r j_l}^{(2)}(\vec{t}_0)} = \frac{\Psi_{i_r j_l}^{(1)}(\vec{t}_0)}{\Psi_{i_r j_l}^{(3)}(\vec{t}_0)}.$$

We call the collection of the pairs  $\mathcal{D}_{\text{dr}, \mathcal{N}'} = \{(\gamma_{i_r j_l}^{(\text{dr})}, V_{i_r j_l}), l \in [N_r - 1], r \in [k]\}$  the dressed network divisor on  $\mathcal{N}'$ .

**Remark 5.5.** *If the Le-network corresponds to a point in an irreducible positroid cell in  $Gr^{TNN}(k, n)$ , then  $\mathcal{D}_{\text{dr}, \mathcal{N}'}$  is a collection of  $g - k$  pairs. If the Le-network corresponds to a point in a reducible positroid cell in  $Gr^{TNN}(k, n)$ , and the reduced cell belongs to  $Gr^{TNN}(k', n')$ , then  $\mathcal{D}_{\text{dr}, \mathcal{N}'}$  is a collection of  $g - k'$  pairs.*

**Definition 5.7.** *The KP edge wave function  $\hat{\Psi}$ . Let  $\Psi_{i_r j_l}^{(m)}(\vec{t})$  be the dressed edge wave function on  $\mathcal{N}'$  with  $\vec{t}_0$  be as above. Then the KP edge wave function on  $\mathcal{N}'$  is*

$$(5.12) \quad \hat{\Psi}_{i_r j_l}^{(m)}(\vec{t}) = \begin{cases} \frac{\Psi_{i_r j_l}^{(m)}(\vec{t})}{\Psi_{i_r j_l}^{(m)}(\vec{t}_0)}, & \text{for all } m \in [3], l \in [N_r], r \in [k], \\ \frac{\mathfrak{D}e^{i\theta_{i_r}}(\vec{t})}{\mathfrak{D}e^{i\theta_{i_r}}(\vec{t}_0)}, & \text{if } m = 3, l = 0 \text{ i.e. on the Darboux edge } e_{i_r}^{(3)}, r \in [k]. \end{cases}$$

**Remark 5.6.** *The dressed network divisor in Definition 5.6 is associated to  $(\mathcal{K}, [A])$  using a specific acyclic orientation of its Le-network. In [4], we prove that any change either of base in the matroid  $\mathcal{M}$  for  $[A]$  or of position of the Darboux edges leaves invariant the KP edge wave function  $\hat{\Psi}$ , and induces a change of the dressed divisor numbers corresponding to the change of coordinates due to the new orientation. Therefore the position of the KP divisor in the ovals is independent on both the orientation of the network and the position chosen for the Darboux source points.*

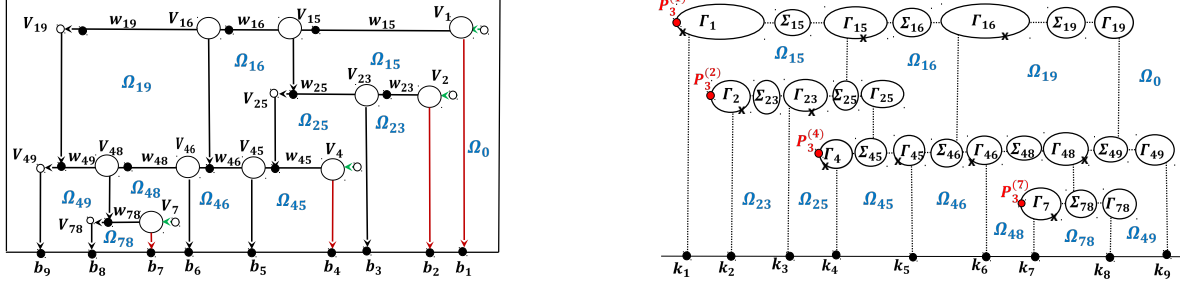


FIGURE 10. The vacuum divisor (crosses) on the M-curve  $\Gamma$  [right] for Example A.2: the local coordinate of the vacuum divisor point on the component  $\Gamma_{ij} \subset \Gamma$  [right] is the divisor number of the vertex  $V_{ij}$  on  $\mathcal{N}'$  [left].

**5.3. The vacuum wave function on  $\Gamma$  and its pole divisor.** In this Section we pass from the edge wave functions on  $\mathcal{N}'$  to functions which are meromorphic on the spectral curve  $\Gamma \setminus \{P_0\}$ . The rule is straightforward: at any given marked point on  $\Gamma \setminus \{P_0\}$ , we impose that the normalized vacuum wave function  $\hat{\phi}(P, \vec{t})$  (respectively the normalized dressed wave function  $\hat{\psi}(P, \vec{t})$ ) coincides with the value of the normalized vacuum (dressed) edge wave function defined in Definition 5.2 (Definition 5.7) on the corresponding edge of  $\mathcal{N}'$  for all  $\vec{t}$ . We then extend the functions from the marked points to  $\Gamma$  as follows:

- (1) On  $\Gamma_0$  the function  $\hat{\phi}(P, \vec{t})$  is the normalized Sato vacuum wave function, while  $\hat{\psi}(P, \vec{t})$  is the normalized Sato dressed wave function;
- (2) On any copy of  $\mathbb{CP}^1$  corresponding either to an internal black vertex or to a bivalent white vertex, both  $\hat{\phi}(P, \vec{t})$  and  $\hat{\psi}(P, \vec{t})$  are constant function with respect to the spectral parameter;
- (3) On any copy of  $\mathbb{CP}^1$  corresponding to a trivalent white vertex  $\hat{\phi}(P, \vec{t})$  is meromorphic of degree 1;
- (4) On any copy of  $\mathbb{CP}^1$  corresponding to a trivalent white vertex and not containing Darboux points  $\hat{\psi}(P, \vec{t})$  is meromorphic of degree 1, while it is constant with respect to the spectral parameter at each copy containing a Darboux point.

Then, by construction,  $\hat{\phi}(P, \vec{t})$  has an essential singularity at  $P_0 \in \Gamma \cap \Omega_0$ , and effective degree  $g$  divisor of poles  $\mathcal{D}_{\text{vac}, \Gamma} = (P_{irjl}^{(\text{vac})})$ ,  $r \in [k]$ ,  $j \in [0, N_r - 1]$  in the real part of  $\Gamma \setminus \{P_0\}$ , such that  $\zeta(P_{irjl}^{(\text{vac})}) = \gamma_{irjl}^{(\text{vac})}$  as in (5.9), where  $\zeta$  is the local coordinate on the corresponding component  $\Gamma_{irjl}$ . Analogously, by construction,  $\hat{\psi}(P, \vec{t})$  has an essential singularity at  $P_0 \in \Gamma \cap \Omega_0$  and its

effective degree  $g$  divisor of poles is the sum of the Sato divisor  $\mathcal{D}_{S, \Gamma_0}(\vec{t}_0)$  on  $\Gamma_0$  and of the points  $\{P_{i_r j_l}^{(\text{dr})}, r \in [k], j \in [N_r - 1]\}$  in the real part of  $\Gamma \setminus \Gamma_0$ , with  $\zeta(P_{i_r j_l}^{(\text{dr})}) = \gamma_{i_r j_l}^{(\text{dr})}$  as in (5.11).

**Definition 5.8. The vacuum wave function  $\hat{\phi}$  on  $\Gamma$ .** Let the data be as in Remark 5.2. Let  $\Gamma$  and its marked points be as in Construction 3.1. Let  $\Phi(\vec{t})$  and  $\hat{\Phi}(\vec{t})$  respectively be the v.e.w. and its normalization as in Definition 5.2 and (5.10), with  $\vec{t}_0 = (x_0, 0, \dots)$  as in Remark 5.4. Define  $\hat{\phi}(P, \vec{t})$  as follows:

- (1)  $\hat{\phi}_0$  denotes the restriction of  $\hat{\phi}$  to  $\Gamma_0$  and is assigned the value of the normalized Sato vacuum wave function  $\hat{\phi}_0(\zeta, \vec{t}) = e^{\theta(\vec{t} - \vec{t}_0)}$ , where  $\theta(\vec{t} - \vec{t}_0) = \zeta(x - x_0) + \sum_{l \geq 2} \zeta^l t_l$ , so that  $\hat{\phi}_0(\kappa_j, \vec{t}) \equiv \hat{\Phi}_j^{(2)}(\vec{t})$ , for any  $j \in [n]$  and for all  $\vec{t}$ .
- (2) For any  $r \in [k]$ ,  $s \in [N_r]$ ,  $\hat{\phi}'_{i_r j_s}(P, \vec{t})$  denotes the restriction of  $\hat{\phi}$  to  $\Sigma_{i_r j_s}$  and is assigned the value of the normalized edge function  $\hat{\Phi}_{i_r j_s}^{(1)}(\vec{t})$ :  $\hat{\phi}'_{i_r j_s}(P, \vec{t}) = \hat{\Phi}_{i_r j_s}^{(1)}(\vec{t})$ ,  $\forall \vec{t}$ ;
- (3) For any  $r \in [k]$ ,  $s \in [0, N_r]$ ,  $\hat{\phi}_{i_r, j_s}(P, \vec{t})$  denotes the restriction of  $\hat{\phi}$  to  $\Gamma_{i_r j_s}$  and is defined as follows:
  - (a) If, for some  $r \in [k]$ ,  $N_r = 0$  (isolated boundary source),  $\hat{\phi}_{i_r}(P, \vec{t})$  is assigned the value  $\hat{\phi}_0(\kappa_{i_r}, \vec{t})$  for all  $P$  and  $\vec{t}$ :  $\hat{\phi}_{i_r}(P, \vec{t}) = \hat{\phi}_0(\kappa_{i_r}, \vec{t})$ ;
  - (b) Otherwise, for  $s \in [0, N_r - 1]$ , let  $\gamma_{i_r j_s}^{(\text{vac})} = \frac{\Phi_{i_r j_s}^{(1)}(\vec{t}_0)}{\Phi_{i_r j_s}^{(3)}(\vec{t}_0)}$  as in (5.9).  $\hat{\phi}_{i_r j_s}(P, \vec{t})$  is assigned to be meromorphic with exactly one real pole  $P_{i_r j_s}^{(\text{vac})}$  with  $\zeta(P_{i_r j_s}^{(\text{vac})}) = \gamma_{i_r j_s}^{(\text{vac})}$  and such that  $\hat{\phi}_{i_r j_s}(P_{i_r j_s}^{(m)}, \vec{t}) = \hat{\Phi}_{i_r j_s}^{(m)}(\vec{t})$ ,  $m \in [3]$ ,  $\forall \vec{t}$ . Therefore, in the local coordinate  $\zeta$ , it takes the form

$$\hat{\phi}_{i_r j_s}(\zeta, \vec{t}) = \frac{\Phi_{i_r j_s}^{(1)}(\vec{t})(\zeta - 1) + \Phi_{i_r j_s}^{(2)}(\vec{t})\zeta}{\Phi_{i_r j_s}^{(3)}(\vec{t}_0) \left( \zeta - \gamma_{i_r j_s}^{(\text{vac})} \right)};$$

- (c) for any  $r \in [k]$ ,  $\hat{\phi}_{i_r j_{N_r}}(P, \vec{t})$  is assigned the value  $\hat{\phi}_{i_r j_{N_r}}(P, \vec{t}) = \Phi_{i_r j_{N_r}}^{(2)}(\vec{t})$ ,  $\forall P \in \Gamma_{i_r j_{N_r}}$  and  $\forall \vec{t}$ .

**Theorem 5.1. The vacuum divisor (Theorem 3.1).**  $\hat{\phi}$  as in Definition 5.8 is the real and regular vacuum wave function on  $\Gamma$  for the soliton data  $(\mathcal{K}, [A])$ , that is it satisfies all the properties of Definitions 3.3 and 3.4 on  $\Gamma \setminus \{P_0\}$ . In particular, it satisfies (3.5), that is

$$\hat{\phi}(P_{i_r}^{(3)}, \vec{t}) = \frac{\sum_{l=1}^n A_l^r \exp(\theta_l(\vec{t}))}{\sum_{l=1}^n A_l^r \exp(\theta_l(\vec{t}_0))}, \quad \text{for } r \in [k], \quad \forall \vec{t},$$

where  $A$  is the RREF representative matrix in  $[A]$ . Finally the vacuum divisor  $\mathcal{D}_{\text{vac}, \Gamma} = \{P_{i_r j_l}^{(\text{vac})}\}$  of  $\hat{\phi}$  satisfies:



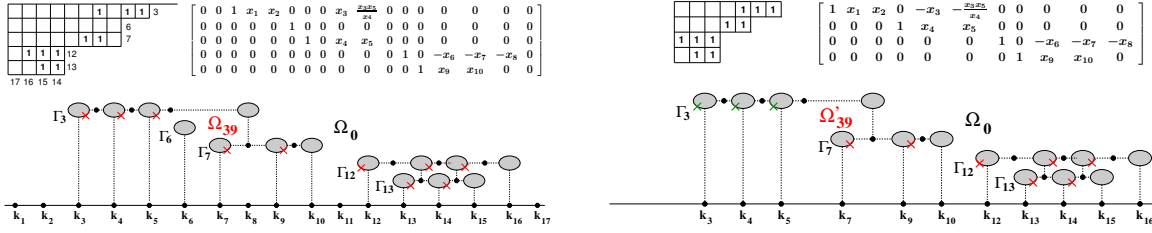


FIGURE 11. We illustrate Case b) in the proof of Theorem 5.1 for the example discussed in Remark 5.7.

- (1) It consists of  $g$  simple poles and no pole belongs to  $\Gamma_0$ ;
- (2) There is exactly one pole on each component  $\Gamma_{i_r j_l}$  corresponding to a trivalent white vertex in  $\mathcal{N}'$ ;
- (3) For any finite oval  $\Omega_s$ ,  $s \in [g]$ , let  $\nu_s = \#\{\mathcal{D}_{\text{vac}, \Gamma} \cap \Omega_s\}$  and  $\mu_s = \#\{P_{i_r}^{(3)} \in \Omega_s, r \in [k]\}$  respectively be the number of poles and the number of Darboux points in  $\Omega_s$ . Then

$$(5.13) \quad \nu_s + \mu_s = \text{odd number}, \quad \text{for any } s \in [g];$$

- (4) Let  $s_0 = \#\{\mathcal{D}_{\text{vac}, \Gamma} \cap \Omega_0\}$  and  $\mu_0 = \#\{P_{i_r}^{(3)} \in \Omega_0, r \in [k]\}$ , respectively be the number of poles and the number of Darboux points in the infinite oval  $\Omega_0$ . Then

$$(5.14) \quad \nu_0 + \mu_0 + k = \text{even number}.$$

*Proof.* The only untrivial statements are properties (3) and (4). Copies of  $\mathbb{CP}^1$  corresponding to isolated boundary sources contribute to the counting only with a Darboux point, while those corresponding to not isolated boundary sources contribute with a pole and a Darboux point. Moreover, by definition, all poles have positive  $\zeta$ -coordinate so that:

- (1) for any fixed  $r \in [k]$  and  $l \in [N_r]$ , the finite oval  $\Omega_{i_r j_l}$  may contain only poles belonging either to  $\Gamma_{i_r j_l}$  or to  $\Gamma_{i_r j_{l-1}}$  or to  $\Gamma_{i_{r+d}}$ , with  $d \in [k-r]$ ;
- (2)  $\Omega_0$  may contain only poles belonging to  $\Gamma_{i_r}$ , with  $r \in [k]$ .

Let's prove (5.14) first.

**Case a)** First of all, let us suppose that there exists a path in  $\mathcal{N}$  joining  $i_1$  to  $j_{N_k}$ : then, either  $i_1 = 1$  and  $N_k = n$  or all  $b_j$ ,  $j \in [i_1 - 1] \cup [j_{N_k} + 1, n]$  are isolated boundary sinks both in  $\mathcal{N}$  and in  $\mathcal{N}'$ . In either case,  $\mu_0 = 1$  in  $\mathcal{N}'$ , since  $\Gamma_{i_s} \cap \Omega_0 \neq \emptyset$  if and only if  $s = 1$ . The pole on  $\Gamma_{i_1}$  has  $\zeta$ -coordinate

$$\gamma_{i_1}^{(\text{vac})} = \frac{\Phi_{i_1}^{(1)}(\vec{t}_0)}{\Phi_{i_1}^{(1)}(\vec{t}_0) + e^{\theta_{i_1}(t_0)}} > 0$$

and  $\text{sign}(\Phi_{i_1}^{(1)}(\vec{t}_0)) = (-1)^{k-1}$  by construction (compare Lemma 5.3 with Theorem 4.1). Then, if  $k$  is even,  $\gamma_{i_1}^{(\text{vac})} > 1$ , the vacuum divisor point  $P_{i_1}^{(\text{vac})} \in \Omega_0$ ,  $\nu_0 = 1$  and (5.14) holds. If  $k$  is odd,  $0 < \gamma_{i_1}^{(\text{vac})} < 1$ ,  $P_{i_1}^{(\text{vac})} \notin \Omega_0$ ,  $\nu_0 = 0$  and (5.14) again holds true.

**Case b)** Otherwise, there exist  $1 \leq s_1 < \dots < s_d \leq k$  such that  $i_{s_l} \in I$ , for any  $l \in [d]$ , and indexes  $\bar{j}_l$ ,  $l \in [d]$ , satisfying  $1 \leq i_{s_1} \leq \bar{j}_1 < i_{s_2} \leq \bar{j}_2 < \dots < i_{s_d} \leq \bar{j}_d \leq n$  such that, for any fixed  $l \in [d]$ , if  $i_{s_l} = \bar{j}_l$  then  $b_{i_{s_l}}$  is an isolated boundary source in  $\mathcal{N}$  (an isolated boundary sink in  $\mathcal{N}'$ ); otherwise  $\bar{j}_l$  is the maximum non pivot index such that there exists a path from the boundary source  $b_{i_{s_l}}$  to the boundary sink  $b_{\bar{j}_l}$ . In this case, in  $\mathcal{N}'$ ,  $\Omega_0 \cap \Gamma_{i_r} \neq \emptyset$  if and only if  $r \in \{s_1, \dots, s_d\}$ . For any fixed  $l \in [d]$ , we apply the argument of Case a) to the subgraph of  $\mathcal{N}'$  containing only boundary vertexes between  $b_{i_{s_l}}$  and  $b_{\bar{j}_l}$ , and again (5.14) holds true. We refer to Figure 11 for an illustrating example.

To prove (5.13), it is sufficient to use an induction argument starting from the ovals associated to the last row ( $r = k$ ) of the Le-diagram and moving along each row from the leftmost box towards the pivot (from  $N_r$  to 0). Notice that any time we add a new oval in this way, we create a provisional infinite oval for which (5.14) holds true.

Let  $r = k$ . If  $b_{i_k}$  is an isolated boundary vertex, then we do not create any finite oval and we pass to next row. If  $N_k \geq 1$ , then all entries of the last row of the RREF representative matrix  $A$  are positive, so that  $\gamma_{i_k j_l}^{(\text{vac})}, \gamma_{i_k}^{(\text{vac})} \in ]0, 1[$  for any  $l \in [N_k - 1]$ . Then each finite oval  $\Omega_{i_k j_l}$ ,  $l \in [N_k]$  contains only the vacuum divisor point  $P_{i_k j_{l-1}}^{(\text{vac})}$  and (5.13) is satisfied.

Now set the counter  $r = k - 1$ .

- (1) If  $b_{i_{k-1}}$  is an isolated boundary vertex, then we do not create any finite oval and we pass to next row. Observe that the provisional infinite oval created using the last two rows of the Le-diagram, contains 2 Darboux points,  $P_{i_{k-1}}^{(3)}, P_{i_k}^{(3)}$  and no vacuum divisor point.
- (2) If  $N_{k-1} \geq 1$  and  $j_{N_{k-1}} < i_k$ , then also all matrix entries of the  $(k-1)$ -th row are positive and again each finite oval  $\Omega_{i_{k-1} j_l}$ ,  $l \in [N_{k-1}]$  contains only the pole  $P_{i_{k-1} j_{l-1}}^{(\text{vac})}$  and (5.13) is satisfied. Finally the provisional infinite oval created after adding all ovals associated to the last two rows of the Le-diagram, contains 2 Darboux points,  $P_{i_{k-1}}^{(3)}, P_{i_k}^{(3)}$  and no vacuum divisor point.
- (3) If  $N_{k-1} \geq 1$  and  $j_{N_{k-1}} > i_k$ , let  $\bar{s} \in [N_{k-1}]$  be the index such that  $\Omega_{i_{k-1} j_{\bar{s}}} \cap \Gamma_{i_k} \neq \emptyset$ .

Then for any fixed oval  $\Omega_{i_{k-1} j_s}$ , with  $s > \bar{s}$ ,  $\Phi_{i_{k-1} j_{s-1}}^{(2)}(\vec{t}_0) \Phi_{i_{k-1} j_{s-1}}^{(1)}(\vec{t}_0) > 0$ ,  $\gamma_{i_{k-1} j_{s-1}}^{(\text{vac})} \in ]0, 1[$ , and  $P_{i_{k-1} j_{s-1}}^{(\text{vac})} \in \Omega_{i_{k-1} j_s}$ . Every such oval contains exactly one vacuum divisor point and no Darboux point, so that (5.13) is satisfied.

For  $s = \bar{s}$ , the oval  $\Omega_{i_{k-1}j_{\bar{s}}}$  contains the Darboux point  $P_{i_k}^{(3)}$ . So by construction,  $\Phi_{i_{k-1}j_{\bar{s}-1}}^{(2)}(\vec{t}_0)\Phi_{i_{k-1}j_{\bar{s}-1}}^{(1)}(\vec{t}_0) < 0$ ,  $\gamma_{i_{k-1}j_{\bar{s}-1}}^{(\text{vac})} > 1$ ,  $P_{i_{k-1}j_{\bar{s}-1}}^{(\text{vac})} \in \Omega_{i_{k-1}j_{\bar{s}-1}}$ . Then  $\Omega_{i_{k-1}j_{\bar{s}}}$  does not contain any pole and exactly one Darboux point, so that (5.13) is satisfied.

For any fixed  $s < \bar{s}$ , by definition  $\Phi_{i_{k-1}j_{s-1}}^{(2)}(\vec{t}_0)\Phi_{i_{k-1}j_{s-1}}^{(1)}(\vec{t}_0) < 0$ ,  $\gamma_{i_{k-1}j_{s-1}}^{(\text{vac})} > 1$ , and  $P_{i_{k-1}j_{s-1}}^{(\text{vac})} \in \Omega_{i_{k-1}j_{s-1}}$ . Then the oval  $\Omega_{i_{k-1}j_s}$  contains exactly one pole  $P_{i_{k-1}j_s}^{(\text{vac})}$  and (5.13) is satisfied.

By construction, the provisional infinite oval created after adding all ovals associated to the last two rows of the Le-diagram, contains the Darboux point  $P_{i_{k-1}}^{(3)}$  and the pole  $P_{i_{k-1}}^{(\text{vac})}$ .

Let us now suppose to have verified (5.13) for all ovals up to row  $\bar{r}+1$  and let's prove it for the  $\bar{r}$ -th row of the Le-diagram. We proceed as for the case  $r = k-1$ , starting by adding the oval  $\Omega_{i_{\bar{r}}j_{N_{\bar{r}}}}$  and proceeding adding ovals following the  $\bar{r}$ -th row of the Le-diagram from left to right. For any  $s \in [N_{\bar{r}}]$ , let  $\bar{d}_s$  be the number of Darboux points and poles contained in the provisional infinite oval before adding  $\Omega_{i_{\bar{r}}j_s}$ , which fall in  $\Omega_{i_{\bar{r}}j_s}$ . By construction,  $(-1)^{\bar{d}_s}\Phi_{i_{\bar{r}}j_{s-1}}^{(2)}(\vec{t}_0)\Phi_{i_{\bar{r}}j_{s-1}}^{(1)}(\vec{t}_0) > 0$ .

If  $\bar{d}_s$  is odd,  $\gamma_{i_{k-1}j_{s-1}}^{(\text{vac})} > 1$ , and  $P_{i_{k-1}j_{s-1}}^{(\text{vac})} \in \Omega_{i_{k-1}j_{s-1}}$ . Then the oval  $\Omega_{i_{k-1}j_s}$  contains exactly  $\bar{d}_s$  poles and Darboux points and (5.13) is satisfied.

If  $\bar{d}_s$  is even,  $\gamma_{i_{k-1}j_{s-1}}^{(\text{vac})} < 1$ ,  $P_{i_{k-1}j_{s-1}}^{(\text{vac})} \in \Omega_{i_{k-1}j_{s-1}}$ . Then the oval  $\Omega_{i_{k-1}j_s}$  contains exactly  $1 + \bar{d}_s$  poles and Darboux points and (5.13) is satisfied.  $\square$

**Remark 5.7. The effect of the isolated boundary vertexes on the effective vacuum divisor.** Any KP soliton solution is associated to a unique irreducible cell in  $Gr^{TNN}(k', n')$  which is obtained eliminating all isolated boundary vertexes from the Le-diagram. Let  $I$  be the pivot set. The elimination of an isolated boundary vertex  $b_j$ ,  $j \in \bar{I}$ , does not affect the vacuum divisor. The elimination of an isolated boundary vertex  $b_{i_s}$ ,  $i_s \in I$ , produces a change of sign in the matrix elements in all the rows  $r \in [1, s-1]$  which lie to the right of the  $i_s$ -th column. This change of sign is automatically encoded in the basis of vectors by the recursion associated to the reduced matrix, and effects both the sign of the vacuum edge wave function and the position of the vacuum divisor not just in the oval where we remove  $\Gamma_{i_s}$ , but also in all the ovals to the left and above it. We show an example in Figure 11 of both the reducible and reduced vacuum divisors. The original Le-diagram in Fig.11[above left] has RREF matrix  $A$  depending on 10 positive parameters  $x_l$ ,  $l \in [10]$  and the corresponding reducible rational M-curve is shown in Fig.11[bottom left]. The crosses are the divisor points of the KP vacuum wave function: here  $k = 5$ ,  $d = 2$ ,  $s_1 = 1$ ,  $s_2 = 4$ ,  $i_1 = 3$ ,  $i_4 = 12$ ,  $j_1 = 10$  and  $j_2 = 16$ . The infinite oval

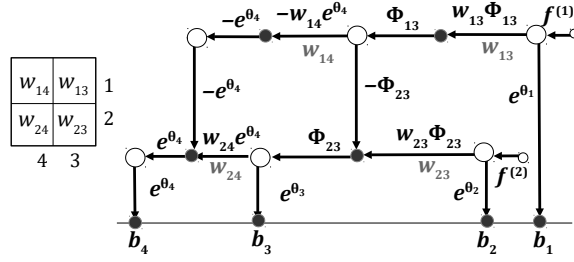


FIGURE 12. The Le-tableau and vacuum edge wave function on the modified Le-network for soliton data in  $Gr^{TP}(2, 4)$ .  $\Phi_{13}(\vec{t}) = -e^{\theta_3(\vec{t})} - (w_{14} + w_{24})e^{\theta_4(\vec{t})}$ , while  $\Phi_{23}(\vec{t}) = e^{\theta_3(\vec{t})} + w_{24}e^{\theta_4(\vec{t})}$ .

$\Omega_0$  intersects  $\Gamma_3$  and  $\Gamma_{12}$  and  $\mu_0 = 2$ .  $\Phi_{12}^{(1)}(\vec{t}_0)$  has the sign of the entry  $A_{12}^4 = -x_8 < 0$ ,  $\Phi^{(2)}(\vec{t}_0) = \exp(\theta_{12}(\vec{t}_0)) > 0$  so that  $\gamma_{12}^{(\text{vac})} > 1$  and  $P_{12}^{(\text{vac})} \in \Omega_0$ .  $\Phi_3^{(1)}(\vec{t}_0)$  has the sign of the entry  $A_{10}^1 = (x_3x_5)/x_4 > 0$ ,  $\Phi^{(2)}(\vec{t}_0) = \exp(\theta_3(\vec{t}_0)) > 0$  so that  $\gamma_3^{(\text{vac})} < 1$  and  $P_3^{(\text{vac})} \notin \Omega_0$ . In conclusion  $\nu_0 = 1$  and  $k + \mu_0 + \nu_0 = 8$  is even.

The reduced Le-diagram and the reduced matrix (see Fig.11[top, right]) are obtained eliminating, respectively, all isolated boundary vertexes. This transformation corresponds to the elimination of the component  $\Gamma_6$  in the reducible rational curve (Fig.11[bottom right]) and to the change of the vacuum pole divisor points (crosses) in the oval  $\Omega'_{39}$  which corresponds to  $\Omega_{39}$  and in all the ovals to the left and above such oval. All other vacuum divisor points (crosses) in the ovals to the right and below respectively of  $\Omega_{39}$  and of  $\Omega'_{39}$  are the same in Figure 11 [bottom, left] and 11[bottom, right].

The proof of Theorem 3.1 on  $\Gamma$  follows immediately from Theorem 5.1.

## 6. CONSTRUCTION OF THE PLANE CURVE AND THE DIVISOR TO SOLITON DATA IN $Gr^{TP}(2, 4)$ AND COMPARISON WITH THE CONSTRUCTION IN [3]

$Gr^{TP}(2, 4)$  is the main cell in  $Gr^{TNN}(2, 4)$  and its elements  $[A]$  are equivalence classes of real  $2 \times 4$  matrices  $A$  with all maximal minors positive. Such matrices are parametrized by the four weights of the Le-tableau (see Figure 12),  $w_{ij}$ ,  $i = 1, 2$ ,  $j = 3, 4$ , and may be represented in the reduced row echelon form (RREF),

$$(6.1) \quad A = \begin{pmatrix} 1 & 0 & -w_{13} & -w_{13}(w_{14} + w_{24}) \\ 0 & 1 & w_{23} & w_{23}w_{24} \end{pmatrix}.$$

The generators of the Darboux transformation  $\mathfrak{D} = \partial_x^2 - \mathfrak{w}_1(\vec{t})\partial_x - \mathfrak{w}_2(\vec{t})$  are

(6.2)

$$f^{(1)}(\vec{t}) = e^{\theta_1(\vec{t})} - w_{13}e^{\theta_3(\vec{t})} - w_{13}(w_{14} + w_{24})e^{\theta_4(\vec{t})}, \quad f^{(2)}(\vec{t}) = e^{\theta_2(\vec{t})} + w_{23}e^{\theta_3(\vec{t})} + w_{23}w_{24}e^{\theta_4(\vec{t})}.$$

In [3] we have proposed a plane curve representation of  $\Gamma(\xi)$  for soliton data in  $Gr^{\text{TP}}(2, 4)$  as the product of a line, a quadric and a cubic and we have desingularized  $\Gamma(\xi)$  to a genus 4 M-curve. In [2] and [5], we use the reduced Le-network  $\mathcal{G}_{\text{red}}$  to implement the construction of the present paper, and represent  $\Gamma(\mathcal{G}_{\text{red}})$  by five lines. We recall that the elimination of  $\mathbb{CP}^1$  copies associated to bivalent vertexes is fully justified since it does not effect neither the properties of the desingularized curve (see Section 3.1) nor the divisor (see Remark 3.7).

In [5] we also desingularize  $\Gamma(\mathcal{G}_{\text{red}})$  to a smooth genus 4 M-curve on which we numerically construct real-regular KP-II finite gap solutions, while in [2] evidence is provided that the asymptotic behavior of the KP soliton zero divisor in  $\|(x, y)\| \gg 1$  for fixed time  $t$  is consistent with the characterization in [16].

In this section, we discuss the same example with a different spirit from our previous publications: we represent

$$\Gamma(\mathcal{G}_{\text{red}}) = \Gamma_0 \sqcup \Gamma'_{13} \sqcup \Gamma_{23} \sqcup \Sigma'_{23} \sqcup \Sigma'_{24},$$

as five lines which are the limit of two lines and a cubic representing

$$\Gamma(\xi) = \Gamma_0 \sqcup \Gamma_1(\xi) \sqcup \Gamma_2(\xi), \quad \xi \gg 1,$$

so that  $\Gamma(\mathcal{G}_{\text{red}}) = \Gamma(\infty)$ . We present the topological model of both  $\Gamma(\mathcal{G}_{\text{red}})$  and  $\Gamma(\xi)$  when  $\xi \gg 1$  in Figure 15[top].

$\Gamma(\xi)$  in Section 6.2 is the reducible curve obtained by the intersection of two lines representing  $\Gamma_0$  and  $\Gamma_2(\xi)$  and a cubic representing  $\Gamma_1(\xi)$ , such that

$$\Gamma_1(\infty) = \Gamma_{23} \sqcup \Sigma'_{23} \sqcup \Sigma'_{24}, \quad \Gamma_2(\infty) = \Gamma'_{13}.$$

We remark that the above representation of  $\Gamma(\xi)$  is different from that proposed in [3]. We also compute the KP divisors both on  $\Gamma(\mathcal{G}_{\text{red}})$  and  $\Gamma(\xi)$ . For  $\xi \gg 1$ , the KP divisor on  $\Gamma(\xi)$  coincides at leading order with that of  $\Gamma(\mathcal{G}_{\text{red}})$  in appropriate coordinates. We remark that the KP divisor is independent on the plane curve representation. Finally, we desingularize both  $\Gamma(\mathcal{G}_{\text{red}})$  and  $\Gamma(\xi)$  to genus 4 M-curves.

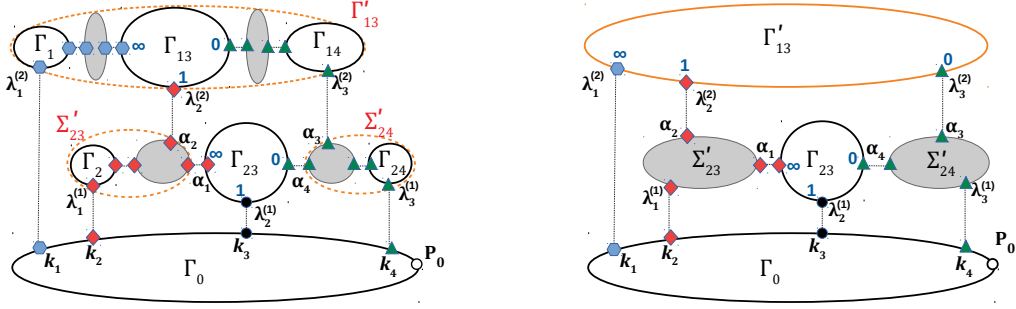


FIGURE 13. The topological model of the spectral curves  $\Gamma(\mathcal{G})$  [left] and  $\Gamma(\mathcal{G}_{\text{red}})$  [right] for soliton data  $Gr^{\text{TP}}(2, 4)$ . In both figures, the value of the KP edge wave function is the same at all points marked with the same symbol.

**6.1. A spectral curve for the reduced Le-network for soliton data in  $Gr^{\text{TP}}(2, 4)$  and its desingularization.** We briefly illustrate the construction of the rational spectral curve  $\Gamma(\mathcal{G}_{\text{red}})$  for soliton data in  $Gr^{\text{TP}}(2, 4)$ . We reduce the degree of the curve from 11 to 5 by eliminating the  $\mathbb{CP}^1$  components corresponding to bivalent vertexes in  $\mathcal{G}$ . We represent the topological model of  $\Gamma(\mathcal{G})$  and of  $\Gamma(\mathcal{G}_{\text{red}})$  in Figure 13: at all double points marked with the same symbol the value of the normalized dressed wave function is the same for all times.

The curve  $\Gamma(\mathcal{G}_{\text{red}})$  is the partial normalization of the nodal plane curve  $\Pi_0(\lambda, \mu) = 0$ , with  $\Pi_0$  as in (6.6), and it is the rational degeneration of the genus 4 M-curve  $\Gamma_\varepsilon$  in (6.7) for  $\varepsilon \rightarrow 0$ . Here we modify the plane curve representation in [5] so that the plane curve representing  $\Gamma(\xi)$  is a rational deformation of  $\Pi_0(\lambda, \mu) = 0$  for  $\xi \gg 1$ . We plot both the topological model and the plane curve for this example in Figure 14.

The reducible rational curve  $\Gamma(\mathcal{G}_{\text{red}})$  is obtained gluing five copies of  $\mathbb{CP}^1$ :  $\Gamma_0$ ,  $\Gamma'_{13}$ ,  $\Gamma_{23}$ ,  $\Sigma'_{23}$  and  $\Sigma'_{24}$  and it may be represented as a plane curve given by the intersection of five lines. To simplify its representation, we impose that  $\Gamma_0$  is one of the coordinate axis in the  $(\lambda, \mu)$ -plane, say  $\mu = 0$ , that  $P_0 \in \Gamma_0$  is the infinite point, that the lines  $\Sigma'_{23}$ ,  $\Sigma'_{24}$  are orthogonal to  $\Gamma_0$ , that  $\Gamma_{23}$  is parallel to the first bisector and that  $\Gamma'_{13}$  and  $\Gamma_{23}$  intersect at a finite point  $\alpha_5$ :

(6.3)

$$\Gamma_0 : \mu = 0, \quad \Gamma'_{13} : \mu - c_{13}(\lambda - \kappa_1) = 0, \quad \Gamma_{23} : \mu - \lambda + \kappa_3 = 0, \quad \Sigma'_{23} : \lambda - \kappa_2 = 0, \quad \Sigma'_{24} : \lambda - \kappa_4 = 0.$$

Notice that here we do not follow the generic construction of Section 3.2 and use parallel lines.

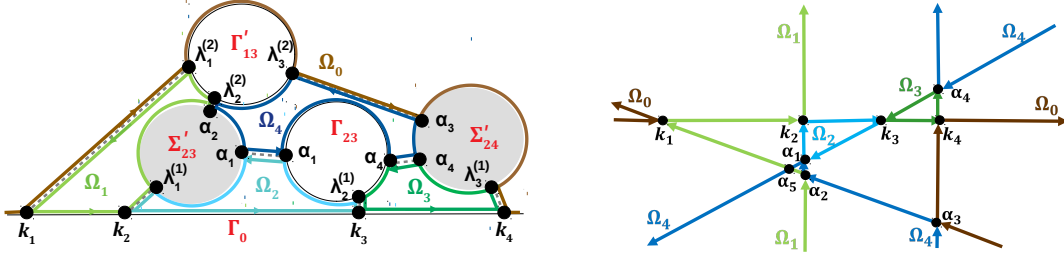


FIGURE 14. The topological model of spectral curve for soliton data  $Gr^{TP}(2, 4)$ ,  $\Gamma(\mathcal{G}_{red})$  [left] is the partial normalization of the plane algebraic curve [right]. The ovals in the nodal plane curve are labeled as in the real part of its partial normalization.

We choose

$$(6.4) \quad c_{13} = \frac{(\kappa_2 + \kappa_4 - 2\kappa_3)(\kappa_4 - \kappa_3)(\kappa_2 - \kappa_1) + (\kappa_3 - \kappa_1)(\kappa_3 - \kappa_2)^2}{(\kappa_4 - \kappa_1)(\kappa_2 - \kappa_1)(\kappa_2 + \kappa_4 - 2\kappa_3)},$$

so that it coincides at leading order in  $\xi$  with the coefficient of the line  $\Gamma_2(\xi)$  in (6.8). Our representation fits generic values of  $\kappa_j$ . The figures in this and the following sections all refer to the case  $\kappa_2 + \kappa_4 - 2\kappa_3 < 0$ .

As usual we denote  $\Omega_0$  the infinite oval, that is  $P_0 \in \Omega_0$ , and  $\Omega_j$ ,  $j \in [4]$ , the finite ovals (see Figure 14). Since the singularity at infinity is completely resolved, the lines  $\Sigma'_{23}$  and  $\Sigma'_{24}$  do not intersect at infinity. Finally the ovals  $\Omega_1$  and  $\Omega_4$  are both finite since neither of them passes through  $P_0$ .

The relation between the coordinate  $\lambda$  in the plane curve representation and the coordinate  $\zeta$  introduced in Definition 3.1 may be easily worked out at each component of  $\Gamma(\mathcal{G}_{red})$ . On  $\Gamma'_{13}$ , we have 3 real ordered marked points, with  $\zeta$ -coordinates:  $\zeta(\lambda_3^{(2)}) = 0 < \zeta(\lambda_2^{(2)}) = 1 < \zeta(\lambda_1^{(2)}) = \infty$ . Comparing with (6.3) we then easily conclude that

$$\lambda = \frac{\kappa_1(\kappa_4 - \kappa_2)\zeta + (\kappa_2 - \kappa_1)\kappa_4}{(\kappa_4 - \kappa_2)\zeta + (\kappa_2 - \kappa_1)}.$$

On  $\Sigma'_{23}$ , we have 3 real ordered marked points, and the following constraints:  $\mu(\lambda_1^{(1)}) = \mu(\kappa_2) = 0$ ,  $\mu(\alpha_1) = \kappa_2 - \kappa_3$ ,  $\mu(\alpha_2) = \mu(\lambda_2^{(2)}) = c_{13}(\kappa_2 - \kappa_1)$ . Similarly on  $\Sigma'_{24}$ , we have 3 real ordered marked points, and the following constraints:  $\mu(\lambda_3^{(1)}) = \mu(\kappa_4) = 0$ ,  $\mu(\alpha_4) = \kappa_4 - \kappa_3$ ,  $\mu(\alpha_3) = \mu(\lambda_1^{(2)}) = c_{13}(\kappa_4 - \kappa_1)$ . Analogously, on  $\Gamma_{23}$  in the initial  $\zeta$  coordinates we have 3 real ordered marked points and  $\zeta(\alpha_4) = 0 < \zeta(\lambda_2^{(1)}) = 1 < \zeta(\alpha_1) = \infty$ , therefore the fractional linear transformation

to the  $\lambda$  is:

$$\lambda = \frac{\kappa_2(\kappa_4 - \kappa_3)\zeta + (\kappa_3 - \kappa_2)\kappa_4}{(\kappa_4 - \kappa_3)\zeta + (\kappa_3 - \kappa_2)}.$$

We remark that  $\Gamma'_{13}$  and  $\Gamma_{23}$  intersect at

$$(6.5) \quad \alpha_5 = (\lambda_5, \mu_5) = \left( -\frac{\kappa_3 - c_{13}\kappa_1}{c_{13} - 1}, -\frac{c_{13}(\kappa_3 - \kappa_1)}{c_{13} - 1} \right).$$

Finally  $\Gamma(\mathcal{G}_{\text{red}})$  is represented by the reducible plane curve  $\Pi_0(\lambda, \mu) = 0$ , with

$$(6.6) \quad \Pi_0(\lambda, \mu) = \mu \cdot (\mu - c_{13}(\lambda - \kappa_1)) \cdot (\lambda - \kappa_2) \cdot (\mu - \lambda + \kappa_3) \cdot (\lambda - \kappa_4).$$

The desingularization of  $\Gamma(\mathcal{G}_{\text{red}})$  gives a genus 4 M-curve  $\Gamma_\varepsilon$  for the following choice ( $0 < \varepsilon \ll 1$ ):

$$(6.7) \quad \Gamma_\varepsilon : \quad \Pi(\lambda, \mu; \varepsilon) = \begin{cases} \Pi_0(\lambda, \mu) + \varepsilon^2 (\lambda - \lambda_5)^2 C_0(\lambda, \mu) = 0, & \text{if } c_{13} \neq 1, \\ \Pi_0(\lambda, \mu) + \varepsilon^2 C_0(\lambda, \mu) = 0, & \text{if } c_{13} = 1, \end{cases}$$

where  $\lambda_5$  is as in (6.5) and  $C_0$  is a cubic polynomial in  $\lambda, \mu$ ,

$$C_0(\lambda, \mu) = \beta_0 + \beta_{1,0}\lambda + \beta_{0,1}\mu + \beta_{2,0}\lambda^2 + \beta_{2,1}\lambda\mu + \beta_{0,2}\mu^2 + \beta_{3,0}\lambda^3 + \beta_{2,1}\lambda^2\mu + \beta_{1,2}\lambda\mu^2 + \beta_{0,3}\mu^3,$$

of which we control the sign at the marked points. If  $\kappa_2 + \kappa_4 - 2\kappa_3 < 0$ , the conditions are

$$\text{sign } (C_0(\kappa_1)) = \text{sign } (C_0(\alpha_2)) \neq \text{sign } (C_0(\kappa_j)), \text{sign } (C_0(\alpha_l)), \quad \text{for } j = 2, 3, 4, \quad l = 1, 3, 4,$$

(see also Figure 6.7 [bottom, left]). The case  $\kappa_2 + \kappa_4 - 2\kappa_3 > 0$  can be treated similarly. For instance, possible choices are  $C_0 = -(35\lambda^3 + \mu^3 + 70\lambda^2)$  for  $\mathcal{K} = \{-3, -1, 2, 3\}$ , and  $C_0 = \mu^2 - 35$  for  $\mathcal{K} = \{-3, -1, 2, 6\}$ .

In Figure 15[left], we represent the topological model of  $\Gamma(\mathcal{G}_{\text{red}})$  [top], which is the partial normalization of the plane curve  $\Pi_0 = 0$  [middle] and the oval structure of the plane curve  $\Gamma_\varepsilon$  as in (6.7) when  $\kappa_2 + \kappa_4 - 2\kappa_3 < 0$ . We remark that the normalized KP wave function takes the same value at all points marked with the same symbol in Figures 13 and 15.

**6.2. Construction of  $\Gamma(\xi)$  as in [3] starting from  $\Gamma(\mathcal{G}_{\text{red}})$ .** In [3] the reducible curve  $\Gamma(\xi) = \Gamma_0 \sqcup \Gamma_1(\xi) \sqcup \Gamma_2(\xi)$  is obtained gluing the three rational irreducible components,  $\Gamma_0, \Gamma_1(\xi)$  and  $\Gamma_2(\xi)$ , at prescribed real points whose position is ruled by the parameter  $\xi \gg 1$ . In Figure 15 [top, right], we represent the topological model of  $\Gamma(\xi)$  for soliton data in  $Gr^{\text{TP}}(2, 4)$  and call  $\tilde{\zeta}$  the local coordinate introduced in Section 4 in [3]. For instance the point  $\alpha_2 \in \Gamma_1(\xi)$  has local coordinate  $\tilde{\zeta}(\alpha_2) = \xi^{-1}$  and is glued to the point  $\lambda_2^{(2)} \in \Gamma_2(\xi)$  having local coordinate  $\tilde{\zeta}(\lambda_2^{(2)}) = -1$ .



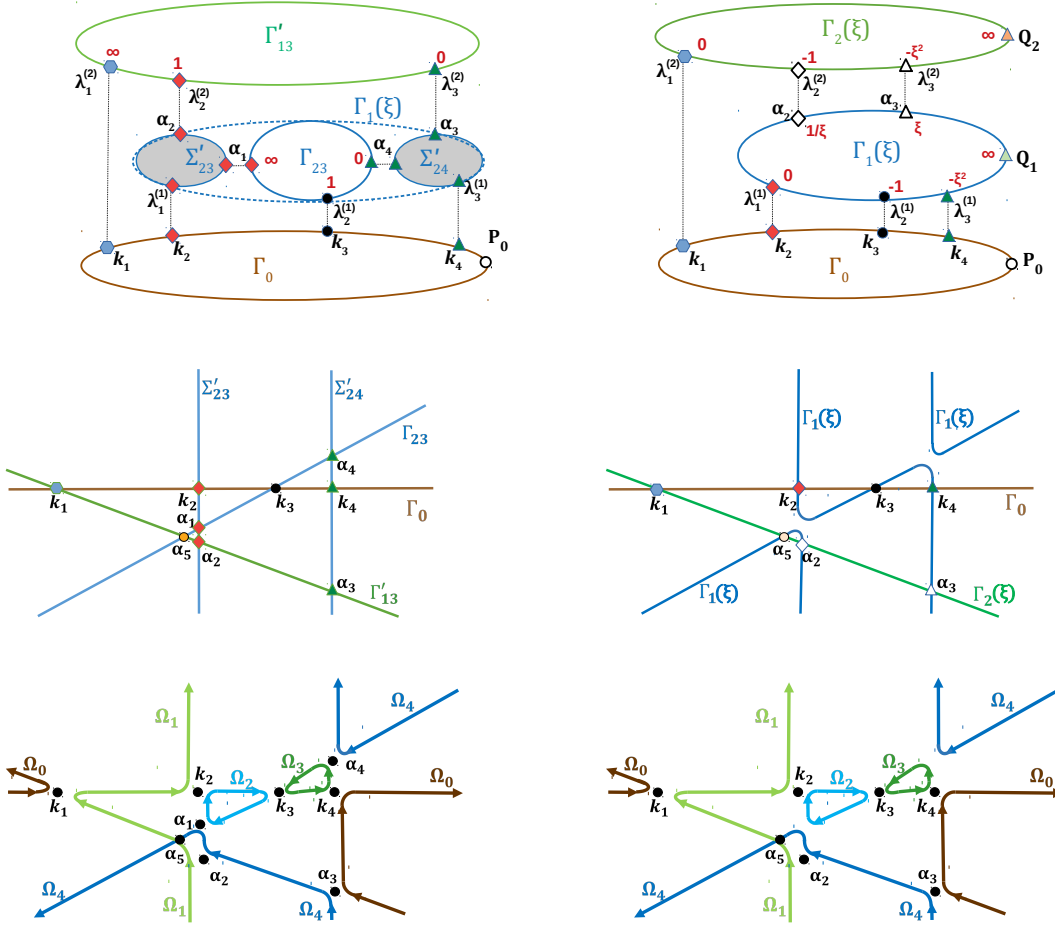


FIGURE 15. For the same soliton data in  $Gr^{TP}(2,4)$  we compare the topological model of the spectral curve [top], its realization as a plane curve [center] and the oval structure of the smooth genus 4 M-curve [bottom] for the reducible rational curves  $\Gamma(\mathcal{G}_{\text{red}}) = \Gamma_0 \sqcup \Gamma_{13}' \sqcup \Gamma_{23} \sqcup \Sigma_{23}' \sqcup \Sigma_{24}'$  [left] and  $\Gamma(\xi) = \Gamma_0 \sqcup \Gamma_1(\xi) \sqcup \Gamma_2(\xi)$  [right]. In all figures the value of the normalized KP wave function for given soliton data in  $Gr^{TP}(2,4)$  is equal for all times at the points marked with the same symbol.

The plane curve  $\Gamma(\xi)$  constructed in this section satisfies  $\Gamma(\infty) = \Gamma(\mathcal{G}_{\text{red}})$ , so it is more suitable than the one presented in [3] for comparing the two models curves and the KP divisors:

- (1)  $\Gamma_0$  is the same rational component both for  $\Gamma(\mathcal{G}_{\text{red}})$  and  $\Gamma(\xi)$ , and we represent it by the line  $\mu = 0$  in both cases;
- (2)  $\Gamma_1(\xi)$  is a rational component which may be obtained from  $\Gamma_{23} \sqcup \Sigma_{23}' \sqcup \Sigma_{24}'$  desingularising it at the double points  $\alpha_1$  and  $\alpha_4$ . This transformation effects the position of the marked points  $\alpha_j \equiv \alpha_j(\xi)$  and  $j = 2, 3$ , which have  $\lambda$ -coordinates  $\lambda_{2,\xi} \equiv \lambda(\alpha_2) = \kappa_2 + O(\xi^{-1})$

and  $\lambda_{3,\xi} \equiv \lambda(\alpha_3) = \kappa_4 + O(\xi^{-1})$  (compare with Section 7 in [3]). Then  $\Gamma_1(\xi)$  may be represented by a cubic depending on  $\xi$  which tends to the product of the three lines when  $\xi \rightarrow \infty$ .

- (3)  $\Gamma_2(\xi)$  has three marked points:  $\lambda_1^{(2)}$  is glued to  $\kappa_1$ , while  $\lambda_j^{(2)}$ ,  $j = 2, 3$  are glued respectively to  $\alpha_j$ ,  $j = 2, 3$ . Then  $\Gamma_2(\xi)$  may be represented by a line which tends to that representing  $\Gamma'_{13}$  when  $\xi \rightarrow \infty$ .

The above ansatz is consistent with the fact that, for any fixed  $\xi \gg 1$  and for all times, the normalized KP wave function on  $\Gamma(\xi)$  coincides exactly with that of  $\Gamma(\mathcal{G}_{\text{red}})$  at the marked points  $\kappa_j$ ,  $j \in [4]$ , and at leading order in  $\xi$  at the marked points  $\alpha_2, \alpha_3$  (see Figure 15).

Let us now construct a plane curve  $\Gamma(\xi)$  satisfying the above requirements.  $\Gamma_0$  is the line  $\mu = 0$  as in the previous section. We require that  $\Gamma_2(\xi)$  is a line passing through the point  $(\kappa_1, 0)$

$$(6.8) \quad \Gamma_2(\xi) : \mu - c_{13}(\xi)(\lambda - \kappa_1) = 0,$$

where  $c_{13}(\xi)$  tends to  $c_{13}$  as in (6.3) in the limit  $\xi \rightarrow \infty$ , so that the line  $\Gamma_2(\infty)$  coincides with that representing  $\Gamma'_{13}$ .

$\Gamma_1(\xi)$  is a cubic which degenerates to the product of the three lines representing  $\Gamma_{23}, \Sigma'_{23}$  and  $\Sigma'_{24}$  in the limit  $\xi \rightarrow \infty$ . We make the following choice

$$(6.9) \quad \Gamma_1(\xi) : \frac{\mu}{\xi} - c_{23}(\xi)(\lambda - \kappa_2)(\lambda - \kappa_3 - \mu)(\lambda - \kappa_4) = 0.$$

The coefficients  $c_{13}(\xi)$ ,  $c_{23}(\xi)$  are uniquely defined by the conditions that  $\Gamma_1(\xi)$  and  $\Gamma_2(\xi)$  intersect at the real points  $\alpha_2 \equiv \alpha_2(\xi)$ ,  $\alpha_3 \equiv \alpha_3(\xi)$  such that in the local coordinate  $\tilde{\zeta}$  used in [3]  $\tilde{\zeta}(\alpha_2) = \xi^{-1}$ ,  $\tilde{\zeta}(\alpha_3) = \xi$  (see also Figure 15 [top,right]). In the coordinate  $\lambda$  used throughout this section, we have

$$\lambda_{2,\xi} \equiv \lambda(\alpha_2) = \frac{\xi^2 \kappa_2(\kappa_4 - \kappa_3) + (1 - \xi)\kappa_3(\kappa_4 - \kappa_2)}{\xi^2(\kappa_4 - \kappa_3) + (1 - \xi)(\kappa_4 - \kappa_2)}, \quad \lambda_{3,\xi} \equiv \lambda(\alpha_3) = \frac{\xi \kappa_4(\kappa_3 - \kappa_2) - \kappa_3(\kappa_4 - \kappa_2)}{\xi(\kappa_3 - \kappa_2) - \kappa_4 + \kappa_2}.$$

The third real intersection point between  $\Gamma_1(\xi)$  and  $\Gamma_2(\xi)$ ,  $\alpha_5 \equiv \alpha_5(\xi)$ , has then  $\lambda$  coordinate

$$(6.10) \quad \lambda_{5,\xi} \equiv \lambda(\alpha_5) = \frac{(\lambda_{2,\xi} \lambda_{3,\xi} \kappa_1 - (\lambda_{2,\xi} + \lambda_{3,\xi})(\kappa_1 \kappa_2 + \kappa_1 \kappa_4 - \kappa_2 \kappa_4) - \kappa_2^2(\kappa_4 - \kappa_1) - \kappa_4^2(\kappa_2 - \kappa_1) + \kappa_1 \kappa_2 \kappa_4)}{\lambda_{2,\xi} \lambda_{3,\xi} - \kappa_1(\lambda_{2,\xi} + \lambda_{3,\xi}) + \kappa_1 \kappa_2 + \kappa_1 \kappa_4 - \kappa_2 \kappa_4}$$

while the coefficients satisfy

$$c_{13}(\xi) = \frac{\lambda_{2,\xi}\lambda_{3,\xi}(\lambda_{2,\xi} + \lambda_{3,\xi} - \sum_{j=1}^4 \kappa_j) + \kappa_1(\lambda_{2,\xi} + \lambda_{3,\xi}) \sum_{j \neq 1} \kappa_j - \kappa_1(\lambda_{2,\xi}^2 + \lambda_{3,\xi}^2 + \sum_{1 < i < j \leq 4} \kappa_i \kappa_j) + \kappa_2 \kappa_3 \kappa_4}{(\lambda_{2,\xi} - \kappa_1)(\lambda_{3,\xi} - \kappa_1)(\lambda_{2,\xi} + \lambda_{3,\xi} - \kappa_2 - \kappa_4)} = c_{13} + O(\xi^{-1}),$$

$$c_{23}(\xi) = -\frac{c_{13}(\xi)(\lambda_{2,\xi} - \kappa_1)}{\xi(\lambda_{2,\xi} - \kappa_4)(\lambda_{2,\xi} - \kappa_2)(c_{13}(\xi)(\lambda_{2,\xi} - \kappa_1) - \lambda_{2,\xi} + \kappa_3)} = -\frac{c_{13}(\kappa_4 - \kappa_1)(\kappa_2 - \kappa_1)(\kappa_2 + \kappa_4 - 2\kappa_3)}{(\kappa_3 - \kappa_1)(\kappa_3 - \kappa_2)(\kappa_4 - \kappa_3)(\kappa_4 - \kappa_2)^2} + O(\xi^{-1}).$$

Therefore  $\Gamma(\xi)$  is represented by the plane curve

$$(6.11) \quad \Gamma(\xi) : \quad \Pi_\xi(\lambda, \mu) = \mu \left( \mu - c_{13}(\xi)(\lambda - \kappa_1) \right) \left( \frac{\mu}{\xi} - c_{23}(\xi)(\lambda - \kappa_2)(\lambda - \kappa_3 - \mu)(\lambda - \kappa_4) \right) = 0.$$

We represent both the plane curve (Figure 15[right,middle]) and its partial normalization (Figure 15[right,top]) in the case  $\kappa_2 + \kappa_4 - 2\kappa_3 < 0$ .

The genus 4 M-curve,  $\Gamma_\varepsilon(\xi)$ , obtained from  $\Gamma(\xi)$  is then a perturbation of  $\Gamma_\varepsilon$ , under the genericity assumption  $c_{13} \neq 1$ :

$$(6.12) \quad \Gamma_\varepsilon(\xi) : \quad \Pi_\xi(\lambda, \mu; \varepsilon) = \Pi_\xi(\lambda, \mu) + \varepsilon^2 (\lambda - \lambda_{5,\xi}^2)^2 C_0(\lambda, \mu) = 0, \quad 0 < \varepsilon \ll 1,$$

where  $\lambda_{5,\xi}$  is as in (6.10), and the coefficients of the cubic polynomial  $C_0$  coincide with those in (6.12), for  $\xi$  fixed and sufficiently big. In Figure 15[right,bottom], we present the oval structure of  $\Gamma_\varepsilon(\xi)$  as in (6.12) in the case  $\kappa_2 + \kappa_4 - 2\kappa_3 < 0$ .

**6.3. The KP divisors on  $\Gamma(\mathcal{G}_{\text{red}})$  and on  $\Gamma(\xi)$ .** In [3], [5] and [2] we have computed the vacuum and the KP divisor for soliton data in  $Gr^{\text{TP}}(2, 4)$  respectively on  $\Gamma(\xi)$ , on  $\Gamma(\mathcal{G}_{\text{red}})$  and on  $\Gamma(\mathcal{G})$ ; therefore we do not repeat this computation here. We just verify that the KP divisors  $\mathcal{D}_{\text{KP},\Gamma} = (P_1^{(S)}, P_2^{(S)}, P_{1,\xi}^{(\text{dr})}, P_{2,\xi}^{(\text{dr})})$  on  $\Gamma(\xi)$  and  $\mathcal{D}_{\text{KP},\Gamma} = (P_1^{(S)}, P_2^{(S)}, P_{13}^{(\text{dr})}, P_{23}^{(\text{dr})})$  on  $\Gamma(\mathcal{G}_{\text{red}})$ , in the coordinate  $\zeta$  introduced in Definition 3.1, satisfy

$$(6.13) \quad \zeta(P_{1,\xi}^{(\text{dr})}) = \zeta(P_{23}^{(\text{dr})}), \quad \zeta(P_{2,\xi}^{(\text{dr})}) = \zeta(P_{13}^{(\text{dr})}) + O(\xi^{-1}).$$

In the following we use the abridged notation  $e^{\theta_{j,0}} = e^{\theta_j(\vec{t}_0)} = e^{\kappa_j x_0}$ . By construction  $\mathcal{D}_{\text{KP},\Gamma}$  consists of the degree 2 Sato divisor  $(P_1^{(S)}, P_2^{(S)})$  defined in (2.7),  $\zeta(P_l^{(S)}) = \gamma_l^{(S)}$ ,  $l = 1, 2$ , and of 2 simple poles  $(P_{13}^{(\text{dr})}, P_{23}^{(\text{dr})})$  respectively belonging to  $\Gamma_{13}$  and  $\Gamma_{23}$ . In the local coordinates induced by the orientation of the Le-network, we have [5, 2]

$$(6.14) \quad \begin{aligned} \zeta(P_1^{(S)}) + \zeta(P_2^{(S)}) &= \mathbf{w}_1(\vec{t}_0), & \zeta(P_1^{(S)})\zeta(P_2^{(S)}) &= -\mathbf{w}_2(\vec{t}_0), \\ \zeta(P_{13}^{(\text{dr})}) &= \frac{w_{14}(\mathfrak{D}e^{\theta_{2,0}} + w_{23}\mathfrak{D}e^{\theta_{3,0}})}{(w_{14} + w_{24})\mathfrak{D}e^{\theta_{2,0}} + w_{23}w_{14}\mathfrak{D}e^{\theta_{3,0}}}, & \zeta(P_{23}^{(\text{dr})}) &= 1 + w_{23} \frac{\mathfrak{D}e^{\theta_{3,0}}}{\mathfrak{D}e^{\theta_{2,0}}}. \end{aligned}$$

In [5, 2], we have also discussed the position of the divisor points in dependence on the signs of  $\mathfrak{D}e^{\theta_{2,0}}$  and  $\mathfrak{D}e^{\theta_{3,0}}$ .

The relation between the local coordinates  $x_{i,j}$  used in [3] and the weights  $w_{ij}$  is

$$x_{1,1} = w_{23}, \quad x_{1,2} = w_{23}w_{24}, \quad x_{2,1} = w_{13}, \quad x_{2,2} = w_{13}w_{14}w_{23}.$$

Applying the Darboux transformation  $\mathfrak{D}$  to the vacuum wave function on  $\Gamma(\xi)$  computed in [3], it is not difficult to prove that on  $\Gamma_1(\xi)$  the divisor point  $P_{1,\xi}^{(\text{dr})}$  has  $\tilde{\zeta}$ -coordinate

$$(6.15) \quad \tilde{\zeta}(P_{1,\xi}^{(\text{dr})}) = -\frac{\xi^2 \mathfrak{D}e^{\theta_{2,0}}}{\xi^2 \mathfrak{D}e^{\theta_{2,0}} + w_{23}(\xi^2 - 1) \mathfrak{D}e^{\theta_{3,0}}}.$$

and that on  $\Gamma_2(\xi)$  the divisor point  $P_{2,\xi}^{(\text{dr})}$  has  $\tilde{\zeta}$ -coordinate

$$(6.16) \quad \tilde{\zeta}(P_{2,\xi}^{(\text{dr})}) = -\frac{\xi^3(\xi - 1) [(w_{14} + w_{24}) \mathfrak{D}e^{\theta_{2,0}} + w_{14}w_{23} \mathfrak{D}e^{\theta_{3,0}}]}{w_{23}(\xi - 1)[w_{14}(\xi^3 + \xi + 1) + w_{24}(1 - \xi^2)] \mathfrak{D}e^{\theta_{3,0}} + \xi^2[(\xi^2 - 1)w_{14} + (1 - \xi)w_{24}] \mathfrak{D}e^{\theta_{2,0}}}.$$

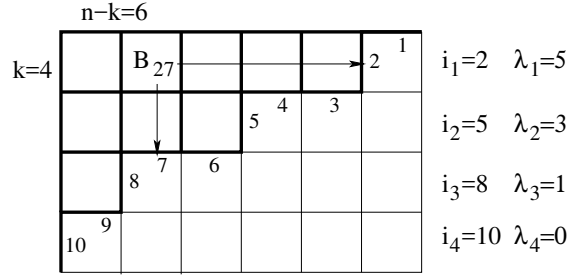
The value of the KP wave function is the same at all points marked with the same symbol in Figure 15 and coincides at leading order in  $\xi$  at the points  $\alpha_2$  and  $\alpha_3$  for  $\xi \gg 1$ . Therefore, for any  $\xi \gg 1$ , the KP divisor point  $P_{1,\xi}^{(\text{dr})} \in \Gamma(\xi)$  coincides with the divisor point  $P_{23}^{(\text{dr})} \in \Gamma(\mathcal{G}_{\text{red}}) \equiv \Gamma(\infty)$ , while  $P_{2,\xi}^{(\text{dr})} \in \Gamma(\xi)$  coincides **at leading order in  $\xi$**  with the divisor point  $P_{13}^{(\text{dr})} \in \Gamma(\mathcal{G}_{\text{red}}) \equiv \Gamma(\infty)$ . The relation between the coordinate  $\tilde{\zeta}$  used in [3] and the coordinate  $\zeta$  at the marked points  $\lambda_s^{(1)}$  in  $\Gamma_{23}$  (resp.  $\lambda_s^{(2)}$  in  $\Gamma_{23}$ ),  $s \in [3]$ , is the following:  $\zeta = \infty, 1, 0$ , respectively correspond to  $\tilde{\zeta} = 0, -1, -\xi^2$ . Finally, inserting the fractional linear transformation

$$\tilde{\zeta} = \frac{\xi^2}{(1 - \xi^2)\zeta - 1},$$

in (6.15) and (6.16) and using (6.14), it is straightforward to verify (6.13).

## APPENDIX A. THE TOTALLY NONNEGATIVE GRASSMANNIAN

In this appendix we recall some useful definitions and theorems from [61] to make the paper self-contained. For more details on the topological properties of  $Gr^{\text{TNN}}(k, n)$  and on generalizations of total positivity to reductive groups we refer to [50, 51, 54, 62, 63]. In particular we use Postnikov rules to represent each Le-tableau  $D$  by a unique bipartite trivalent oriented network  $\mathcal{N}$  in the disk. In Section 3.1 we use the graph  $\mathcal{G}$  of  $\mathcal{N}$  to construct a curve  $\Gamma(\mathcal{G})$ , which is a rational degeneration of a smooth M-curve of genus equal to the dimension  $|D|$  of the corresponding positroid cell.

FIGURE 16. The Young diagram associated to the partition  $(5, 3, 1, 0)$ ,  $k = 4$ ,  $n = 10$ .

**Definition A.1. The totally non-negative part of  $Gr(k, n)$ .** The totally non-negative Grassmannian  $Gr^{TNN}(k, n)$  is the subset of the Grassmannian  $Gr(k, n)$  with all Plücker coordinates non-negative, i.e. it may be defined as the following quotient:  $Gr^{TNN}(k, n) = GL_k^+ \backslash Mat_{kn}^{TNN}$ . Here  $GL_k^+$  is the group of  $k \times k$  matrices with positive determinant, and  $Mat_{kn}^{TNN}$  is the set of real  $k \times n$  matrices  $A$  of rank  $k$  such that all maximal minors are non-negative, i.e.  $\Delta_I(A) \geq 0$ , for all  $k$ -element subsets  $I \subset [n]$ .

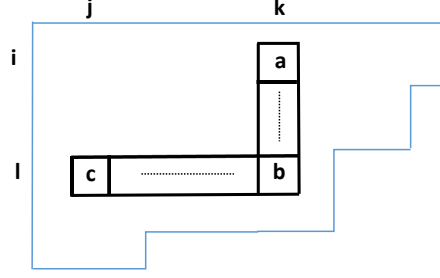
The totally positive Grassmannian  $Gr^{TP}(k, n) \subset Gr^{TNN}(k, n)$  is the subset of  $Gr(k, n)$  whose elements may be represented by  $k \times n$  matrices with all strictly positive maximal minors  $\Delta_I(A)$ .

It is well-known that  $Gr(k, n)$  is decomposed into a disjoint union of Schubert cells  $\Omega_\lambda$  indexed by partitions  $\lambda \subset (n - k)^k$  whose Young diagrams fit inside the  $k \times (n - k)$  rectangle (we use the so-called English notation in our text). A refinement of this decomposition was proposed in [32], [33]. Intersecting these strata with  $Gr^{TNN}(k, n)$  one obtains the totally non-negative Grassmann cells [61] with the following property: each cell is birationally equivalent to an open octant of appropriate dimension, and this birational map is also a topological homeomorphism.

Let us recall these constructions. The Schubert cells are indexed by partitions, or, equivalently by pivot sets. To each partition  $\lambda = (\lambda_1, \dots, \lambda_k)$ ,  $n - k \geq \lambda_1 \geq \lambda_2 \geq \dots \geq \lambda_k \geq 0$ ,  $\lambda_j \in \mathbb{Z}$  there is associated a pivot set  $I(\lambda) = \{1 \leq i_1 < \dots < i_k \leq n\}$  defined by the following relations:

$$(A.1) \quad i_j = n - k + j - \lambda_j, \quad j \in [k].$$

Each Schubert cell is the union of all Grassmannian points sharing the same set of pivot columns. Therefore, any point in  $\Omega_\lambda$  with pivot set  $I$  can be represented by a matrix in canonical reduced row echelon form, i.e. a matrix  $A$  such that  $A_{i_l}^l = 1$  for  $l \in [k]$  and all the entries to the left of these 1's are zero. The Young diagram representing the Schubert cell  $\Omega_\lambda$  is a collection of boxes arranged in  $k$  rows, aligned on the left such that the  $j$ -th row contains  $\lambda_j$  boxes,  $j \in [k]$ .

FIGURE 17. The Le-rule  $a, c \neq 0$  imply  $b \neq 0$ .

**Remark A.1.** In this paper we use the ship battle rule to enumerate the boxes of the Young diagram of a given partition  $\lambda$ . Let  $I = I(\lambda)$  be the pivot set of the  $k$  vertical steps in the path along the SE boundary of the Young diagram proceeding from the NE vertex to the SW vertex of the  $k \times (n-k)$  bound box, and let  $\bar{I} = [n] \setminus I$  be the non-pivot set is. Then the box  $B_{ij}$  corresponds to the pivot element  $i \in I$  and the non-pivot element  $j \in \bar{I}$  (see Figure 16 for an example).

Each stratum in the refined decomposition of  $Gr(k, n)$  into matroid strata [32] is composed by the points of the Grassmannian which share the same set of non-zero Plücker coordinates. Each Plücker coordinate is indexed by a base, i.e. a  $k$ -element subset in  $[n]$ , and, for a given stratum, the set of these bases forms a matroid  $\mathcal{M}$ , i.e. for all  $I, J \in \mathcal{M}$  for each  $i \in I$  there exists  $j \in J$  such that  $I \setminus \{i\} \cup \{j\} \in \mathcal{M}$ . Then the stratum  $\mathcal{S}_{\mathcal{M}} \subset Gr(k, n)$  is defined as

$$\mathcal{S}_{\mathcal{M}} = \{[A] \in Gr(k, n) : \Delta_I(A) \neq 0 \iff I \in \mathcal{M}\}.$$

A matroid  $\mathcal{M}$  is called realizable if  $\mathcal{S}_{\mathcal{M}} \neq \emptyset$ . The pivot set  $I$  is the lexicographically minimal base of the matroid  $\mathcal{M}$ . In [61], Postnikov studies the analogous stratification for  $Gr^{TNN}(k, n)$ .

**Definition A.2. Positroid cell.** [61] The totally nonnegative Grassmann (positroid) cell  $\mathcal{S}_{\mathcal{M}}^{TNN}$  is the intersection of the matroid stratum  $\mathcal{S}_{\mathcal{M}}$  with the totally nonnegative Grassmannian  $Gr^{TNN}(k, n)$ :

$$\mathcal{S}_{\mathcal{M}}^{TNN} = \{GL_k^+ \cdot A \in Gr^{TNN}(k, n) : \Delta_I(A) > 0 \text{ if } I \in \mathcal{M}, \text{ and } \Delta_I(A) = 0 \text{ if } I \notin \mathcal{M}\}.$$

The matroid  $\mathcal{M}$  is totally nonnegative if the matroid stratum  $\mathcal{S}_{\mathcal{M}}^{TNN} \neq \emptyset$ .

**Example A.1.**  $Gr^{TP}(k, n)$  is the top dimensional cell and corresponds to the complete matroid  $\mathcal{M} = \binom{[n]}{k}$ .

A useful tool to classify positroid cells are Le-diagrams and Le-graphs [61].

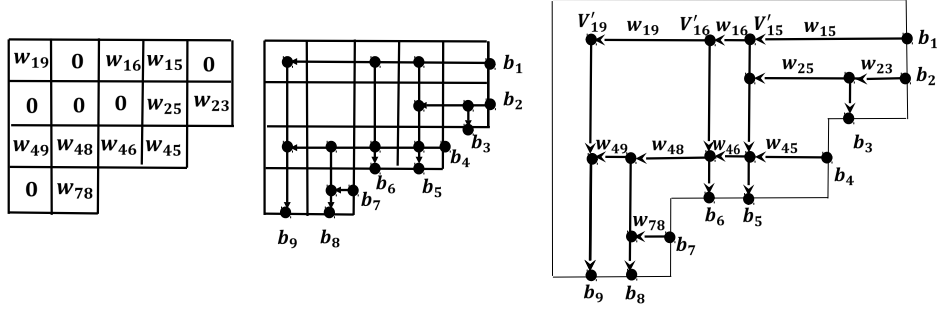


FIGURE 18. The Le-diagram and the Le-network of Example A.2. The horizontal edges are oriented from right to left while the vertical ones from top to bottom.

**Definition A.3. Le-diagram and Le-tableau.**[61] For a partition  $\lambda$ , a Le-diagram  $D$  of shape  $\lambda$  is a filling of the boxes of its Young diagram with 0's and 1's such that, for any three boxes indexed  $(i, k)$ ,  $(l, k)$ ,  $(l, j)$ , where  $i < l$  and  $k < j$ , filled correspondingly with  $a, b, c$ , if  $a, c \neq 0$ , then  $b \neq 0$  (see Figure 17). For such a diagram denote by  $|D|$  the number of boxes of  $D$  filled with 1s.

The Le-tableau  $T$  is obtained from a Le-diagram  $D$  of shape  $\lambda$ , by replacing all 1s in  $D$  by positive numbers  $w_{ij}$  (weights).

The construction of the Le-graph  $\mathcal{G}$  associated to a given Le-diagram is as follows [61]. The boundary of the Young diagram of  $\lambda$  gives the lattice path of length  $n$  from the upper right corner to the lower left corner of the rectangle  $k \times (n - k)$ . A vertex is placed in the middle of each step in the lattice path and they are marked  $b_1, \dots, b_n$  proceeding NE to SW. The vertexes  $b_i$ ,  $i \in I \equiv I(\lambda)$  corresponding to vertical steps are the sources of the network and the remaining vertexes  $b_j$ ,  $j \in \bar{I}$ , corresponding to horizontal steps are the sinks. Then the upper right corner is connected to the lower left corner by another path to obtain a simple close curve containing the Young diagram. For each box of the Le-diagram  $(i, j)$  filled by 1 an internal vertex  $V_{ij}$  is placed in the middle of the box; from such vertex one draws a vertical line downwards to the boundary sink  $b_j$  and a horizontal line to the right till it reaches the boundary source  $b_i$ . By the Le-property any intersection of such lines is also a vertex. All edges are oriented either to the left or downwards.

To obtain a Le-network  $\mathcal{N}$  from a Le-tableaux of shape  $\lambda$  one constructs the Le-graph from the corresponding Le-diagram, assigns the weight  $w_{ij} > 0$  from the box  $B_{ij}$  to the horizontal edge

$e$  which enters  $V_{ij}$  and assigns unit weights  $w_e = 1$  to all vertical edges [61]. The correspondence between the Le-tableau and the Le-network is illustrated in Figure 18.

The map  $T \mapsto \mathcal{N}$  gives the isomorphism  $\mathbb{R}_{>0}^{|D|} \simeq \mathbb{R}_{>0}^{E(G)}$  between the set of Le-tableaux  $T$  with fixed Le-diagram  $D$  and the set of Le-networks (modulo gauge transformations) with fixed graph  $\mathcal{G}$  corresponding to the diagram  $D$  as above.

Given a Le-tableau  $T$  with pivot set  $I$  it is possible to reconstruct both the matroid and the representing matrix in reduced row echelon form using the Lindström lemma.

**Proposition A.1.** [61] *Let  $\mathcal{N}$  be the Le-network associated to the Le-diagram  $D$  and let  $I$  be the pivot set. For any  $k$ -elements subset  $J \subset [n]$ , let  $K = I \setminus J$  and  $L = J \setminus I$ . Then the maximal minor  $\Delta_J(A)$  of the matrix  $A = A(\mathcal{N})$  is given by the following subtraction-free polynomial expression in the edge weights  $w_e$ :*

$$\Delta_J(A) = \sum_P \prod_{i=1}^r w(P_i),$$

where the sum is over all non-crossing collections  $P = (P_1, \dots, P_r)$  of paths joining the boundary vertexes  $b_i$ ,  $i \in K$  with boundary vertexes  $b_j$ ,  $j \in L$ .

Let  $i_r \in I$ , where  $r \in [k]$  and  $j \in [n]$ . Then the element  $A_j^r$  of the matrix  $A$  in reduced row echelon form (RREF) associated to the Le-network  $\mathcal{N}$  is

$$(A.2) \quad A_j^r = \begin{cases} 0 & j < i_r, \\ 1 & j = i_r, \\ (-1)^{\sigma_{i_r j}} \sum_{P: i_r \mapsto j} \left( \prod_{e \in P} w_e \right) & j > i_r, \end{cases}$$

where the sum is over all paths  $P$  from the boundary source  $b_{i_r}$  to the boundary sink  $b_j$ ,  $j \in \bar{I}$ , and  $\sigma_{i_r j}$  is the number of pivot elements  $i_s \in I$  such that  $i_r < i_s < j$ .

**Example A.2.** Let us consider the Le-diagram  $D$  and Le-network as in Figure 18. Then  $I = (1, 2, 4, 7)$  and the matrix in reduced row echelon form is

$$A = \begin{pmatrix} 1 & 0 & 0 & 0 & w_{15} & w_{15}(w_{16} + w_{46}) & 0 & -w_{15}w_{48}(w_{16} + w_{46}) & -w_{15}w_{48}w_{49}(w_{16} + w_{46}) - w_{15}w_{16}w_{19} \\ 0 & 1 & w_{23} & 0 & -w_{23}w_{25} & -w_{23}w_{25}w_{46} & 0 & w_{23}w_{25}w_{46}w_{48} & w_{23}w_{25}w_{46}w_{48}w_{49} \\ 0 & 0 & 0 & 1 & w_{45} & w_{45}w_{46} & 0 & -w_{45}w_{46}w_{48} & -w_{45}w_{46}w_{48}w_{49} \\ 0 & 0 & 0 & 0 & 0 & 0 & 1 & w_{78} & 0 \end{pmatrix}.$$

The same example is used in [45] to illustrate the combinatorial properties of the KP-soliton tropical asymptotics in the limit  $t \rightarrow -\infty$ .



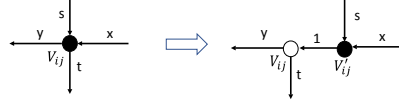


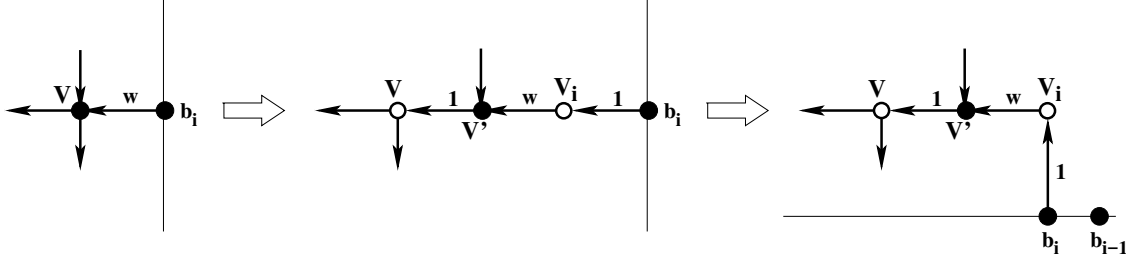
FIGURE 19. All internal vertexes of the Le-network are transformed to trivalent vertexes, preserving the boundary measurement map.

**Remark A.2. Reducible positroid cells** A totally non-negative cell  $\mathcal{S}_{\mathcal{M}}^{TNN} \subset Gr^{TNN}(k, n)$  is reducible if its Le-diagram contains either rows or columns filled by 0s [61].

If the  $j$ -th column of the Le-diagram is filled by zeroes, then there is no path in the Le-network with destination  $j$ , the RREF matrix  $A$  has the  $j$ -th column filled by zeroes. One may then represent the same point in a totally non-negative cell  $\mathcal{S}_{\mathcal{M}'}^{TNN} \subset Gr^{TNN}(k-1, n)$ , by eliminating the  $j$ -th column from the Le-diagram and the  $j$ -th column from the matrix  $A$ .

If the  $r$ -th row of the Le-diagram is filled by zeroes, then there is no path in the Le-network starting from the boundary source  $b_{i_r}$  and the  $r$ -th row of  $A$  contains just the pivot element. One may then represent the same point in a totally non-negative cell  $\mathcal{S}_{\mathcal{M}'}^{TNN} \subset Gr^{TNN}(k-1, n-1)$ , by eliminating the  $r$ -th row of the Le-diagram, eliminating the  $r$ -th row and the  $i_r$ -th columns from the matrix  $A$  and changing the sign of all elements of  $A_j^i$  with  $i < r$  and  $j > i_r$ .

In section 3.1 we associate an unique universal curve to each positroid cell, and we model the construction of a rational degeneration of an M-curve on the Le-graph: vertexes of the graph correspond to copies of  $\mathbb{CP}^1$  and the gluing rules are ruled by its edges. To provide a construction of the curve without parameters, we require that each copy of  $\mathbb{CP}^1$  associated to an internal vertex has three marked points. Moreover, the recursive construction of the wave function and the characterization of its divisor is technically simpler if modeled on a bipartite graph where black and white vertexes alternate. For the above reasons we follow Postnikov's rules to transform the Le-network  $\mathcal{N}$  into a planar bipartite perfect network with internal vertexes of degree at most three, and we continue to denote it with  $\mathcal{N}$ , since this transformation is well-defined. In the perfect network each boundary vertex has degree one and each internal vertex in  $\mathcal{G}$  is either the initial vertex of exactly one edge or the final vertex of exactly one edge. For the Le-graph the only relevant transformation concerns degree four internal vertexes to a couple of trivalent vertexes of opposite colour as in [61] (see Figure 19).

FIGURE 20. Transformation of graph at the boundary source  $b_i$ .

Following Postnikov [61], we assign black color to each internal vertex with exactly one outgoing edge and white color to each trivalent internal vertex with exactly one incoming edge. We also assign black color to all boundary vertexes. Finally we move all boundary vertexes to the same line (see Figure 20).

**Definition A.4.** *The trivalent bipartite Le-network used to construct the curve  $\Gamma(\mathcal{G})$*  The acyclically oriented network associated to the Le-diagram  $D$  is transformed into a **perfect trivalent bipartite network  $\mathcal{N}$**  in the disk with the following rules:

- (1) If the box  $B_{ij}$  of  $D$  is filled with 1, the vertex  $V_{ij}$  is transformed into a couple of one black vertex  $V'_{ij}$  and one white vertex  $V_i$  (see Figure 19[left]); following [61] the horizontal edge joining the black vertex  $V'_{ij}$  to the white vertex  $V_i$  has unit weight, while all other weights are unchanged (see Figure 19[right]);
- (2) All boundary vertexes have black colour and degree one. Any isolated boundary source  $b_i$  is joined by a vertical edge to a white vertex  $V_i$ . If the boundary source  $b_i$  is not isolated, we add a white vertex  $V_i$  to the edge of weight  $w$  starting at  $b_i$ , we assign unit weight to the edge joining  $b_i$  to  $V_i$  and weight  $w$  to the other edge at  $V_i$  (see Figure 20 middle);
- (3) All internal vertexes corresponding to a given row  $r$  in  $D$ , included  $V_{i,r}$ , lie on a common horizontal line;
- (4) The contour of the disk is continuously deformed in such a way that all of the boundary sources and boundary sinks lay on the same horizontal segment and the edge at each boundary vertex is vertical; in this process the positions of all internal vertexes are left invariant (see Figure 20 right).

In Figure 21 we show the bipartite Le-network for Example A.2.

**Remark A.3.** Let  $\mathcal{G}$  be the bipartite Le-graph associated to the Le-diagram  $D$ . Then in  $\mathcal{G}$

- (1) Each black vertex has **at most** one vertical edge;

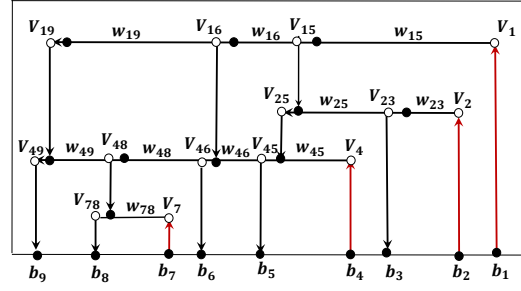


FIGURE 21. The bipartite Le-network for Example A.2 (see Figure 18). The weights refer to the perfect orientation associated to the pivot base  $[1, 2, 4, 7]$  of the matroid: the vertical edges starting at the boundary sources  $b_1, b_2, b_4$  and  $b_7$  are oriented upwards, all other vertical edges are oriented downwards, while all horizontal edges are oriented from right to left.

- (2) Each white vertex has **exactly** one vertical edge;
- (3) The total number of white vertexes is  $|D| + k$ ;
- (4) If  $D$  is irreducible, then the total number of trivalent white vertexes is  $|D| - k$ , while the total number of trivalent black vertexes is  $|D| - n + k$ .

For any  $r \in [k]$ , we denote  $N_r$  the number of boxes filled with 1 in the  $r$ -th row of the Le-diagram  $D$ . By construction we have

$$(A.3) \quad |D| \equiv \sum_{i_r \in I} N_r, \quad \text{with } N_r \equiv \# \{ \text{boxes } B_{i_r j} \text{ filled by 1, for } j \in \bar{I} \}$$

We also introduce an index to simplify the counting of boxes filled by ones. For any fixed  $r \in [k]$ , let  $1 \leq j_1 < j_2 \cdots < j_{N_r} \leq n$  be the non-pivot indexes of the boxes  $B_{i_r j_s}$ ,  $s \in \hat{N}_r$ , filled by one in the  $r$ -th row. Then for any  $r \in [k]$ , we define the index

$$(A.4) \quad \chi_l^{i_r} = \begin{cases} 1 & \text{if there exists } s \in [N_r] \text{ such that } l = j_s, \\ 0 & \text{if } B_{i_r l} \text{ is filled by 0 or } l < i_r. \end{cases}$$

## REFERENCES

- [1] S. Abenda *On a family of KP multi-line solitons associated to rational degenerations of real hyperelliptic curves and to the finite non-periodic Toda hierarchy*, J.Geom.Phys. **119** (2017) 112–138
- [2] S. Abenda *On some properties of KP-II soliton divisors in  $Gr^{TP}(2, 4)$* , Ricerche di Matematica (2018), <https://doi.org/10.1007/s11587-018-0381-0>
- [3] S. Abenda, P.G. Grinevich *Rational degenerations of M-curves, totally positive Grassmannians and KP-solitons*, Commun.Math.Phys. (2018), <https://doi.org/10.1007/s00220-018-3123-y>; arXiv:1506.00563
- [4] S. Abenda, P.G. Grinevich *KP theory, plane-bipartite networks in the disk and rational degenerations of M-curves*, arXiv:1801.00208

- [5] S. Abenda, P.G. Grinevich *Real periodic soliton lattices of KP-II and desingularization of spectral curves: the  $Gr^{TP}(2, 4)$  case*, arXiv:1803.10968
- [6] E. Arbarello, M. Cornalba, P.A. Griffiths *Geometry of algebraic curves. Volume II. With a contribution by Joseph Daniel Harris*, Grundlehren der Mathematischen Wissenschaften 268, Springer, Heidelberg, (2011) xxx+963 pp.
- [7] N. Arkani-Hamed, J.L. Bourjaily, F. Cachazo, A.B. Goncharov, A. Postnikov, J. Trnka *Scattering Amplitudes and the Positive Grassmannian*, arXiv:1212.5605
- [8] N. Arkani-Hamed, J.L. Bourjaily, F. Cachazo, A.B. Goncharov, A. Postnikov, J. Trnka *Grassmannian geometry of scattering amplitudes*, Cambridge University Press, Cambridge, (2016), ix+194 pp.
- [9] M. Atiyah, M. Dunajski, L.J. Mason *Twistor theory at fifty: from contour integrals to twistor strings*, Proc. A. **473** (2017), 20170530, 33 pp.
- [10] G. Biondini, S. Chakravarty *Soliton solutions of the Kadomtsev-Petviashvili II equation*. Journal of Mathematical Physics, **47**, (2006), 033514; doi:10.1063/1.2181907
- [11] M. Boiti, F. Pempinelli, A.K. Pogrebkov, B. Prinari *Towards an inverse scattering theory for non-decaying potentials of the heat equation*, Inverse Problems **17** (2001) 937–957
- [12] V. Buchstaber, A. Glutsyuk *Total positivity, Grassmannian and modified Bessel functions*, arXiv:1708.02154
- [13] V.M. Buchstaber, A.A. Glutsyuk *On determinants of modified Bessel functions and entire solutions of double confluent Heun equations*, Nonlinearity, **29** (2016), 3857–3870
- [14] V.M. Buchstaber, S. Terzic *Topology and geometry of the canonical action of  $T^4$  on the complex Grassmannian  $G_{4,2}$  and the complex projective space  $\mathbb{CP}^5$* , Mosc. Math. J., **16:2** (2016), 237–273
- [15] V.M. Buchstaber, S. Terzic *Toric topology of the complex Grassmann manifolds*, (2018), arXiv: 1802.06449v2
- [16] S. Chakravarty, Y. Kodama *Classification of the line-solitons of KP-II*, J. Phys. A Math.Theor. **41** (2008), 275209
- [17] S. Chakravarty, Y. Kodama *Soliton solutions of the KP equation and application to shallow water waves*, Stud. Appl. Math. **123** (2009) 83–151
- [18] L.A. Dickey *Soliton equations and Hamiltonian systems*, Second edition. Advanced Series in Mathematical Physics, 26. World Scientific Publishing Co., Inc., River Edge, NJ, 2003. xii+408 pp.
- [19] A. Dimakis, F. Müller-Hoissen *KP line solitons and Tamari lattices*, J. Phys. A **44** (2011), no. 2, 025203, 49 pp.
- [20] V. S. Dryuma *Analytic solution of the two-dimensional Korteweg-de Vries (KdV) equation*, JETP Letters, **19:12** (1973), 387–388
- [21] B.A. Dubrovin *Theta functions and non-linear equations*, Russian Math. Surveys, **36:2** (1981), 11–92
- [22] B.A. Dubrovin, T.M. Malanyuk, I.M. Krichever, V.G. Makhankov *Exact solutions of the time-dependent Schrödinger equation with self-consistent potentials*, Soviet J. Particles and Nuclei, **19:3** (1988), 252–269
- [23] B.A. Dubrovin, I.M. Krichever, S.P. Novikov *Integrable systems*. Dynamical systems, IV, 177–332, Encyclopaedia Math. Sci., 4, Springer, Berlin, (2001)
- [24] B. A. Dubrovin, S.M. Natanzon *Real theta-function solutions of the Kadomtsev-Petviashvili equation*. Izv. Akad. Nauk SSSR Ser. Mat. **52** (1988) 267–286

- [25] V.Fock, A. Goncharov *Moduli spaces of local systems and higher Teichmüller theory*, Publ.Math. I.H.E.S. **103** (2006), 1–211
- [26] S. Fomin, A. Zelevinsky *Double Bruhat cells and total positivity*. J. Amer. Math. Soc. **12** (1999) 335–380
- [27] S. Fomin, A. Zelevinsky *Cluster algebras I: foundations*. J. Am. Math. Soc. **15** (2002) 497–529
- [28] N.C. Freeman, J.J.C. Nimmo *Soliton solutions of the Korteweg de Vries and the Kadomtsev-Petviashvili equations: the Wronskian technique*, Proc. R. Soc. Lond. A **389** (1983), 319–329
- [29] F.R. Gantmacher, M.G. Krein *Sur les matrices oscillatoires*. C.R. Acad. Sci. Paris **201** (1935) 577–579
- [30] F.R. Gantmacher, M.G. Krein *Oscillation Matrices and Kernels and Small Vibrations of Mechanical Systems*, (Russian), Gostekhizdat, Moscow-Leningrad, (1941), second edition (1950); revised English edition from AMS Chelsea Publ. (2002)
- [31] M. Gekhtman, M. Shapiro, A. Vainshtein *Cluster algebras and Poisson geometry*, Mathematical Surveys and Monographs, 167. American Mathematical Society, Providence, RI, 2010. xvi+246 pp
- [32] I. M. Gel'fand, R. M. Goresky, R. D. MacPherson, V. V. Serganova *Combinatorial geometries, convex polyhedra, and Schubert cells*, Adv. in Math. **63** (1987), no. 3, 301–316
- [33] I.M Gel'fand and V.V. Serganova *Combinatorial geometries and torus strata on homogeneous compact manifolds*, Russian Mathematical Surveys, **42** (1987), no. 2, 133–168
- [34] A.B. Goncharov, R. Kenyon *Dimers and cluster integrable systems*, Ann. Sci. Éc. Norm. Supér. (4) **46** (2013), no. 5, 747–813
- [35] P. Griffiths, J. Harris *Principles of Algebraic Geometry*, John Wiley & Sons, (1978)
- [36] D.A. Gudkov *The topology of real projective algebraic varieties*, Russ. Math. Surv. **29** (1974) 1–79
- [37] A. Harnack *Über die Vieltheiligkeit der ebenen algebraischen Curven*, Math. Ann. **10** (1876) 189–199
- [38] R. Hirota *The direct method in soliton theory*, Cambridge Tracts in Mathematics, 155. Cambridge University Press, Cambridge, (2004), xii+200 pp.
- [39] B.B. Kadomtsev, V.I. Petviashvili *On the stability of solitary waves in weakly dispersive media*, Sov. Phys. Dokl. **15** (1970) 539–541
- [40] S. Karlin *"Total Positivity, Vol. 1*. Stanford, (1968)
- [41] R. Kenyon, A. Okounkov, S. Sheffield *Dimers and amoebae*, Ann. of Math. (2) **163** (2006), no. 3, 1019–1056
- [42] Y. Kodama *Young diagrams and N-soliton solutions of the KP equation*, J Phys. A Math. Gen. **37** (2004), 11169–11190
- [43] Y. Kodama *KP solitons in shallow water* J. Phys. A: Math. Theor. **43** (2010), 434004
- [44] Y. Kodama, L.K. Williams *The Deodhar decomposition of the Grassmannian and the regularity of KP solitons*, Adv. Math. **244** (2013), 979–1032
- [45] Y. Kodama, L.K. Williams *KP solitons and total positivity for the Grassmannian*, Invent. Math. **198** (2014) 637–699
- [46] I.M. Krichever *An algebraic-geometric construction of the Zakharov-Shabat equations and their periodic solutions*, Sov. Math., Dokl. **17** (1976), 394–397
- [47] I.M. Krichever *Integration of nonlinear equations by the methods of algebraic geometry*, Functional Analysis and Its Applications, **11:1** (1977), 12–26

- [48] I.M. Krichever *Spectral theory of finite-zone nonstationary Schrödinger operators. A nonstationary Peierls model*, Functional Analysis and Its Applications, **20**:3 (1986), 203–214
- [49] I.M. Krichever *Spectral theory of two-dimensional periodic operators and its applications*, Russian Math. Surveys, **44**:8 (1989), 146–225
- [50] G. Lusztig *Total positivity in reductive groups*, Lie Theory and Geometry: in honor of B. Kostant, Progress in Mathematics **123**, Birkhäuser, Boston, (1994), 531–568
- [51] G. Lusztig *Total positivity in partial flag manifolds*, Representation Theory, **2** (1998), 70–78
- [52] T.M. Malanyuk *A class of exact solutions of the Kadomtsev-Petviashvili equation*, Russian Math. Surveys, **46**:3 (1991), 225–227
- [53] N. E. Mnëv *The universality theorems on the classification problem of configuration varieties and convex polytope varieties*, in Topology and Geometry – Rohlin Seminar, O. Ya. Viro ed., Lecture Notes in Mathematics **1346**, Springer, Heidelberg.
- [54] R. Marsh, K. Rietsch *Parametrizations of flag varieties*, Representation Theory, **8**, (2004), 212–242
- [55] V.B. Matveev *Some comments on the rational solutions of the Zakharov-Shabat equations*, Letters in Mathematical Physics, **3** (1979), 503–512
- [56] G. Mikhalkin *Enumerative tropical algebraic geometry in  $\mathbb{R}^2$* , J. Amer. Math. Soc. **18** (2005), 313–377
- [57] T. Miwa, M. Jimbo, E. Date *Solitons. Differential equations, symmetries and infinite-dimensional algebras*, Cambridge Tracts in Mathematics, 135. Cambridge University Press, Cambridge, (2000), x+108 pp.
- [58] S.M. Natanzon *Moduli of real algebraic surfaces, and their superanalogues. Differentials, spinors, and Jacobians of real curves*, Russian Mathematical Surveys, **54**:6 (1999), 1091–1147
- [59] S.P. Novikov *The periodic problem for the Korteweg-de Vries equation*, Functional Analysis and Its Applications, **8**:3 (1974), 236–246
- [60] A. Pinkus *Totally positive matrices*, Cambridge Tracts in Mathematics, **181**, Cambridge University Press, Cambridge, (2010), xii+182.
- [61] A. Postnikov *Total positivity, Grassmannians, and networks*, arXiv:math/0609764 [math.CO]
- [62] A. Postnikov, D. Speyer, L. Williams *Matching polytopes, toric geometry, and the totally non-negative Grassmannian*, J. Algebraic Combin. **30** (2009), no. 2, 173–191
- [63] K. Rietsch *An algebraic cell decomposition of the nonnegative part of a flag variety*, Journal of Algebra **213** (1999), no. 1, 144–154.
- [64] M. Sato *Soliton Equations as Dynamical Systems on a Infinite Dimensional Grassmann Manifolds*, RIMS Kokyuroku, **439** (1981), 30–46
- [65] I. Schoenberg *Über variationsvermindende lineare Transformationen*, Math. Zeit. **32**, (1930), 321–328.
- [66] I.A. Taimanov *Singular spectral curves in finite-gap integration*, Russian Mathematical Surveys, **66**:1 (2011), 107–144
- [67] D.P. Thurston *From dominoes to hexagons*, Proc. Centre Math. Appl. Austral. Nat. Univ., **46**, Austral. Nat. Univ., Canberra, (2017), 399–414
- [68] O. Ya. Viro *Real plane algebraic curves: constructions with controlled topology*, Leningrad Math. J. **1** (1990), no. 5, 1059–1134

- [69] V.E. Zakharov, A. B. Shabat *A scheme for integrating the nonlinear equations of mathematical physics by the method of the inverse scattering problem. I*, *Funct. Anal. and Its Appl.*, **8** (1974), Issue 3, 226–235
- [70] Y. Zarmi *Vertex dynamics in multi-soliton solutions of Kadomtsev-Petviashvili II equation*, *Nonlinearity* **27** (2014), 1499–1523

DIPARTIMENTO DI MATEMATICA, UNIVERSITÀ DI BOLOGNA, P.ZZA DI PORTA SAN DONATO 5, I-40126 BOLOGNA BO, ITALY

*E-mail address:* `simonetta.abenda@unibo.it`

L.D.LANDAU INSTITUTE FOR THEORETICAL PHYSICS, PR. AK SEMENOVA 1A, CHERNOGOLOVKA, 142432, RUSSIA, `pgg@landau.ac.ru`, LOMONOSOV MOSCOW STATE UNIVERSITY, FACULTY OF MECHANICS AND MATHEMATICS, RUSSIA, 119991, MOSCOW, GSP-1, 1 LENINSKIYE GORY, MAIN BUILDING,, MOSCOW INSTITUTE OF PHYSICS AND TECHNOLOGY, 9 INSTITUTSKIY PER., DOLGOPRUDNY, MOSCOW REGION, 141700, RUSSIA.